Fall 2014

The impacts of climate change and agricultural activities on water cycling of Northern Eurasia

Yaling Liu
Purdue University

Graduate School Form 30
(Revised 08/14)

PURDUE UNIVERSITY
GRADUATE SCHOOL
Thesis/Dissertation Acceptance

This is to certify that the thesis/dissertation prepared

By Yaling Liu

Entitled
THE IMPACTS OF CLIMATE CHANGE AND AGRICULTURAL ACTIVITIES ON WATER CYCLING OF NORTHERN EURASIA

For the degree of Doctor of Philosophy

Is approved by the final examining committee:

Qianlai Zhuang

Laura Bowling

Dev Niyogi

Melba Crawford

To the best of my knowledge and as understood by the student in the Thesis/Dissertation Agreement, Publication Delay, and Certification/Disclaimer (Graduate School Form 32), this thesis/dissertation adheres to the provisions of Purdue University's "Policy on Integrity in Research" and the use of copyrighted material.

Qianlai Zhuang

Approved by Major Professor(s): _____

_____

Approved by: Indrajeet Chaubey 10/13/2014

Head of the Department Graduate Program Date

THE IMPACTS OF CLIMATE CHANGE AND AGRICULTURAL ACTIVITIES ON WATER CYCLING OF NORTHERN EURASIA

A Dissertation

Submitted to the Faculty

of

Purdue University

by

Yaling Liu

In Partial Fulfillment of the

Requirements for the Degree

of

Doctor of Philosophy

December 2014

Purdue University

West Lafayette, Indiana

Dedicated to my beloved parents, husband and daughter

献给我至爱的父母，丈夫和女

ACKNOWLEDGEMENTS

When it comes to this section, I realize that I am indebted to so many people. The PhD life of past three and half years is enjoyable and fruitful as well as stressful. This is a precious and unique journey, where I enriched my knowledge background and skills, expanded my collaboration connections and also made a lot of awesome friends. The beautiful scenery along this journey deserves all the struggles and efforts.

I would express my sincerest gratitude to my major professor Qianlai Zhuang. He offered me an opportunity – pursuing the PhD degree at Purdue University– that have changed the trajectory of my life and made the transfer from a high school Geography teacher to a researcher possible so that I could possibly fulfill my career goal – being a scientist doing research on the interactions between human and nature. All his solid support, stimulating instructions, and inspiring encouragement are really profitable and nutritious to my growth.

Deepest appreciation is made here to my advisory committee members Drs. Laura Bowling, Melba Crawford and Dev Niyogi. I benefited a lot from Laura's courses as well as face-to-face meetings, her insights and instructions could always enlighten me and guide me to a solution. Melba gave me huge encouragement on life as well as instructions on research and course work; she serves as a successful role model in my PhD life and in

the future. I gained so much from Dev's exciting course and pleasant coffee meetings, as well as his insightful suggestions upon my papers.

Gratitude is also extended to my collaborators across different institutions. Special acknowledgement is made here to Drs. Diego Miralles, Ryan Teuling, David Kicklighter, Jiquan Chen, Tonlin Zhang and Nadja Tchebakova for their continuous support. I also acknowledge the academic, technical and miscellaneous support from Purdue boilermakers and financial support from the funding agencies NASA, NSF and DOE.

I would also thank all my labmates, colleagues and friends for the exciting discussions, stimulating brainstorms, as well as sharing my ups and downs. Finally, heartfelt gratitude is made here to my beloved family, to whom this dissertation is dedicated. While I was pursuing my PhD degree, my daughter YoYo was attending preschool and kindergarten here, we then grew together at Purdue. Finishing the PhD program without the passionate and constant support from my family is a mission impossible.

Again, all your support made this happen, thank you!

TABLE OF CONTENTS

Page

Page

Page

Page

ABSTRACT

Liu, Yaling. Ph.D., Purdue University, December 2014. The Impacts of Climate Change and Agricultural Activities on Water Cycling of Northern Eurasia. Major Professor: Qianlai Zhuang.

The ecosystems in Northern Eurasia (NE) are important due to their vast land coverage, high rate of observed and projected warming, and the potential feedbacks they can cause on the global climate system. To understand the impacts of climate change and agricultural activities on water cycling in NE, I analysed a variety of datasets and conducted series of studies by applying a combination of modeling, in-situ observations and remote sensing data, uncertainty analysis, and model-data fusion.

Long-term unique *in-situ* measurements on soil moisture across multiple stations and discharge records at the outflow basins in Northern China (NC) provide us robust evidence to assess the trends of soil moisture and discharge in this region (Chapter 2). NC overlaps with NE and is one of the hot-spots experiencing the most severe water shortage in the world. Declines in soil moisture and stream flow detected via *in-situ* measurements in the last three decades indicate that water scarcity has been exacerbated. Multiple linear regression results indicate that intensification of agricultural activities including increase in fertilizer use, prevalence of water-expensive crops and cropland expansion appear to have aggravated these declines in this region.

Scarce evapotranspiration (*ET*) measurements make *ET* estimation via model a necessary step for better regional-scale water management. Penman–Monteith based algorithms for plant transpiration and soil evaporation were introduced into the Terrestrial Ecosystem Model (TEM) to calculate *ET* (Chapter 3). I then examined the response of *ET* and water availability to changing climate and land cover on the Mongolian Plateau during the 21st century. It is shown that use of the Penman–Monteith based algorithms in the TEM substantially improved *ET* estimation on the Mongolia Plateau. Results show that regional annual *ET* varies from 188 to 286 mm yr^{-1} – with an increasing trend – across different climate change scenarios during the 21st century. Meanwhile, the differences between precipitation and *ET* suggest that the available water for human use will not change significantly during the 21st century. In addition, analyses also suggest that climate change is more important than land cover change in determining changes in regional *ET*.

Improvement in the accuracy of *ET* estimation by introducing Penman–Monteith based algorithms into the TEM motivated me to further improve the model representation of *ET* processes. I further modified the TEM to incorporate more detailed *ET* processes including canopy interception loss, *ET* (evaporation) from wet land surfaces, wetlands and water bodies, and snow sublimation to examine spatiotemporal variation of *ET* in NE from 1948 to 2009 (Chapter 4). Those modifications lead to substantial enhancement in the accuracy of estimation of *ET* and runoff. The consideration of snow sublimation substantially improved the *ET* estimates and highlighted the importance of snow in the hydrometeorology of NE. The root mean square error of discharge from the six largest watersheds in NE decreased from 527.74 km^3 yr^{-1} to 126.23 km^3 yr^{-1}. Meanwhile, a

systematic underestimation of river discharge after 1970 indicates that other water sources or dynamics not considered in the model (e.g., melting glaciers, permafrost thawing and fires) or bias in the precipitation forcing may also be important for the hydrology of the region.

To better understand the possible causes of systematic bias in discharge estimates, I examined the impacts of forcing data uncertainty on *ET* and runoff estimation in NE by driving the modified TEM with five widely-used forcing data sets (Chapter 5). Estimates of regional *ET* vary between 263.5–369.3 mm yr^{-1} during 1979-2008 depending on the choice of forcing data, while the spatial variability of *ET* appears more consistent. Uncertainties in *ET* forcing propagate as well to estimates of runoff. Independent of the forcing dataset, the climatic variables that dominate *ET* temporal variability remain the same among all the five TEM simulated *ET* products. *ET* is dominated by air temperature in the north and by precipitation in the south during the growing season, and solar radiation and vapour pressure deficit explain the dynamics of *ET* for the rest of the year. While the Climate Research Unit (CRU) TS3.1 dataset of the University of East Anglia appears as a better choice of forcing via our assessment, the quality of forcing data remains a major challenge to accurately quantify the regional water balance in NE.

CHAPTER 1. INTRODUCTION

1.1 Research background

Ecosystems in Northern Eurasia (NE) plays a critical role in regulating Earth's climate due to its vast land coverage, its high sensitivity to global warming (Serreze et al. 2000; IPCC 2007, 2013), and its significant feedbacks on the global climate system (Adam and Lettenmaier 2008; Groisman et al. 2010). NE accounts for 19% of the Earth's land surface and contains about 70% of the Earth's boreal forests and more than two-thirds of the Earth's permafrost (NEESPI, 2004). There is a growing consensus that larger temperature increases and more drastic climate changes are occurring in this region compared with lower latitude ecosystems (IPCC 2007, 2013).

The hydrological cycle in NE plays an important role in the global climate system. Recent increases in the total terrestrial freshwater flux from NE into the Arctic Ocean have been suggested as the cause for the weakening of the Atlantic thermohaline circulation (Rahmstorf and Ganopolski 1999) and the slow-down of the transport of CO_2 to the deep ocean (ACIA 2005). Moisture condition varied spatially and temporally, the western half of high latitudinal NE domain became more humid during the 20^{th} century, whereas east of the Ural Mountains was drier (Groisman et al. 2010). In addition, permafrost degradation has occurred in this permafrost-dominated region as warming

prevails. A significant warming trend during the last 30 years was detected in the long-term records of near-surface permafrost temperature (e.g., Romanovsky, 2002), with some areas showing permafrost temperatures close to 0°C and some sites showing that degradation has already occurred (e.g., Fedorov, 1996). Thawing permafrost has changed ecosystem structure and biogeochemistry including the carbon cycling (e.g., Zhuang et al., 2003; Euskirchen et al., 2006) and the release of the greenhouse gases CO_2 and CH_4 (Zhuang et al., 2004, 2007) to the atmosphere. These changes may consequently lead to changes to global climate.

Given an increasing frequency in forest fires in NE in recent years (McClelland et al. 2004), fire disturbances alter the ecosystem structure, succession and biogeochemical processes to a large extent (Alexeyev and Birdsey, 1998; Soja et al., 2004a and b; Sukhinin et al., 2004; Groisman et al., 2007). As warming increases, wildfires increase in frequency and area burned. Fires have multifaceted effects on ecosystem structure and functioning. Fire disturbances release carbon, but also replace an absorptive tree canopy with a reflective snow surface during the non-growing season, which increases albedo. The positive feedback to climate induced from carbon release may be offset by increasing negative feedback due to snow cover. Nonetheless, these two-sided effects have not been well understood for this region.

Other types of land use and land cover changes (LUCC) also prevail in this region. For instance, over 500 million m^3 of wood per year have been lost due to stand-replacing disturbances (fire, insects, etc.) between 1993 and 2003 (Shvidenko et al., 2008). Forest industry practices have further degraded the regional environment. In addition, climate change has contributed to “green desertification” (i.e. potentially irreversible replacement

of forests by grassy glades and bogs), which has already been observed over millions of hectares of previously forested land (Shvidenko et al., 2008). In the Mongolia Plateau, overgrazing in permafrost-dominated steppe-grassland areas has accelerated the degradation of permafrost and peatlands (Bohannon 2008; Minayeva et al 2004, 2005). The LUCC regulates the land-atmosphere interactions, changes albedo, affects the surface energy budget, and alters the partitioning of available energy, in turn impacts the climate system. Furthermore, LUCC will likely increase in the future to meet increasing human demands for food, fiber, and energy in this region.

Overall, the above-mentioned changes are accelerating in the region, and they jointly affect the global climate system. These concurrent complex changes also pose challenges to understanding the evolution of land-atmosphere interactions as well as the mechanisms of changes in water and carbon cycling in this region.

1.2 Research motivation

Recent years have seen the progress in understanding the dynamics of the hydrological cycle, and the interactions between climate change, human activities and changes in water cycling in this region. For example, Peterson et al. (2002) reported an increasing fresh water discharge into the Arctic ocean from this region; Adam et al. (2007, 2008) reported the impacts of reservoir regulations on the streamflow and analyzed the streamflow trends using new precipitation and reconstructed streamflow products. Troy et al. (2012) highlighted the role of winter precipitation and temperature in the streamflow trends in this region. Saurer et al. (2004) showed that the water-use efficiency of trees has improved in this region over the last 100 years based on measurements of the

carbon isotope ratio in tree rings. Dye et al. (2003) indicated that snow-cover season has declined and vegetation growth has been enhanced in the past decades in this region.

Nonetheless, accurate quantification of evapotranspiration (*ET*), long-term spatiotemporal variability of *ET* and water availability (i.e., *P*-*ET*, *P*: precipitation), and uncertainties in estimating *ET* over this region has not been adequately studied. This knowledge gap motivates me to look into these issues to advance understanding in variability of water cycling and uncertainty in quantification of water balances in this region. Another goal is to investigate the impact of agricultural activities on water cycling of this region by looking at an adjacent overlapping region – Northern China (NC), because NC is a hot-spot of droughts and the available field data are limited in the domain of NC.

This thesis starts from analysis of soil moisture and discharge field data, and then moves on to estimation of *ET* and water availability using a biogeochemical model, with a focus on *ET* variability and uncertainty in the estimation of *ET*. The primary focus on *ET* is justified with three reasons. First, *ET* is an essential process in the Earth system as it governs the energy, water and carbon cycling between land and atmosphere (Dolman and de Jeu 2010; Wang and Dickinson 2012). *ET* conveys about half of the solar energy absorbed by the land back to the atmosphere as latent heat flux (Stephens et al. 2012), and thus regulates the Earth's energy balance and therefore its temperature. In addition, *ET* returns more than 60% of annual precipitation (*P*) back to the atmosphere, constraining the water availability over the continents (Vörösmarty et al. 1998; Miralles et al. 2011a; Kumar et al. 2014), and providing climate feedbacks via precipitation recycling (Seneviratne et al., 2010). Second, enhanced accuracy in the estimation of *ET* is

critical to improving the estimation of other water quantities such as soil moisture and available water resources, which is directly associated with water management. Third, accurate estimation of *ET* is crucial for the determination of the status of the atmospheric boundary layer in General Circulation Models (GCM) for accurate climate prediction.

1.3 Research Tasks and Outline of Thesis

1.3.1 Research tasks

The dissertation research focuses on the dynamics of water cycling in NE, with the study region expanding from NC, to the Mongolia Plateau and to the entire NE. The primary tasks lie in addressing a series of questions:

1. What are the trends of precipitation, soil moisture and discharge in NC in the past three decades? What are the impacts of agricultural activities on the dynamics of soil moisture and discharge in this region?
2. How can representation of atmospheric evaporative demand (AED) be improved in the TEM so as to improve the accuracy of *ET* estimation? How will *ET* and water availability change on the Mongolia Plateau during the 21st century? Is climate change or climate-induced land cover change more important in determining regional *ET*?
3. How can the accuracy of *ET* estimation be further improved in the TEM? What is the crucial part of model representation for *ET* estimation in NE? How have *ET* and water availability changed in NE?

4. What are the impacts of forcing data on the uncertainty in the estimation of *ET*? Which forcing data set appears to be a better choice? What are the main climatic drivers in determining *ET* in this region?

1.3.2 Outline of Thesis

In Chapter 2, I assessed soil moisture, discharge and precipitation trends in NC with a robust long-term soil moisture field dataset, discharge measurements and meteorological observations. Next, I investigated the effects of agricultural activities on these trends using multiple linear regression models. This work highlights the acceleration of soil moisture and discharge decline derived from agricultural intensification. The study is currently in review at *Scientific Reports*.

Chapter 3 is motivated by the study in Chapter 2 – although the decline of soil moisture and discharge derived from agricultural practices are majorly due to increased *ET*, *ET* was not involved due to unavailability of *ET* measurements. Here, I use biogeochemical model as a tool to simulate *ET* changes at regional scale. I modified an early version of TEM by introducing Penman–Monteith based algorithms to calculate *ET*. The modified model has been calibrated using eddy-covariance (EC) measurement data and evaluated by a variety of satellite-based *ET* products so that I gained considerable confidence in the skill of the model in estimating regional spatiotemporal variabilities. The modified model was run from 1970-2100 driven by climate data of six climate scenarios and two land cover datasets to examine the response of *ET* and water

availability to changing climate and land cover on the Mongolian Plateau during the 21st century. This study has been published in *Global and Planetary Change* (Liu et al. 2013).

In Chapter 4, I further modified the TEM *ET* algorithms to estimate: 1) transpiration separately for uplands and wetlands; 2) evaporation separately for uplands, wetlands, and water bodies; and 3) snow sublimation. These modifications aim at improving the representation of the interactions between the terrestrial energy and water budgets and to increase their realism in high-latitude regions. The different *ET* components are aggregated to grid cell scale weighted by the fraction of each land cover per grid cell. The updated TEM is calibrated using *in-situ* measurements at thirteen EC towers and also evaluated against a variety of satellite-based *ET* products to gain confidence in performance. Then the updated TEM is used to examine the temporal and spatial variations in *ET,* water availability and river discharge in NE for the period 1948–2009. This study has been published in *Climatic Change* (Liu et al. 2014).

In Chapter 5, motivated by looking into the possible causes of systematic errors in the discharge estimates by TEM in Chapter 4, I investigated the *ET* estimation uncertainty that is derived from the use of forcing data, by driving TEM with five widely-used climate datasets for NE during 1979-2008. I also explored the dominant climatic drivers for *ET* to better understand the sources of uncertainties in *ET* estimation. This study aims to investigate the plausible *ET* dynamics, the spatiotemporal variability of *ET* estimates in response to uncertainties in forcing data, as well as the regional changes in the sensitivity of *ET* to different climatic drivers. This study is currently in review at *Journal of Geophysical Research: Atmosphere*.

In Chapter 6, I provide a summary to this dissertation research, discuss the limitations, and delineate the possible future research directions.

CHAPTER 2. AGRICULTURE INTENSIFICATION ACCELERATES SOIL MOISTURE AND DISCHARGE DECLINE IN NORTHERN CHINA[1]

2.1 Abstract

Northern China is one of the most densely populated regions in the world. Agricultural activities have intensified since the 1980s to provide food security to the region. However, this intensification has likely contributed to an increasing scarcity in water resources, which may in turn be endangering the region's food security. Based on *in-situ* measurements of soil moisture collected during 1983–2012, we find that topsoil (0–50 cm) water content has declined significantly ($p<0.01$) during the growing season, with a trend of 0.38–0.70% per year. Furthermore, the river discharge measured at the outlet of the three main hydrological basins has also declined, at rates of 0.05–1.10 km^3 yr^{-1}. Our results indicate that the regional aggravation of these negative trends is consistent with the effect of agricultural intensification. Increased fertilizer application has favoured biomass growth and increased transpiration rates, thus reducing the water yield of the region. The rapid proliferation of water-expensive crops (e.g., maize and

[1] Liu, Y., Pan, Z., Zhuang, Q., Miralles, D., Teuling, A.J., Zhang, T., An, P., Dong, Z., Zhang, J., He, D., Wang, L., Pan, X., Niyogi, D. Agriculture intensification aggravates drought in Northern China, *Scientific Reports* in review

rapeseed), and the expansion of the area dedicated to food production, have contributed to the drying of the soils and the declines in streamflow. Alternative agricultural practices that can meet the immediate demand without compromising future water resources seem critical for the sustainability of food production in Northern China.

2.2 Introduction

Droughts are one of the most costly natural hazards in China due to their unusual severity and persistence (Wang et al. 2011); they resulted in an average annual loss of $48.8 billion during 1978–2003 (ADRC, 2003). While on a global scale drought has not increased (Sheffield et al. 2012), Northern China (NC) is facing an increasing water scarcity (Wang et al. 2011; Zou et al. 2005; Ma et al. 2006). In fact, China is one of thirteen countries considered to be facing extreme water shortages, with four times less water resources per capita than the world average (Piao et al. 2010). Additionally, distribution of water resources does not proportionally match demand. With only 18% of China's water resources, NC accounts for 65% of the arable land and 40% of the population (Piao et al. 2010; Population census Office of China, 2011). This imbalance leads to a high exploitation of water in NC, which induces severe ecological and environmental problems such as degradation of land and freshwater (Chen et al. 2011). In the past three decades, droughts affected an average annual area of 23.9 million ha in NC, accounting for 35.6% of the planting area (National Bureau of Statistics of China). Moreover, dry extremes are likely to become more frequent and intense in the region (Wetherald et al. 2002; Trenberth et al. 2014).

While droughts are associated with declines in precipitation, soil moisture and discharge (Heim et al. 2002), the drivers of this aggravation of these declines in NC and the role of agricultural intensification are still poorly understood. More specifically, despite recent analyses of meteorological drought looking at trends in rainfall (Sheffield et al. 2012; Zou et al. 2005; Ma et al. 2006; Trenberth et al. 2014) and studies of soil moisture using model-simulated or satellite-retrieved soil moisture changes (Wang et al. 2011; Dorigo et al. 2012), there is a lack of ground truth based on observational assessment of the soil moisture trends measured in situ. Previous studies have identified a long-term decline in the regional river runoff, and attributed this decline to a precipitation decrease and human interventions such as reservoir regulation, water withdraw and deep groundwater pumping (Piao et al. 2010; Zhang et al. 2009; Fu et al. 2004). However, the regional impacts of the intensification of human agricultural practices have received so far little attention. Current agricultural practices –such as crop type selection, farming measures, fertilizer application, or irrigation management – affect physical and biogeochemical interactions within ecosystems (Alley et al. 2003; Rosenzweig et al. 2008) and have therefore the potential to be a major driving force in the dynamics of soil moisture (Fu et al. 2003). Consequently, investigating the mechanisms behind this dry-out appears crucial for the improvement of the regional management of agricultural practices and water resources, and to evaluate the sustainability of the current food production mode in the region.

This study aims at understanding NC soil moisture and discharge trends using robust observational evidence and to understand how regional agricultural activities have impacted these trends. We use unique *in-situ* soil moisture measurements collected

between 1983–2012, long-term discharge measurements, meteorological observations and satellite remote sensing to assess the regional dynamics of soil moisture, discharge and precipitation[18] during the past three decades. The effects of agricultural intensification on these dynamics are assessed through multiple linear regressions using data of fertilizer application rates and information on crop types and crop area. The Xinjiang autonomous region and the Qinghai province are excluded from the analysis, as population density is lower and agriculture is less intensive, and there is a lack of ground observations and historical records of agricultural activities.

2.2Methods

2.2.1 Overview

We analyse the trends of soil moisture in NC using long-term soil moisture measurements from 40 agricultural meteorological stations during 1983-2012, and support our analysis with a study of the discharge (Q) trends from the three outflow river basins in the region. The study region and location of the 40 stations as well as the boundary of river basins are shown in Fig. 2.1b. To isolate the long-term impact of precipitation trends, we examine how meteorological drought has evolved across NC using measurements of precipitation from 307 weather stations. We calculate the Palmer Drought Severity Index (PDSI, Palmer, 1965) based on the tool in Jacobi et al. (2013), but we use FAO56 Penman-Monteith equation (Allen et al. 1998) instead of Thornthwaite or Hamon equation to estimate potential evapotranspiration as suggested by Sheffield et al. (2012) and An et al. (1985). We use a Mann-Kendall test to evaluate the

significance of trend. Multiple linear regression models are used to assess the correlated effects for changes in soil moisture and *Q*.

2.2.2 Data

The observations used in the analyses include: (a) soil moisture measurements during the growing season (generally April-September, 3-5 observations per month) from 40 different agricultural meteorological stations across Northern China for 1983–2012 (Fig. 2.1b, note that these stations are located in rain-fed dry-land area and no irrigation is applied). The soil moisture is measured using the gravimetric technique; (b) a long-term monitoring-field data set of soil moisture in different crop fields in the Wuchuan Agricultural Meteorology Observation Station for 1983-2009; (c) a dataset on crop water consumption with different fertilizer use rates in the Wuchuan field experiment station in Inner Mongolia of China; (d) monthly discharge data at the outlets of the Yellow, Haihe and Liaohe river basins for 1980-2012, note that we use the *Q* data at Tieling gauge station, which is close to the outlet, for the Liaohe river basin as there is frequent seawater backwash at the outlet; (e) meteorological observations at 307 weather stations across NC, which include monthly *T*, *P*, *u*, *RH* and *R*. We then use the methods in Andrews (2010) to derive *VPD* from *T* and *RH*. These meteorological observations are interpolated into 0.5°×0.5° spatially explicit regional meteorological data via IDW for regional analysis.

Historical records contain county level and province level agricultural activities statistical data for 1983-2010, which include the crop area and yield for each major crop,

total fertilizer use weight, and total crop area. Note that the sequence of administrative hierarchy in China is province, city, county, town and village.

Other ancillary data include satellite-based soil moisture, land-use/land-cover change (LUCC) and radiation products. Satellite retrieved CCI-WACMOS land surface soil moisture data that merges active and passive microwave observations and refers to a depth of 0.5-2cm (Dorigo et al. 2012) during 1983-2010 and GRACE terrestrial water storage data – the mean of three solutions CSR, GFZ and JPL ensemble (Landerer et al. 2012) during 2003-2013 are also used in this study to investigate the spatial variability of the trends in soil moisture and understand their magnitude within the global context. LUCC data of year 2010 derived from Landsat TM/ETM digital images (Liu et al. 2002) are used to calculate fraction coverage of cropland in each 0.25°×0.25° pixel of the CCI-WACMOS soil moisture product. Monthly average NASA/GEWEX Surface Radiation Budget (SRB) Release-3.0 data sets from 1984-2007 are used to calculate potential evaporation via the FAO-56 Penman-Monteith equation, and subsequently the PDSI.

2.2.3 Multiple linear regression model

Since the locations of the 40 stations where the soil moisture measurements are conducted are different from those of the weather stations, the meteorological data used for each site in the regression is interpolated from observations at the four nearest weather stations using the inverse distance weighting method (IDW, Shepard, 1968). Historical records of (chemical) fertilizer use rates at those 40 stations are not available. To cope with this site-level data scarcity we use county-average rates as in Muramatsu (2003). Data at these 40 stations is combined in one multiple regression model.

Volumetric soil moisture (θ_v) measurements are converted to relative soil moisture values (θ_r) – θ_v divided by measured field capacity – to avoid the effects of different soil texture among different stations, allowing averaging of soil moisture measurements from different stations.

In the regression for soil moisture changes, we consider the impacts of meteorological variables like air temperature (T, ^oC), precipitation (P, mm yr^{-1}), wind speed (u, m s^{-1}), relative humidity (RH), vapour pressure deficit (VPD, hPa) and radiation hours (R, hr), and agricultural activities like fertilizer use rate (F, kg/ha, calculated as total weight of fertilizer use divided by crop area) and crop types (c), as well as county effects representing differences in soil moisture level across different counties (C_m, the overall effects of county level environmental variables like topography, soil texture and microclimate). F is calculated as total weight of fertilizer use divided by crop area. We jointly consider nitrogen, phosphorus, and potassium fertilizers due to the unavailability of historical records of their separate use. These fertilizers we considered are active ingredients as nitrogen, phosphorus pentoxide, and potassium oxide, respectively. Based on multiple experiments on the crop water consumption that have been conducted in NC region by many Chinese scientists (e.g., Xie et al. 1996; Ren et al. 2004; Liu et al. 2010; Zhang et al. 2010; Feng et al. 2010; He et al. 2012), we categorize the main crop types in NC into 3 groups: 1) soybean and potato; 2) wheat; and 3) maize and rapeseed.

We use ANCOVA model (Kutner et al. 2005) to investigate the correlated effects between the dependent and explanatory variables, and the model can be summarized as:

$$Y_m = \beta_{m,0} + \beta_{m,1}X_1 + \cdots + \beta_{m,i}X_i + \sum_{j=2}^{3} \beta_{c,m,j} I(c = j) + C_m + \varepsilon_m \qquad (2.1)$$

where Y_m stands for the mean θ_r in growing season of each year during 1983-2010. $\beta_{m,0}$ is the intercept term, $C_m = \sum_{j=2}^{k} \beta_{C,m,j} I(County = j)$ represents the county effect, $X_1 \sim X_i$ (i.e., *T*, *P*, *RH*, *R*, *u, VPD* and *F*) represent the *ith* explanatory variable and $\beta_{m,1} \sim \beta_{m,i}$ are corresponding slopes, $I(\cdot)$ is the indicator function, and ε_m is a normally distributed error term. Since we have classified the crops into three groups, we use two parameters ($\beta_{c,m,2}$ for group 2 and $\beta_{c,m,3}$ for group 3) to represent the crop effect. The factor terms do not contain the first level in their expression since we choose the first level of both county effects and crop effects as baselines. Note that the choice of baseline does not affect the regression results.

We build three models for the three river basins – Yellow, Haihe and Liaohe river basins – to investigate the effects of meteorological and agricultural variables on *Q* decline. We use the *Q* data at the outlet of each river basin as a dependent variable. Explanatory variables involve meteorological variables (i.e., *T*, *P*, *RH*, *R*, *u* and *VPD*) and agricultural activities (i.e., *F*, crop area of each major crop type) that aggregated from all counties within each basin. A full model with all of the explanatory variables is represented as follows.

$$Y_d = \beta_{d,0} + \beta_{d,1} X_1 + \cdots + \beta_{d,i} X_i + \sum_{k=1}^{5} \beta_{d,k} A_k + \varepsilon_d \qquad (2.2)$$

where Y_d stands for growing season mean *Q* for each year during 1983-2012 ($km^3\ yr^{-1}$), $\beta_{d,0}$ is the intercept term, $X_1 \sim X_i$ (i.e., *T*, *P*, *RH*, *R*, *u, VPD* and *F*) represent the *ith* explanatory variable and $\beta_{d,1} \sim \beta_{d,i}$ are corresponding slopes, A_k stands for the planting

area of *kth* crop (i.e., wheat, maize, soybean, potato, rapeseed) and $\beta_{d,k}$ is corresponding slope, and ε_d is a normally distributed error term. Besides this full model, a few reduced models that assign some of the coefficients equal to zero are also investigated. This is important because of the possible impact of the Simpson paradox on parameter estimates as well as on the significance of effects (Simpson 1951).

2.2.4 Fertilizer use experiment

Water consumption experiment of potato was conducted at Wuchuan field experiment station (41.60 °N，111.27 °E) in Inner Mongolia of China from 2008 to 2010. This station is located in the middle of the north agro-pastoral transitional zone, and is considered as a good representative of semi-arid farming-pastoral transitional area. The experiment was designed as an increasing gradient of fertilizer use rate: N0P0, N1P1, N2P2, N3P3, and N4P4 (Table 2.1). Fertilizer was applied before planting in each plot. Each plot area was 6 × 10 m^2, row spacing was 50 cm, and the planting density was 6 m^{-2}. Soil moisture was measured 3-5 times per month using gravimetric technique, and the water consumption for the whole growing season was then calculated using the water balance method, and the runoff was neglected as the station is located in semi-arid dry-land agriculture region.

2.3 Results

2.3.1 Soil moisture and discharge assessment

Across the 40 agricultural meteorological stations in NC, we find that the average relative soil moisture (θ_r) during the growing season decreased significantly in the last

three decades (Fig. 2.1a) – here θ_r is defined as the volumetric soil moisture (θ_v) divided by the measured field capacity. We find a significant ($p<0.01$) θ_r trend of -0.38%, -0.43% and -0.70% per year in the top 0–10 cm, 10–20 cm, and 20–50 cm of soil, respectively. This analysis provides solid evidence of soil drying-out in the entire NC region.

Satellite observations of surface soil moisture (Dorigo et al. 2012) and total soil water storage (Landerer et al. 2012) agree on the presence of a hot-spot of soil moisture decline in NC (Fig. 2.1b,c) and provide us a more complete picture of soil moisture trend in NC. The trends in satellite surface soil moisture are generally in line with the ground measurements for the 0–10cm soil layer at the 40 stations (Fig. 2.1b, correlation coefficient between trend magnitudes $r = 0.75$). Disagreements in the magnitude of the trends might occur due to the scale-mismatch between the point measurements and the gridded satellite data, in conjunction with the fact that agriculture practices do not cover the entire area of each pixel (Fig. 2.1d); additionally, the satellite sensors can only detect the conditions in the top 0.5–2 cm soil layer, while the measurements have been taken as the mean soil moisture for the 0–10 cm of soil.

The growing season Q at the outlets of the Yellow river basin, Haihe river basin and Liaohe river basin unanimously show significant declining trends during 1983–2012 (Fig. 2.1e). The Yellow river basin presents the largest decline, which is consistent with the reports of a frequent dry out of the stream on its lower reach since 1972 (Chen et al., 2003). The reduced soil moisture available and the concurrent Q decline at the three basins highlights the prevalence of reduced water availability in the past three decades over NC.

An overall decline of PDSI (Fig. 2.1f) – a widely used metric to monitor meteorological drought – during the 1984–2007 period also indicates that the NC region has been experiencing higher temperatures (Fig. 2.1g) and receiving increasingly less rainfall (Fig. 2.1h). The most dramatic decline in PDSI occurs in the northeast part of Inner Mongolia, where the drying trend and warming trend are higher.

2.3.2 Impacts of agricultural intensification on soil moisture and discharge

We disentangle the effects of climate change from those of agricultural practices on the generation of drought in the region through multiple linear regression analysis. Results show that, shows that, among all the meteorological and agricultural explanatory variables considered (see Section 2.2.3), P, F and c are the most significant variables determining the soil moisture for the three soil layers. Here we take the 20–50 cm soil layer, which comprises a large portion of the root zone (Liu et al. 2008; Liu et al. 2009) and is directly affected by transpiration, to illustrate the correlated effects of declining soil moisture. The analysis yields slopes of 0.031 (% mm^{-1} yr), –0.13 (% kg^{-1} ha), –6.33 and –12.66, for P, F, crop group 2 (i.e., wheat) and group 3 (i.e., maize, rapeseed), respectively (see model (2.1) in Section 2.2.3). This model can explain 68% of variance in θ_r ($R^2 = 0.68$), suggesting that the model may be capturing the dynamics reasonably well. Regression results show the expected positive covariance between P and θ_r, as θ_r responds directly to P. However, the significant negative effects of F and c on θ_r may be less straightforward.

To further explore this negative correlation, we examine the data gathered at a field experiment station in Wuchuan, where in a fertilizer use experiment soil moisture

was monitored during 2008-2010. Results show a clear raise in field water consumption as the input of fertilizer increases, by 10%–37.2% depending on the specific fertilizer treatment (Table 2.1–2.2, Fig. 2.2a), resulting in a significant decrease in soil moisture. Therefore, the increase in fertilizer use in the past three decades across NC (Fig. 2.2b) is likely to have aggravated the soil desiccation in the region.

Cultivation of different crop types also shows significant effects on θ_r dynamics. Taking the crop group 1 (i.e., soybean and potato) as baseline, the regression results indicate that group 2, and specially group 3, have negative effects due to their higher water consumption, which is consistent with previous field experiments conducted in NC (Xie et al. 1996; Ren et al. 2004; Liu et al. 2010; Zhang et al. 2010; Feng et al. 2010; He et al. 2012). Those experiments indicate that crop water consumption during the growing season follows the order: group 1 (326-452 mm) < group 2 (450-500 mm) < group 3 (398-568 mm). These results suggest that the increase of fertilizer use (Fig. 2.2b) and the expansion of croplands (Fig. 2.3c) in NC, with a disproportionate proliferation of high water-consuming crops (Fig. 2.3a), all have contributed significantly to the widespread soil moisture decline in the region.

A pair-wise experiment conducted at the Wuchuan Agricultural Meteorology Observation Station further supports the hypothesis that agricultural activities have accelerated soil moisture decline. During several decades (1983–2009), soil moisture has been monitored at two contiguous sites: a pristine pasture and an agricultural site. Measurements reveal a significant (p<0.05) decreasing trend of soil moisture in the first 50 cm of soil for the cropland (for all crop types), contrasting with the slightly increasing – but statistically significant (p<0.05) – trend observed in the pristine pasture (Fig. 2.4).In

potato, naked oats and spring wheat fields, θ_v decreased by 0.11%, 0.11% and 0.06% per year (respectively), while in the pristine natural pasture, where changes only reflect climate effects (the effects of soil development is neglected), there was an increase of 0.03% per year. Since there are no significant differences in soil texture, topography and microclimate between the cropland and pasture sites, differences in θ_v are here attributed to the agricultural activities.

Discharge dynamics was also assessed for the three study basins based on multiple linear regression models. Regression results for the three basins are consistent, in the following we focus on the Yellow river basin, due to its larger coverage and dense population. Our regression model for the Yellow river (see model (2.2) in Section 2.2.3) explains 82% of the long-term variance in discharge ($R^2 = 0.82$). Results indicate that P has a significant positive effect on Q (slope of 0.12 $km^3\ mm^{-1}$), whereas F and A_w (crop area of wheat) have significant negative effects (($-0.29\ km^3\ yr^{-1}\ kg^{-1}$ ha and $-0.06\ km^3\ yr^{-1}\ 10^{-3}\ ha^{-1}$, respectively). The crop area of maize (A_{mz}) is not considered to have significant effects on Q ($p \approx 1$) despite the high correlation between A_{mz} and Q ($r = -0.76$, $p<10^{-5}$). This occurs due to the so-called "Simpson Paradox" (Simpson 1951), in which two strongly dependent variables like F and A_{mz} ($r = 0.92$) cannot co-exist in the model. Replacing A_w with A_{mz} in the model, we find A_{mz} also have significant negative effects on Q ($p < 0.001$). Overall, the effects of P, F, plantation of maize and wheat on Q are consistent with those on θ_r.

2.4 Discussion

Food sufficiency has been achieved after nearly 50 years' efforts in China (Ju et al. 2009), and agriculture has intensified greatly since the early 1980s, with large inputs of chemical fertilizers and implementation of farming techniques (Guo, et al., 2010). Meanwhile, the amount of fertilizer use in China accounts for 31.4% of global total consumption in 2008 (Xin et al, 2012), and the fertilizer use rate is more than twice the world average (World Bank, 2006) and far greater than crop demand (Ju et al. 2009; Huang et al. 2010). Conversely, the efficiency of fertilizer use in China is much lower than world average (Raun and Johnson, 1999). While the yield per hectare for all crops has increased from 1.21 t/ha to 4.83 t/ha, the yield per unit chemical fertilizer use decreased dramatically for the 3 main crops in China during 1961-1998: 164 to 10 for rice, 44 to 6 for wheat and 93 to 9 for maize (Tong et al., 2003).

Though the impacts of excessive fertilizer use on agriculture and environment in China have been investigated in recent years (e.g., Ju et al. 2009; Kahrl et al. 2010a,b), little attention has been paid on the impacts of fertilizer overuse on hydrological cycling. Excessive fertilizer use increases water consumption (Fig 2.4a), while having little effect on crop yield (Ju et al. 2009). Previous studies also indicate that fertilizer use boost crop growth and transpiration (Gaiser et al. 2004; Huang et al. 2003), which in turn will deplete soil moisture and lead to a decline in runoff. In addition, the use of chemical fertilizers is usually accompanied by an increase in irrigation that may further deplete water resources. Our results reveal the propelling feedback of fertilizer overuse on both soil moisture and discharge decline, suggesting that over-fertilization may lead to drought

exacerbation, as well as environment deterioration and economic loss of unnecessary expenditure on fertilizer.

Crop area has been increasing in recent years (Fig. 2.3c), despite the decline from 2001–2003 that is likely the result of a government program aimed to convert degraded farmland into forest and grassland (Feng et al. 2005).The yield per unit area for each of the main crops (wheat, maize, soybean, potato and rapeseed) presents increasing trends in the last 3 decades (Fig. 2.3b), which is an integrated effect of multiple factors such as increase of fertilizer use, improvement in crop varieties, enhancement in farming practices and increase of irrigation. The coefficient of determination (R^2) between soil moisture and crop yield at the 40 stations varies from 0.53–0.85, suggesting that the increase of crop yield per unit area has resulted in an increased depletion of soil moisture.

Some other factors such as reservoir regulations, water withdraw, groundwater pumping, which have not been considered in this study, are likely to contribute as well to intensification of droughts. For example, twelve dams were built during 1950s–1990s, and there are 3147 reservoirs, 29200 pump sites and 875000 wells in the Yellow river basin (Fu et al., 2004). These facilities have certainly altered the regional distribution of water, although no available records may allow us to scrutinize their impacts on current drought conditions.

Another important human intervention that has not been yet discussed is irrigation. Irrigation has been locally used to counteract agricultural drought, reducing the soil moisture decline but still contributing to a decline in runoff, as most of the water for irrigation is withdrawn from river system (Zhu et al., 2013). While irrigation area has dramatically expanded in recent decades in NC (Fu et al. 2004; Chen et al. 2003), the

limited historical records of irrigation practices do not allow a thorough investigation of their contribution to regional droughts. Remote sensing may have the potential to monitor the irrigation practices and support the investigation in the future.

2.5 Conclusions

Trends of soil moisture and discharge in Northern China have been examined with long-term *in-situ* observations, and correlated relationship between these trends and agricultural activities have been investigated using multiple linear regression model. We unequivocally corroborate the soil drying and discharge declining trend in Northern China with ground truth observation datasets. Apart from the effects of climate changes, current agricultural activities aggravated this trend. Increased fertilizer use, widespread cultivation of water-expensive crops, and cropland expansion contribute to the decline in soil moisture and discharge in this region. Existing agricultural activities tend to accelerate soil moisture and discharge decline and decrease ecosystem resilience under the warming climate. Alternative agricultural practices that without detriment to future water resources and can meet the immediate demand seem critical for the region.

2.5 Acknowledgements

This research is supported by the National Natural Science Foundation of China (Grant Nos. 41371232 and 41271110), the National Basic Research Program of China (No. 2012CB956204), the National Science and Technology Support Program (No. 2012BAD09B02), the NASA Land Use and Land Cover Change program (NASA-NNX09AI26G, NN-H-04-Z-YS-005-N, and NNX09AM55G), the Department of Energy (DE-FG02-08ER64599), the National Science Foundation (NSF-1028291 and NSF-0919331, NSF-CAREER), the NSF Carbon and Water in the Earth Program (NSF-0630319). We acknowledge Chinese Meteorological Administration, Ministry of Water Resources of China and National Bureau of Statistics of China for provision of data used in this study.

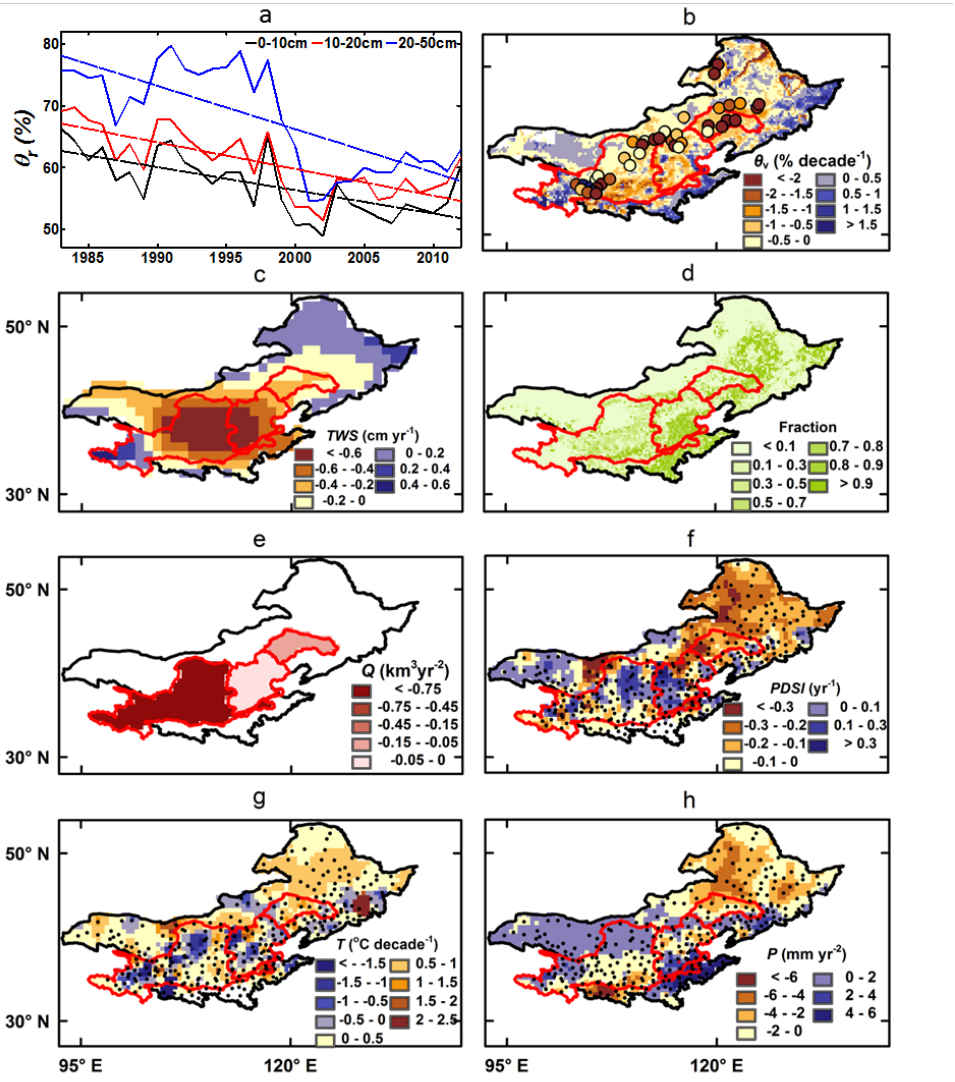

Figure 2.1 Growing season drought trends in Northern China (NC): a) Average relative soil moisture (θ_r) trends in 0–10 cm, 10–20 cm and 20–50 cm soil across the 40 agricultural meteorological stations during 1983–2012. b) Volumetric soil moisture (θ_v) trend during 1983–2010 across NC and at the 40 stations (circles on the map) during 1983–2012. The former is derived from CCI-WACMOS soil moisture product[9] and the latter is from *in-situ* measurements of the top 0–10cm soil. The red polygons delineate the boundaries of the Yellow, Haihe and Liaohe river basins from west to east, respectively. c) Terrestrial water storage (TWS) trend during 2003–2013. d) Fraction coverage of cropland in 2010. e) Discharge (Q) trends in the three basins during 1980–2012. f-h) *PDSI*, air temperature (T) and Precipitation (P) trend during 1984–2007. The black dots in g-h) represent the locations of 307 weather stations.

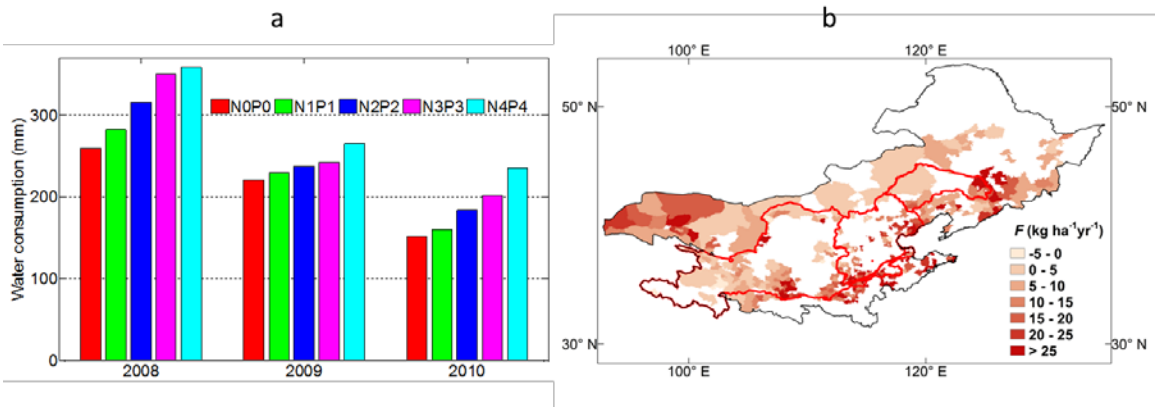

Figure 2.2 Fertilizer use experiment and fertilizer use trend in Northern China: a) fertilizer use experiment between 2008–2010 in Wuchuan Field Experiment Station, where N0P0–N4P4 stand for an increasing fertilizer use gradient that correspond to Table S1; and b) fertilizer use (*F*) trend during 1983–2006 across the region. Note that area without fertilizer use data is left vacant.

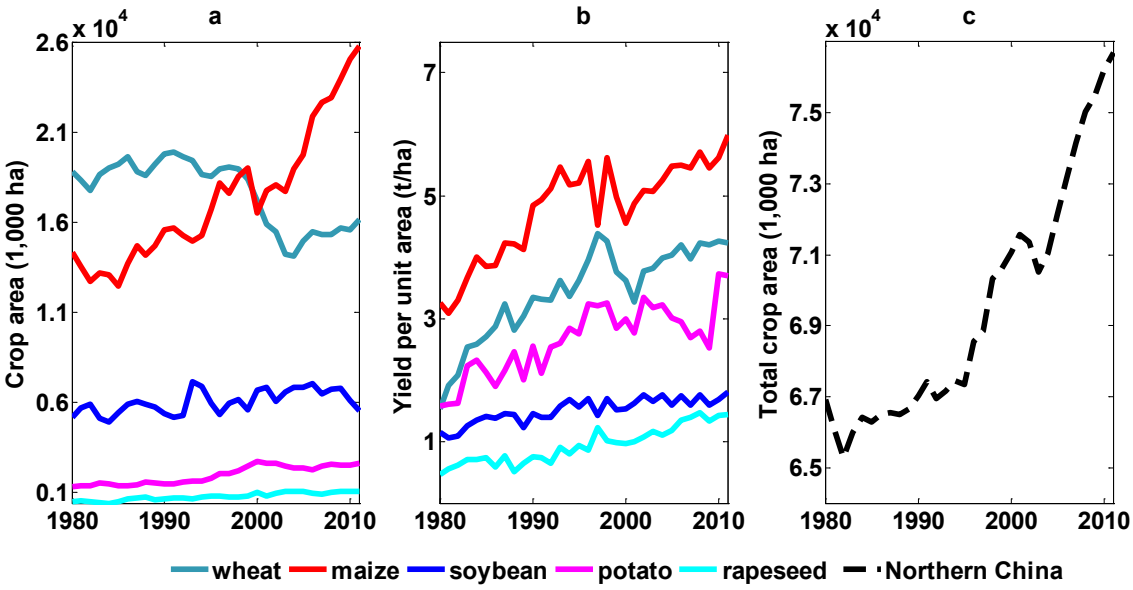

Figure 2.3 Changes of crop area and yield per unit area in Northern China during 1980–2011: a) planting area for each major crop; b) yield per unit area for each major crop; and c) total crop area in the region.

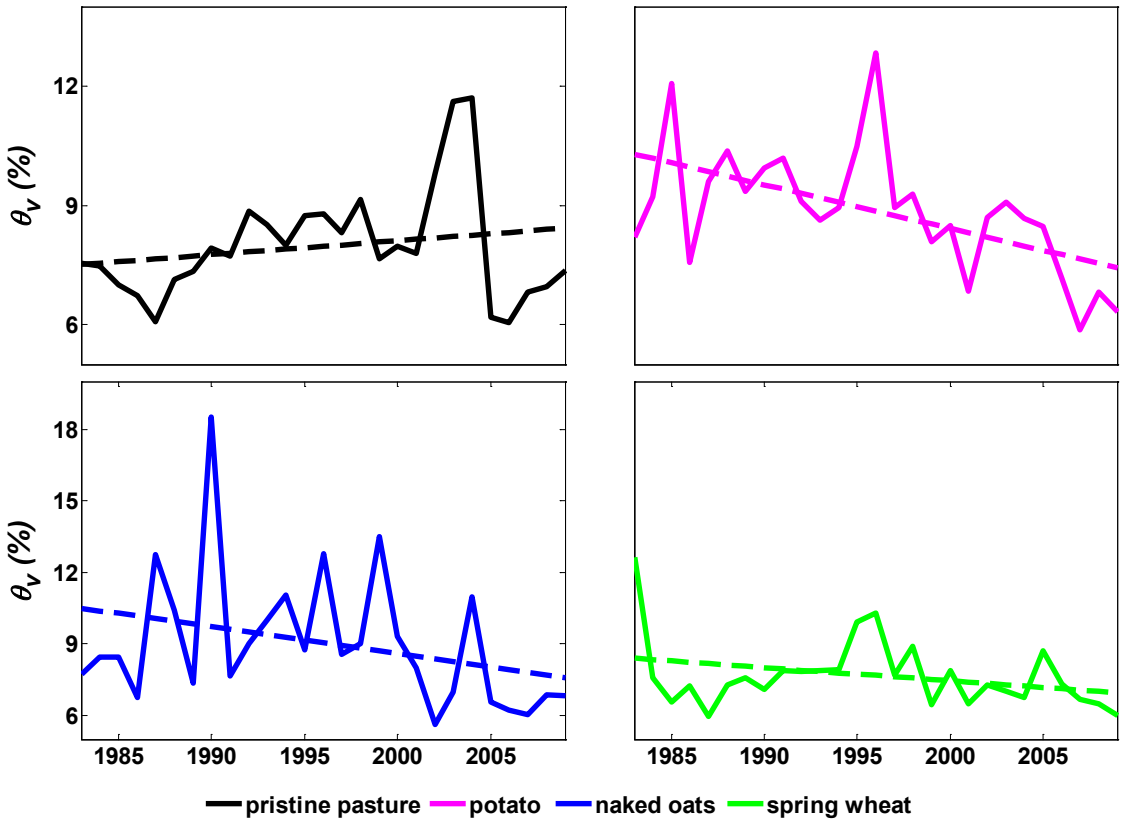

Figure 2.6 Variation of volumetric soil moisture (θ_v) in topsoil (0–50 cm) of pristine pasture and different crop fields in Wuchuan Agricultural Meteorology Observation Station during 1983–2009.

Table 2.1 Fertilizer use experimental design

number	treatment	Pure fertilizing amount (kg/ hm^2)		Actual fertilizer amount (kg hm^{-2})	
		N	P_2O_5	Urea	Triple superphosphate
1	N_0P_0	0	0	0	0
2	N_1P_1	45	45	97.5	97.5
3	N_2P_2	90	90	195	195
4	N_3P_3	135	135	294	294
5	N_4P_4	180	180	391.5	391.5

Table 2.2 Changes of water consumption with different fertilization use rate in potato plot of Wuchuan Field Experiment Station. Water consumption values followed by the same lowercase letters for each year are not significantly different at $p < 0.05$.

	Treatment	**Water consumption（mm）**		
		2008	2009	2010
Fertilization	N_0P_0	260.3a	221.5a	152.0a
	N_1P_1	282.6b	230.3ab	160.2a
	N_2P_2	316.3c	237.5bc	184.2b
	N_3P_3	350.5d	242.3c	202.1c
	N_4P_4	359.3d	265.7d	235.3d

CHAPTER 3. RESPONSE OF EVAPOTRANSPIRATION AND WATER AVAILABILITY TO CHANGING CLIMATE AND LAND COVER ON THE MONGOLIAN PLATEAU DURING THE 21ST CENTURY[2]

3.1 Abstract

Adequate quantification of evapotranspiration (*ET*) is crucial to assess how climate change and land cover change (LCC) interact with the hydrological cycle of terrestrial ecosystems. The Mongolian Plateau plays a unique role in the global climate system due to its ecological vulnerability, high sensitivity to climate change and disturbances, and limited water resources. Here, we used a version of the Terrestrial Ecosystem Model that has been modified to use Penman-Monteith (PM) based algorithms to calculate *ET*. Comparison of site-level *ET* estimates from the modified model with *ET* measured at eddy covariance (EC) sites showed better agreement than *ET* estimates from the MODIS *ET* product, which overestimates *ET* during the winter months. The modified model was then used to simulate *ET* during the 21st century under six climate change scenarios by excluding/including climate-induced LCC. We found that regional annual *ET* varies from 188 to 286 mm yr^{-1} across all scenarios, and that it increases between 0.11 mm yr^{-2} and 0.55 mm yr^{-2} during the 21st century. A spatial gradient of *ET* that increases from the southwest to the northeast is consistent in all scenarios. Regional *ET* in grasslands, boreal forests and semi-desert/deserts ranges from 242 to 374 mm yr^{-1}, 213 to 278 mm yr^{-1} and 100 to 199 mm yr^{-1}, respectively; and the degree of the *ET* increase follows the order of

[2] Liu, Y., Zhuang, Q., Chen, M., Tchebakova, N., Pan, Z., Sokolov, A., Kicklighter, D., Melillo, J., Zhou, G., He., Y., Chen, J., Bowling, L., Miralles, D., Parfenov, E. (2013) Response of evapotranspiration and water availability to changing climate and land cover on the Mongolian Plateau during the 21st century. Global Planet Change,108: 85-99

grassland, semi-desert/desert, and boreal forest. Across the plateau, climate-induced LCC does not lead to a substantial change (<5%) in *ET* relative to a static land cover, suggesting that climate change is more important than LCC in determining regional *ET*. Furthermore, the differences between precipitation and *ET* suggest that the available water for human use (water availability) on the plateau will not change significantly during 21st century. However, more water is available and less area is threatened by water shortage in the Business-As-Usual emissions scenarios relative to level-one stabilization emissions scenarios.

3.2 Introduction

ET is an essential component of the hydrologic cycle, and is central to earth system science because it governs interactions (e.g., energy exchange and biogeochemical cycling) between the atmosphere and terrestrial ecosystems (Betts, 1996; Mu et al., 2007, 2011; Weiß et al., 2008; Dolman and De Jeu, 2010; Wang et al., 2010, 2012; Sun et al., 2011a, 2011b; Katul et al., 2012). *ET* returns more than 60% of annual land precipitation back to the atmosphere (Shiklomanov and Sokolov, 1985; L'vovich and White, 1990; Oki and Kanae, 2006; Miralles et al., 2011a), and thereby constrains water availability over the continents. Future trends of *ET* may lead to an overall intensification or weakening of the water cycle, with implications for the recycling of precipitation and generation of runoff (Shukla et al., 1990; Lean et al., 1995). With a growing scientific consensus about global warming (Hansen et al., 2005; Barnett et al., 2005; IPCC, 2007), there is an increasing concern about how climatic change will impact the water supply, especially in arid and semi-arid regions (Peterson et al., 2002, 2006; Vorosmarty et al., 2000; Serreze and Barry, 2005; IPCC, 2007; Bates et al., 2008). These

issues are directly relevant to human society and play an important role in the policy-making process related to water management.

Quantitative predictions of regional water balances, management of water resources, irrigation scheduling, or climate and weather prediction, all require the accurate quantification of ET. (Valiantzas, 2006; Cleugh et al., 2007; Jiang et al., 2009; Wang et al., 2010, 2012; Mu et al., 2011). Simulations from models which have been calibrated and parameterized with measured data (e.g., measurements at EC towers), and satellite-based estimates can then be used for continuous predictions over time and space(Jung et al., 2010; Xiao et al., 2012).

The Mongolian Plateau offers an interesting opportunity to study the state-of-the-art ET dynamics. It is located in a farming-pastoral ecotone adjoining the Gobi desert in the south and the Altai-Sayan Mountains in the north, and is dominated by arid and semi-arid climate (He et al., 2009; Lu et al., 2009; Liu et al., 2011). The plateau covers vast arid and semi-arid area, and is expected to experience earlier and more drastic climate changes (e.g., surface air temperature) compared with lower latitude regions (IPCC, 2001; Zhuang, 2004; Lu et al., 2009). Additionally, the high vulnerability of the ecosystem makes it especially sensitive to climate change and disturbances (Sun, 2002; Sankey et al., 2006; Dulamsuren et al., 2009; Lu et al., 2009; Chen, 2012;). The plateau is therefore considered to play a critical role in the global climate system (Galloway and Melillo, 1998; Li et al., 2008; Lu et al., 2009). As in other arid and semi-arid regions – where water loss from ET can account for > 95% of the annual precipitation (Kurc et al., 2004; Huxman et al., 2005; Lu et al., 2011; Wang et al., 2011; Sun et al., 2011b; Katul et al., 2012) – ET is crucial in controlling the hydrology, climate and ecology in the plateau. As

the climate and land cover of the plateau have been projected to change during the 21st century (Lu et al., 2009; Tchebakova et al., 2009; Groisman et al., 2010), the regional ET could change significantly.

Investigation of future trends in *ET* under changing climate and climate-induced LCC on the plateau can provide insights into how climate policies might influence future water supplies, and contribute to the understanding of future hydrological, ecological and societal changes in this region and their feedbacks to the global climate system. To date, there is a lack of studies on the quantification of *ET* and water availability under changing climate and land cover on the Mongolian Plateau. This study is a pioneer effort toward filling that knowledge gap. The first objective of this study is to improve the *ET* algorithms of a process-based biogeochemistry model – the Terrestrial Ecosystem Model (TEM; Zhuang et al., 2003, 2010). Then, we aim to validate and apply the improved model to examine how *ET* will respond to the changes of climate and land cover over the plateau during the 21st century. The implications of the results for the water availability in the region will be discussed in detail.

3.3 Methods

The Terrestrial Ecosystem Model (TEM) is a process-based biogeochemistry model using spatially referenced data of climate, soils, land cover, and elevation to simulate C, N, and water fluxes and pool sizes of the terrestrial biosphere (e.g., Raich et al., 1991; McGuire, 1992; Zhuang et al., 2001, 2002, 2003, 2004). In this study, we modified TEM version 5.0 (Zhuang et al. 2003, 2010) to incorporate algorithms based on the Penman-Monteith (PM) equation (Monteith, 1965; Allen et al., 1998) to estimate ET.

These modifications allowed better consideration of interactions between terrestrial energy and water budgets when estimating *ET* with TEM. To evaluate these model improvements, site-level *ET* estimates of the TEM, with and without modifications of the *ET* algorithms, were compared against *ET* measurements from two eddy covariance sites on the Mongolian Plateau. In addition, regional *ET* estimates by TEM, with and without modifications of the *ET* algorithms, were compared to the regional estimates from three recent studies (Miralles et al. 2011a,b; Mu et al., 2011; Vinukollu et al. 2011). The modified TEM was then used with six climate change scenarios and two land cover scenarios to examine how *ET* might respond to changes of climate and land cover over the plateau during the 21st century.

3.3.1 Modeling algorithms

In the previous version of monthly time-step TEM (Zhuang et al., 2003, 2010), the *ET* algorithms (hereafter referred to as AL1) are based on both the atmospheric demand for water vapor and the ability of the land surface to supply such water vapor (Vörösmarty et al., 1998). In the previous TEM, the atmospheric demand for water vapor is determined from potential evapotranspiration (PET, mm mon^{-1}), which is estimated via the Jensen-Haise (1963) formulation:

$$PET = [(0.014 \times (1.8 \times T + 32) - 0.37)] \times R_s \times 0.016742 \times MD \qquad (3.1)$$

where T is the monthly average air temperature (°C), R_s is the mean monthly short-wave radiation at the top of the canopy (Cal cm^{-2} d^{-1}) calculated in TEM using latitude, date and cloudiness (Pan et al., 1996), and MD is the number of days per month. This PET algorithm does not consider the effects of net outgoing long-wave radiation from the land

surface, ground heat flux, and the aerodynamic aspects of *ET* on the atmospheric demand for water vapor. PET calculated in Eq. (3.1) tends to be underestimated in the spring and overestimated in the summer, as the sensitivity of PET to T is larger, and the sensitivity to R_s is lower than in nature (Feddes et al., 1994). Biases in the calculation of PET will then be propagated to the *ET* estimates.

ET is then derived from PET in conjunction with a water balance model (WBM), where the ability of the land surface to supply water for *ET* depends on the amount of soil moisture (SM), rainfall and snowmelt (Vörösmarty et al., 1998). In the WBM, direct surface runoff is not separated from total runoff from a grid cell, which is assumed to go through soils and contribute to neighboring stream networks. If the sum of monthly rainfall and snowmelt is greater or equal to monthly PET, then *ET* is assumed to equal PET. If SM reaches field capacity under these conditions, then any additional water is assumed to be runoff to neighboring river networks. If the sum of monthly rainfall and snowmelt is less than monthly PET, then no runoff is assumed to occur and *ET* is calculated by subtracting the change in SM during the month from the sum of monthly rainfall and snowmelt. A unitless soil drying function is used to determine the change in SM within a month based on relative soil wetness, PET, rainfall and snowmelt.

To improve *ET* estimates within the monthly time-step TEM, we introduced new *ET* algorithms (hereafter referred to as AL2), based on the PM algorithm as applied by Mu et al (2007, 2011) that explicitly incorporates both physiological and aerodynamic constraints (Monteith, 1965; Allen et al., 1998). In these new AL2 algorithms, we calculated *ET* (mm mon^{-1}) by estimating transpiration of the vegetation canopy (T_c, mm mon^{-1}) separately from evaporation from the soil surface (E_{soil}, mm mon^{-1}):

$$ET = T_c + E_{soil} \quad (3.2a)$$

$$T_c = \frac{sA_c + \rho c_p (VPD)/r_a}{\lambda(s + \gamma(1 + r_s/r_a))} \times secs2day \times MD \quad (3.2b)$$

$$E_{soil\_pot} = \frac{sA_{soil} + \rho c_p (VPD)/r_{as}}{\lambda(s + \gamma(1 + r_{tot}/r_{as}))} \times secs2day \times MD \quad (3.2c)$$

$$E_{soil} = E_{soil\_pot} \times f_{SM} \quad (3.2d)$$

$$f_{SM} = RH^{VPD/\beta} \quad (3.2e)$$

where A_c (W m^{-2}) is the available energy in the vegetation canopy, A_{soil} (W m^{-2}) is the available energy in the soil, s is the slope of the saturation vapor pressure curve (Pa K^{-1}) and is a function of air temperature, ρ (kg m^{-3}) is the air density, c_p (J kg^{-1} K^{-1}) is the specific heat capacity of air, VPD (Pa) is the vapor pressure deficit (i.e., saturated air vapor pressure minus actual air vapor pressure), r_a (s m^{-1}) is the aerodynamic resistance, r_s (s m^{-1}) is the surface resistance to transpiration from the plant canopy, r_{as} is the aerodynamic resistance at the soil surface, r_{tot} is the sum of r_{as} and surface resistance to evaporation, λ (J kg^{-1}) is the latent heat of vaporization, ρ (kg m^{-3}) is the air density, γ (Pa K^{-1}) is the psychometric constant, secs2day (secs day^{-1}) is the number of seconds in a day, E_{soil_pot} is the potential evaporation from soils, f_{SM} is a proxy of soil water deficit used to constrain soil evaporation, RH is relative humidity, and β is the relative sensitivity of RH to VPD (Fisher et al., 2008).

As described by Mu et al. (2011), the available energy in the vegetation canopy (A_c) to support transpiration is determined by multiplying the net radiation flux at the surface (R_n, W m^{-2}) by the fraction of ground covered by vegetation (F_c), whereas the available energy in the soil depends on R_n multiplied by the fraction of ground not

covered by vegetation ($1 - F_c$) minus the sensible heat exchange from the surface into the soil (G, W m^{-2}). R_n is the balance of incoming and outgoing shortwave and longwave radiation and is calculated from the incoming shortwave radiation (R_s), albedo, and air temperature as described by Cleugh et al. (2007). Mean monthly values for albedo and air temperature are used when calculating R_n.

Based on the protocols of Mu et al. (2007), and the relationships among the Fraction of Absorbed Photosynthetically Active Radiation (FPAR), leaf area index (LAI) and enhanced vegetation index (Turner et al., 2003; Heinsch et al., 2006; Hu et al., 2007; Chen et al., 2009), F_c is calculated as:

$$F_c = \frac{\exp(-LAI_{\min} \times k) - \exp(-LAI \times k)}{\exp(-LAI_{\min} \times k) - \exp(-LAI_{\max} \times k)} \quad (3.3)$$

where LAI_{min} and LAI_{max} are the minimum and maximum LAI in a year, respectively, and k is the canopy light extinction coefficient and assumed to be 0.5 (Running and Coughlan, 1988). Monthly LAI is estimated by TEM as follows:

$$LAI = SLA \times ALLEAF \times LEAF \quad (3.4)$$

where SLA is the specific leaf area (m^2 g C^{-1}) (Pierce et al., 1994; Garnier et al., 1997; Poorter and Evans, 1998; White et al., 2000; Milner et al., 2003), ALLEAF is the maximum leaf biomass (g C m^{-2}), and LEAF is a phenology term that represents the relative amount of leaf biomass in a specific month to ALLEAF and is estimated by TEM (Zhuang et al., 2002).

G is estimated based on monthly air temperature (Allen et al., 1998):

$$G = 1.6198(T_i - T_{i-1}) \quad (3.5)$$

where T_i is the mean air temperature of month i (°C) and T_{i-1} is that of the previous month (°C).

Soil evaporation is calculated from potential soil evaporation (E_{soil_pot}) and is constrained by a proxy of soil water deficit f_{SM}. The estimate of f_{SM} is based on the complementary relationship of land-atmosphere interactions from VPD and RH, where it is assumed that SM has a strong link with the adjacent atmospheric moisture (Bouchet, 1963; Mu et al., 2007; Fisher et al., 2008).

The detailed methods for calculating the r_s and r_a of plant transpiration, the r_{tot} and r_{as} of soil surface evaporation are documented in Mu et al. (2007, 2011). r_s in Eq. (3.2b), is calculated from canopy conductance C_c (the inverse of r_s), which is based on the mean potential stomatal conductance per unit leaf area (C_L), LAI, VPD, and air temperature (Mu et al., 2007). The effects of environmental factors such as VPD and air temperature on the stomatal resistance (converted to r_s using 1/LAI as a scalar), r_{tot} and r_{as} have been taken into account in this study, and the effects of air temperature on r_a have also been considered. In addition, although the effects of SM on r_{tot} and stomatal resistance have not been directly incorporated in their calculation, f_{SM} has been applied as a SM constraint on soil evaporation, and further control is represented as *ET* estimates are constrained by the soil water balance in TEM. Some other *ET* methodologies like the one by Miralles et al. (2011a, 2011b) explicitly use SM and vegetation water content observations to estimate evaporative stress. Additionally, many previous studies consider other environmental factors for calculating resistances than those considered in this study, such as net radiation, photosynthetically active radiation flux (PAR), ambient CO_2 concentrations and wind (Jarvis, 1976; Sellers et al., 1986; Ball et al., 1987; Dolman et al.,

1991; Xu, 1994; Wright et al., 1995; ASCE, 1996; Dickinson et al., 1998; Mueller, 2011). While consideration of these factors allows the calculation of resistance to capture more detailed effects of biophysical properties on ET, but provide limited benefits to our simulations at the monthly time step and also introduce additional uncertainties. Given that r_a and r_{as} are very sensitive to wind speed variation (ASCE, 1996; Liu et al., 2006; Zhang et al., 2007; Bonan, 2008), an averaged monthly wind will smooth most of the "noise" and short-term variation so that it is likely to fail to capture the effects of wind on r_a and r_{as}. Moreover, the current unavailability of wind speed data in the Integrated Global System Model (ISGM) climate scenarios data (driving data of this study) makes it unfeasible to incorporate wind into the parameterizations of r_a and r_{as}. Similarly, the diurnal cycle of stomatal resistance responds to the diurnal variability of R_n and PAR (Landsberg et al., 1997), but most of this response would be lost using averaged monthly aggregates.

Finally, after calculating *ET* with the new AL2 algorithms, the *ET* estimates were then constrained by the available water in soils as determined by water balance in TEM. Thus, *ET* estimated using either the AL1 or AL2 algorithms (hereafter referred to as AL1-ET and AL2-ET, respectively) is constrained by the soil water balance, but the AL2 now consider more aspects of the concurrent energy balance and more effects of environmental and biophysical factors on *ET* than the AL1 of the previous TEM.

3.3.2 Model parameterization

As described above, here we modified TEM version 5.0 (Zhuang et al. 2003, 2010) by adapting algorithms developed by Mu et al. (2007, 2011) based on the PM equation

(Monteith, 1965; Allen et al., 1998) for estimating *ET* by TEM. Many parameters involved in the new AL2 algorithms were defined from literature values (e.g., Running and Coughlan, 1988; Shuttleworth, 1992; ASCE, 1996; Milner et al., 2003; Cleugh et al., 2007; Mu et al., 2007, 2011), while other parameters such as the relative sensitivity of RH to VPD (β), specific leaf area (SLA), and mean potential stomatal conductance per unit leaf area (C_L) for grasslands and boreal forests were adjusted within the referenced range until model values were closest to field-based measured *ET*. The major parameters that were introduced into or adjusted in this study are listed in Table 3.1.

For albedo, we used MODIS albedo (MCD43C3) of year 2005 for the region to determine the mean monthly albedo of each land cover type (Schaaf et al., 2002; Jin, 2003a; Jin, 2003b; Salomon et al., 2006), which was assumed to remain unchanged during 1971-2100 due to unavailability of time series albedo data. Then the monthly albedo of each land cover was used as land cover-specific parameters to estimate monthly R_n.

3.3.3 Data

Overall, TEM needs input data on air temperature, precipitation, cloudiness, vapor pressure, atmospheric CO_2 concentrations, land cover type, albedo, elevation, and soil texture to estimate ET. As indicated earlier, TEM can use cloudiness data to estimate incoming shortwave radiation. Soil texture and elevation vary spatially over the study regions and are assumed to remain static throughout 1971-2100, whereas other inputs vary over time and space. In this study, we conducted our simulations at a spatial

resolution of 0.5° latitude × 0.5° longitude resolution so that all spatially-explicit input data sets were reorganized to this resolution.

3.3.3.1 Historical data

Data on soil texture, elevation, and historical climate and atmospheric CO2 concentrations from 1971 to 2000 were collected from several sources. The soil texture data were from the Food and Agriculture Organization/Civil Service Reform Committee (FAO/CSRC) digitization of the FAO-UNESCO (1971) soil map (Zobler, 1986). Elevation data were from the Shuttle Radar Topography Mission (Farr et al., 2007). Gridded historical data on monthly air temperature, precipitation, cloudiness, and vapor pressure were obtained from the Climate Research Unit (CRU) of the University of East Anglia. Annual global atmospheric CO2 concentration data for the historical period were acquired from atmospheric observations (Keeling et al., 2005).

3.3.3.2 Future scenarios data

Modeling estimates of changes in air temperature, precipitation, cloudiness, vapor pressure, and atmospheric CO_2 concentrations associated with six climate scenarios (X901M, X902L, X903H, X904M, X905L, and X906H; Sokolov et al., 2005; Zhu et al., 2011; Jiang et al., 2012) generated by the IGSM of the Massachusetts Institute of Technology (MIT) (Sokolov et al., 2005) were used for future projections over the 21st century. The X901M, X902L, and X903H scenarios represent Business-As-Usual (BAU) emissions scenarios with a median climate response, a low climate response, and a high climate response, respectively. The X904M, X905L, and X906H scenarios represent level-one stabilization emissions (450 ppm CO_2) scenarios with a median climate

response, a low climate response, and a high climate response, respectively. The largest increases in air temperature and precipitation occur in the X903H scenario and the smallest increases occur in the X905L scenario on the plateau (Fig. 3.1).

Each of the six climate scenarios were used to drive a biogeography model, Siberian BioClimatic Model (SiBCliM, Tchebakova et al., 2009, 2011), to simulate land cover distribution for the years 2000, 2025, 2050, 2075 and 2100. Other than climate change, the SiBCliM simulations did not consider the influence of any anthropogenic activities on land cover distribution. Land cover simulations of 2000 are used to represent a static land cover throughout 1971-2100 (referred to as VEG1). To examine the effects of climate-induced LCC, the simulated land cover were used to develop a time series of annual land cover over five time periods from 2001 to 2100. The SiBCliM results for 2000, 2025, 2050, 2075 and 2100 were used to describe land cover during 2000-2024, 2025-2049, 2050-2074, 2075-2099, and 2100, respectively (referred to as VEG2). The annual land cover distribution in VEG2 is assumed to remain unchanged from year to year throughout each period but varies among the five periods (Fig. 3.2).

3.3.3.3 Data for model evaluation

Data were obtained to evaluate the performance of the modifications to TEM at both the site and regional levels. In addition to latent heat fluxes, EC data of air temperature, precipitation, RH, and incoming shortwave radiation were collected from two Mongolian sites (http://www.asianflux.com) to allow the development of site level *ET* estimates by TEM: a larch forest site at Southern Khentei Taiga (SKT) and a grassland site at Kherlenbayan Ulaan (KBU). The half-hourly data at SKT and KBU are

available from 2003 to 2006, and 2003 to 2009, respectively. An Artificial Neural Network method (Papale, 2003) was used to fill any gaps in the data caused by system failure or data rejection. We then averaged half-hourly air temperature, RH, latent heat flux, and solar radiation, and summed the half-hourly precipitation to get monthly values.

Monthly *ET* estimates from MODIS (referred to as MODIS-ET, Mu et al. 2011) and from GLEAM (Global Land-surface Evaporation: the Amsterdam Methodology – Miralles et al. 2011a, b) were also collected and compared to site-level *ET* estimates by TEM. Although AL2-ET and MODIS-ET estimates are both based on PM framework, they are different in LAI acquisition, calculation of F_c and G, parameterization of C_L, β and SLA, forcing data, and whether is constrained by available soil water.

For evaluation of spatial and temporal patterns of *ET* estimated by TEM across the plateau, AL2-ET results were also compared to gridded estimates selected out of global results by Vinukollu et al. (2011) in addition to MODIS-ET and GLEAM for the time period 2000 to 2008. Vinukollu et al. (2011) also used a PM based approach extended by Mu et al. (2007) to estimate *ET* (known as PM-Mu *ET*) whereas GLEAM is based on a Priestley-Taylor approach with an evaporative constraint base on satellite-derived soil moisture and vegetation water content (Miralles et al., 2011a, b). For these regional evaluations, TEM was driven with monthly air temperature, precipitation, dew point temperature (used to derive vapor pressure), and cloudiness data over the 2000-2008 time period obtained from the European Centre for Medium-Range Weather Forecasts (ECMWF). MODIS land cover data of 2001 were used (MCD12C1), with an assumption that the land cover of the plateau during 2000-2008 was the same as 2001.

3.3.4 Regional simulations

ET simulations were conducted for both static and changing land cover conditions. The model was first run to equilibrium using the long-term averaged historical monthly climate data from 1971 to 2000, and was then spun up for 120 years to develop initial conditions for TEM at the beginning of the 21st century for the plateau. Then, we conducted twelve simulations using the AL2 algorithms to examine the effects of future climate change and LCC on ET. To examine the effects of climate change alone on ET, we conducted six simulations using the VEG1 land cover, historical climate from 1971 to 2000, and each of the six climate scenarios from 2001 to 2100. To examine the effects of both climate change and climate-induced LCC on *ET* during the 21st century, we conducted six simulations using the VEG2 land cover, historical climate from 1971 to 2000, and each of the six climate scenarios from 2001 to 2100. Differences in *ET* between the VEG1 and VEG2 simulations for corresponding climate scenarios were used to estimate the effects of climate-induced LCC on *ET*.

3.3.5 Statistical analysis

Root mean square error (RMSE), Nash–Sutcliffe model efficiency coefficient (NS) and mean percentage error (MPE) were used to evaluate the accuracy of *ET* estimates. The smaller values of RMSE and MPE, and NS values close to 1 (range from $-\infty$ to 1) indicate more accurate model estimates. The non-parametric Mann-Kendall test for trends was applied to determine significant time-series trends (Hamed and Rao, 1998).

3.4 Results and Discussion

3.4.1 Evaluation of site-level *ET* estimates

Comparisons of site-level AL1-ET and AL2-ET estimates with measured *ET* at the two EC sites (Table 3.2, Fig. 3.3) indicate that the AL2 greatly outperforms AL1. The MPE of 5.94% and 6.42% for annual AL2-ET, at the SKT and KBU sites, respectively, suggest that the AL2-ET generally agrees well with measured *ET* at the site level. The seasonal changes of AL2-ET, GLEAM and MODIS-ET match well with the measured *ET* at both sites, except from November to March (Fig. 3.3). During the winter months, the AL2-ET and GLEAM estimates are very close to the measured *ET* whereas MODIS-ET estimates are much higher. The overestimation of *ET* by MODIS-ET during the winter is probably due to increased uncertainties of driving data, e.g., land cover, albedo, LAI and reanalysis climate data (Strahler et al., 2002; Jin et al., 2002, 2003; Wang et al., 2004, 2005; Gao et al., 2005; Heinsch et al., 2006; Zhao et al., 2006; Sprintsin et al., 2009; Decker, 2011). In contrast, AL1-ET tends to overestimate *ET* during the summer, which is likely due to the overestimation of PET in the summer by the AL1 (Feddes et al., 1994) and the bias is passed on to the AL1-ET.

3.4.2 Evaluation of regional *ET* estimates

Regional AL2-ET (regional *ET* was determined by summing area-weighted *ET* estimates across all grid cells within the study region) matches well with regional MODIS-ET and GLEAM during the growing season, and performs better than regional AL1-ET (Figure 3.4). The regional AL1-ET is much higher during the growing season,

especially in July (18.6-41.5% higher), which is probably due to overestimation of *ET* by AL1-ET in the summer as shown in the site-level analyses (Section 3.1). In contrast, GLEAM during the growing season is similar to AL2-ET and MODIS-ET. The regional AL2-ET is lower than the regional MODIS-ET in the non-growing season (Fig. 3.4), which is likely due to the overestimation of MODIS-ET during this time as indicated in the site-level analyses. Overall, GLEAM reports an average annual *ET* of 210.07 mm yr^{-1} in the region during 2000-2008, which compares well to the 223.6 mm yr^{-1} by AL2-ET. Estimates by MODIS-ET (282.86 mm yr^{-1}) and AL1-ET (305.56 mm yr^{-1}) are much higher, which are likely due to their overestimation of *ET* in the winter and summer, respectively.

Across the plateau, the average annual AL1-ET and AL2-ET estimates over the 2000-2008 time period, show an increasing gradient from southwest to northeast that compares well with patterns observed by GLEAM and MODIS-ET (Fig. 3.5). At the same time, the AL1-ET of the eastern and northern parts of the plateau are obviously higher than that of MODIS-ET and GLEAM, likely because the AL1-ET is overestimated during the summer (Feddes et al., 1994) and the errors are unevenly distributed. The overall magnitude of MODIS-ET, however, is higher than that of AL1-ET and AL2-ET and the gradient of MODIS-ET across the plateau is not as strong as in the AL1-ET and AL2-ET estimates. This might be partially caused by the higher *ET* estimates during the winter when the monthly MODIS-ET estimates are 8-20 mm higher than those of AL1-ET and AL2-ET, and the differences are not evenly distributed across the plateau. Spatially, there are small differences between whole-year *ET* and growing season *ET* for AL1-ET and AL2-ET because their *ET* amounts in the winter are very small. However,

there are notable differences when it comes to MODIS-ET because MODIS-ET in winter tends to be higher, accounting for 24.6% of the average annual *ET* over 2000-2008. In contrast, the PM-Mu *ET* estimates of Vinukollu et al. (2011) are much lower than the other *ET* estimates (Fig 3.5), which is similar with the evaluation in the Vinukollu et al. (2011) that PM-Mu *ET* have sizeable negative bias (-132 mm yr^{-1} over 26 basins across continents), large discrepancy with observed data, and large RMSE. Although PM-Mu *ET* estimates by Vinukollu et al. (2011) and MODIS-ET are both based on PM framework, the parameterization and forcing data are different (Mu et al., 2007; Vinukollu et al., 2011). In addition, the former was based on the methods in Mu et al. (2007), whereas the latter was based on the methods in Mu et al. (2011) which further improved those of 2007. Moreover, the aerodynamic resistance in PM-Mu is calculated from Surface Energy Balance System (SEBS) model instead using the methods described in Mu et al. (2007) (Vinukollu et al., 2011). These differences may explain why PM-Mu *ET* estimates of Vinukollu et al. (2011) are much lower than MODIS-ET.

Due to the significant improvements demonstrated by the AL2 algorithms over the AL1 algorithms at both the site and regional levels, the AL2 algorithms were used in the TEM simulations to examine how climate change and LCC might influence *ET* in the future.

3.4.3 Climate change effects on ET

ET ranges from 188 mm yr-1 to 286 mm yr-1 across all scenarios using the VEG1 land cover during the 21st century, but increases in ET differ in magnitude among the six climate scenarios (Fig, 3.6, Table 3.3). The largest ET increases (0.55 mm yr-2) occurred

in the X903H scenario and the smallest ET increases (0.11 mm yr-2) occurred in the X905L scenario. Larger increases in ET occurred in the scenarios based on the BAU emissions policy (X903H, X901M, X902L) than in the emissions stabilization policy (X906H, X904M, X905L). Within an emissions policy, higher ET and larger increases in ET occurred in the climate scenarios that had a higher climate response than a lower climate response (X903H > X901M > X902L > X906H > X904M > X905L). Moreover, the order of ET estimates among the climate scenarios is also consistent with the projected increases in air temperature and precipitation among the climate scenarios (Table 3.3, Fig. 3.1). Higher precipitation would increase the supply of water for ET whereas higher air temperatures would increase atmospheric demand for water vapor by increasing the vapor pressure deficit (Anderson 1936). Thus, our results indicate the water cycling on the plateau will intensify in the future, but the level of this intensification will depend on the climate policy being implemented and the response of climate to greenhouse gas forcings.

The southwest to northeast gradient in *ET* is projected to continue to exist in the future in all six scenarios following a similar gradient in precipitation (Fig. 3.7). However, the spatial patterns of changes in AL2-ET vary among the climate scenarios. In the BAU emissions scenarios, AL2-ET increases almost over the entire region (Fig. 3.8). In contrast, AL2-ET decreases in some regions of the plateau and increases in other regions in the level-one stabilization emissions scenarios. Furthermore, the southwestern region, where the land cover is predominantly semi-desert/desert (Fig. 3.2), has the smallest increases in AL2-ET from the 1990s to 2090s in all scenarios.

Land cover influences both the rate of ET and the relative importance of ET to water cycle, which may be represented as a ratio of ET to precipitation (ET/P). Grasslands, boreal forests and semi-desert/deserts account for 90% of the vegetated area in the region. For all scenarios, the regional grassland ET ranges from 242 to 374 mm yr-1 (Table 3.4 and Fig. 3.9), with an average ET/P of 90%, which coincides with that at the KBU grassland site. Regional boreal forest ET ranges from 213 to 278 mm yr-1, with an average ET/P of 72%, which falls in the range of ratio at the boreal forest site SKT (70%-89%). The semidesert/desert ET varies from 100 to 199 mm yr-1 and accounts for 95-100% of the precipitation, which is consistent with previous studies in arid areas (Kurc et al., 2004; Sun et al., 2011a; Wang et al., 2012; Katul et al., 2012), and the average regional semidesert/desert ET ~145 mm yr-1 during 21st century for all scenarios is comparable to the current average estimates for these ecosystems (Jiménez et al., 2011; Miralles et al., 2011a). The simulated ET differences for various land cover types are mainly due to the climate variations across different land covers, e.g., the precipitation and air temperature in the grassland being higher than those of the boreal forest, or precipitation in the semidesert/desert being lower than that of the grassland or boreal forest. In particular, in the X903H scenario, precipitation during the growing season in grasslands is 23 mm higher than that of the boreal forest, 190 mm higher than that of the semidesert/desert, and mean air temperature during the growing season in grasslands is 5.34 °C higher than that of the boreal forest.

3.4.4 Land cover effects on ET

The regional AL2-ET estimates using the VEG2 land cover were slightly higher than the estimates using the VEG1 land cover in all six scenarios (Fig. 3.10). The differences in *ET* between the two land cover scenarios are more apparent in the BAU emissions scenarios than in the level-one stabilization emissions scenarios, but these differences are < 5% of the AL2-ET estimates using the VEG1 land cover. Likewise, LCC appeared to have subtle effects on the spatial distribution of AL2-ET (Figs. 3.7 – 3.8). Thus, the direct effects of climate change on *ET* appeared to be more important than the indirect effects of climate-induced LCC on *ET*.

There are two possible reasons for the inconspicuous effects of LCC on ET. First, the positive response of *ET* to LCC in some areas is offset by the negative response in other areas and, as a result, the change of aggregated *ET* over the whole plateau is small. The positive effect includes the change from forest to grassland, and the negative effect is due to the change from forest and grassland to semidesert/desert and from grassland to forest. For example, in the X903H scenario with the largest LCC among the six scenarios, the boreal forests and temperate forests will largely become grasslands and the semidesert/desert coverage will expand from 34.5% to 50% of the plateau by the end of the 21st century, specifically, 20.1% of the vegetated area will change from forests to grassland and 14.5% will change from grassland to semidesert/desert. Furthermore, the change area in all scenarios accounts for only 9-36% of the total area (Fig. 3.2). These relatively small changes in land cover appeared to have subtle effects on the spatial distribution of *ET* and regional *ET* estimates.

3.4.5 Implications of projected *ET* trends on the water availability

It is becoming recognized that water availability is a crucial limiting natural resource for human development, especially in arid and semiarid areas (Vorosmarty, 2000; Fekete, 2004). Our simulation results indicate that annual mean volumetric soil moisture varies very slightly from year to year, with trends ranging from -0.0069% ~ -0.021% yr^{-1} in all scenarios. Because the variation of soil moisture is negligible over the long run, net precipitation, the difference between precipitation and *ET* (hereafter *P-ET*), can approximately represent water availability, in other words, how much water may be available for human use.

Regional *P-ET* fluctuates without a significant trend in all the scenarios using the VEG1 land cover during the 21st century (Fig. 3.6). In addition, changes in *P-ET* from the 1990s to 2090s (Δ (*P-ET*)) are insignificant (±20 mm) across most of the plateau (Fig. 3.8).These results imply that without considering further anthropogenic impacts, projected climate change itself will not significantly increase threats to the water availability as increasing *ET* rates are being compensated by increasing precipitation rates. However, the threats to the water availability differ from scenario to scenario due to inconsistent trends between *ET* and precipitation. With the VEG1 land cover, *P-ET* will increase from the 1990s to 2090s across a large portion of the plateau (Fig. 3.8) with larger changes in the BAU scenarios (X901M: 10.4 mm or +58.3%; X902L: 2.4 mm or +52.8%; X903H: 5.4 mm or +56.9%) than the stabilized emissions scenarios (X904M: 2.5 mm or +49.6%; X905L: 0.4 mm or +48.9%; X906H: 2.8 mm or +51.5%). These results suggest that, as a whole, the BAU emissions scenarios tend to have slightly more

available water for human use and less area will be threatened by water shortage relative to the level one stabilization emissions scenarios.

With climate-induced LCC, fewer areas are likely to suffer from water shortage, although the increase in average *P-ET* from the 1990s to the 2090s using the VEG2 is slightly less than that using the VEG1 (Fig. 3.8). This discrepancy is likely due to the uneven effects of LCC across the plateau. At the same time, one common feature across all the scenarios is that future water supplies tend to be threatened in the northeastern part of the plateau where boreal forests are currently located.

3.4.6 Model limitations and simulation uncertainties

ET estimation is challenging because it involves a large number of biophysical factors such as landscape heterogeneity, plant biophysics for specific species, leaf angle, canopy structure, soil properties, soil moisture, and microclimate (ASCE, 1996; Wang et al., 2010; Mu et al., 2011). The algorithms used in this study do not account for biodiversity effects, as different species within a single plant functional type can have different ET rates that also vary with stand age. Uncertainties also exist in a number of the biophysical parameters in the AL2 algorithms, and all parameters are assumed to have the same value for a given biome type across the entire plateau. Moreover, the algorithms for soil evaporation are based on an assumption that SM has a strong link with the adjacent atmospheric moisture during an entire month, whereas the strongest link occurring at midday during convective conditions (Fisher et al., 2008). The application of the model at a monthly step might then contribute to ET errors. Another limitation of the algorithms is that the effect of high-CO2-induced partial stomatal closure on stomatal

resistance (Jarvis, 1976; Gedney et al., 2006; Lammertsma et al., 2011; Miglietta et al., 2011) has not been taken into account. Although the influence of available water on stomatal closure has been considered in the simulation of atmospheric CO2 fertilization effects on gross primary production (Raich et al., 1991; McGuire et al., 1997; Zhuang et al., 2003), the corresponding influence of CO2 on partial stomatal closure has not been considered in simulating ET and needs to be examined in future work.

ET is very sensitive to short-term weather conditions (ASCE, 1996; Allen et al., 1998) so the input of relatively coarse monthly meteorological data into TEM may bias *ET* estimates. In addition, the omission of some processes such as snow sublimation, evaporation from wet canopy surface, and wet soil surface will also lead to underestimation of total *ET*. In the case of forested regions, the omission of wet canopy evaporation may lead to an underestimation of *ET*, as the rates of interception loss may overcome several times those of transpiration (Gash and Shuttleworth, 2007; Miralles et al., 2010). The AL2-ET during the non-growing season is underestimated (Fig. 3.3), because the LAI is estimated to be zero by TEM in most cases during this period, which results in transpiration being zero. Low vapor pressure leads to low RH during this period, which also results in low soil evaporation (see Eq. (3.2c, 3.2d and 3.2e)). Then, a daily version of the TEM that has incorporated with the aforementioned processes and improvements on LAI and soil evaporation may produce better *ET* estimates.

All input driving data for the TEM have inherent uncertainties (Zobler, 1986; Mitchell and Jones, 2005; Sokolov et al., 2005; Webster et al., 2002; Farr et al., 2007). Spatially-interpolated CRU climate data are based on sparse and irregular meteorological stations in this region (New et al., 1999, 2000; Mitchell and Jones, 2005;), whereas

climate and terrain conditions vary in this region, the CRU data therefore have inherent uncertainties. The reanalysis ECMWF data and IGSM scenario climate data were simulated by models (Sokolov et al., 2005; Dee et al., 2011) so that the innate uncertainties in the model outputs will be inherited into the TEM ET estimation. Further, the VEG2 data are not continuously changing over time, our assumption that land cover remains the same over a period of 25 years may result in further errors. A data set with more continuous changes in land cover over the 21st century would improve the prediction of ET for future scenarios.

EC tower measurements used for validation also have different sources of uncertainty. Flux measurements are often affected by systematic errors such as energy balance disclosure and incomplete measurement of nocturnal flux exchange (Aubinet et al., 1999; Hollinger et al., 2005). Energy closure imbalance is common in eddy covariance studies and varies from a small percentage to 30-40% as a result of limitations in instrumentation, spatial heterogeneity of EC footprints, and the partial shortage of measured turbulent and advective fluxes (Anthoni et al., 1999; Wilson et al., 2002; Tchebakova et a., 2002). Further, there is likely a spatial-scale mismatch between the source area of the available energy (R_n - G) and the turbulent flux source areas (Schmid, 1994, 1997, 1999; Scott, 2010). For example, the source area of the available energy derived from ridge-top locations may be mismatched with the fluctuating turbulent flux source areas, which are often located on sloped surfaces with varied aspects (Schmid, 1994; Scott, 2010). Moreover, all EC systems attenuate the true turbulent signals at sufficiently high and low frequencies, especially at night (Moore, 1986; Massmana et al.,

2002). As a result, *ET* estimates from the EC towers have uncertainties ranging 10-30% (Glenn, 2008).

Finally the satellite-based *ET* estimates used here for comparison (e.g. MODIS-ET, GLEAM and the PM-Mu *ET* by Vinukollu et al, 2011) have uncertainties that are either cascaded from the inputs used to drive the methods or inherent to the algorithms themselves. This study has revealed potential uncertainties of MODIS *ET* during the winter on the plateau. The input climate data of the Global Modeling and Assimilation Office (GMAO) re-analyses used to drive MODIS-ET tends to have high uncertainties in winter (Zhao et al., 2006; Decker, 2011). Other possible error source lie in the input MODIS land cover data, where the accuracies are in the range of 70-80% (Strahler et al., 2002), and the inherited uncertainties from the MODIS albedo (MOD43C1). The uncertainties of albedo in the winter are especially distinct on the plateau since it is dominated by grassland (Fig. 3.2) and its albedo is most sensitive to snow cover when compared with other land cover (Jin et al., 2002, 2003; Gao et al., 2005;). An additional potential source of error is the input MODIS LAI, which tends to overestimate (Wang et al., 2004; Heinsch et al., 2006). The uncertainties in the MODIS land cover and albedo will propagate to the MODIS LAI in addition to their direct impacts on MODIS *ET* (Yang et al., 2006; Sprintsin et al., 2009). Some studies show that MODIS LAI have more apparent uncertainties in winter relative to summer (Wang et al., 2005; Sprintsin et al., 2009).

3.5 Conclusions

Despite the deficiencies and uncertainties of our model simulations described above, our analyses indicates that the modified TEM captures current spatial and temporal variations in ET as well as, or better than other approaches, and provides helpful insights about how ET and water availability on the Mongolian Plateau may change in the future in response to climate change and climate-induced LCC.

For the three dominant land cover types on the plateau, ET are all projected to increase. Grasslands have the highest regional annual ET, followed by the boreal forest and semi-desert/desert, whereas the increasing trends of ET is highest at grassland and lowest in boreal forest. The spatial gradients of annual ET across the plateau are expected to remain throughout the 21st century, increasing from the southwestern region to the northeastern region.

The magnitude and spatial pattern of changes in ET will depend on the climate policy being implemented and the sensitivity of climate to the energy forcing from greenhouse gas emissions. Larger changes in ET are expected from a BAU policy than a policy that attempts to stabilize greenhouse gas emissions as a result of larger changes in precipitation and air temperatures under the BAU policy. Furthermore, ET is expected to increase across most of the Mongolian Plateau under the BAU policy whereas ET will increase in some regions but decrease in other regions under a level-one stabilization emissions policy. Under both policies, a larger climate response to greenhouse gas forcing is expected to result in larger increases in ET. The enhanced ET is not expected to threaten water availability across most of the Mongolian Plateau because of concurrent increases in projected precipitation. An exception, however, may be the north-central

and northeastern parts of the plateau where large decreases in net precipitation are projected to occur in some climate scenarios.

Climate-induced changes in land cover are expected to have only minor effects on future regional ET with most of the regional ET changes (>95%) resulting directly from climate changes. Nevertheless, climate-induced LCC will induce visible changes in spatial distribution of net precipitation across the plateau during the 21st century, suggesting that future ET and water availability studies over time period of decades may need to consider the effects of LCC on ET.

3.6 Acknowledgements

This research is supported by the NASA Land Use and Land Cover Change program (NASA-NNX09AI26G, NN-H-04-Z-YS-005-N, and NNX09AM55G), the Department of Energy (DE-FG02-08ER64599), the National Science Foundation (NSF-1028291 and NSF- 0919331), and the NSF Carbon and Water in the Earth Program (NSF-0630319). The computing is supported by the Rosen Center of High Performance Computing at Purdue University. Special acknowledgment is made here to Prof. Eric Wood of Princeton University for his generous provision of *ET* dataset in the Vinukollu et al. (2011). Diego Miralles acknowledges the support by the European Space Agency WACMOS-ET project (contract no. 4000106711/12/I-NB).

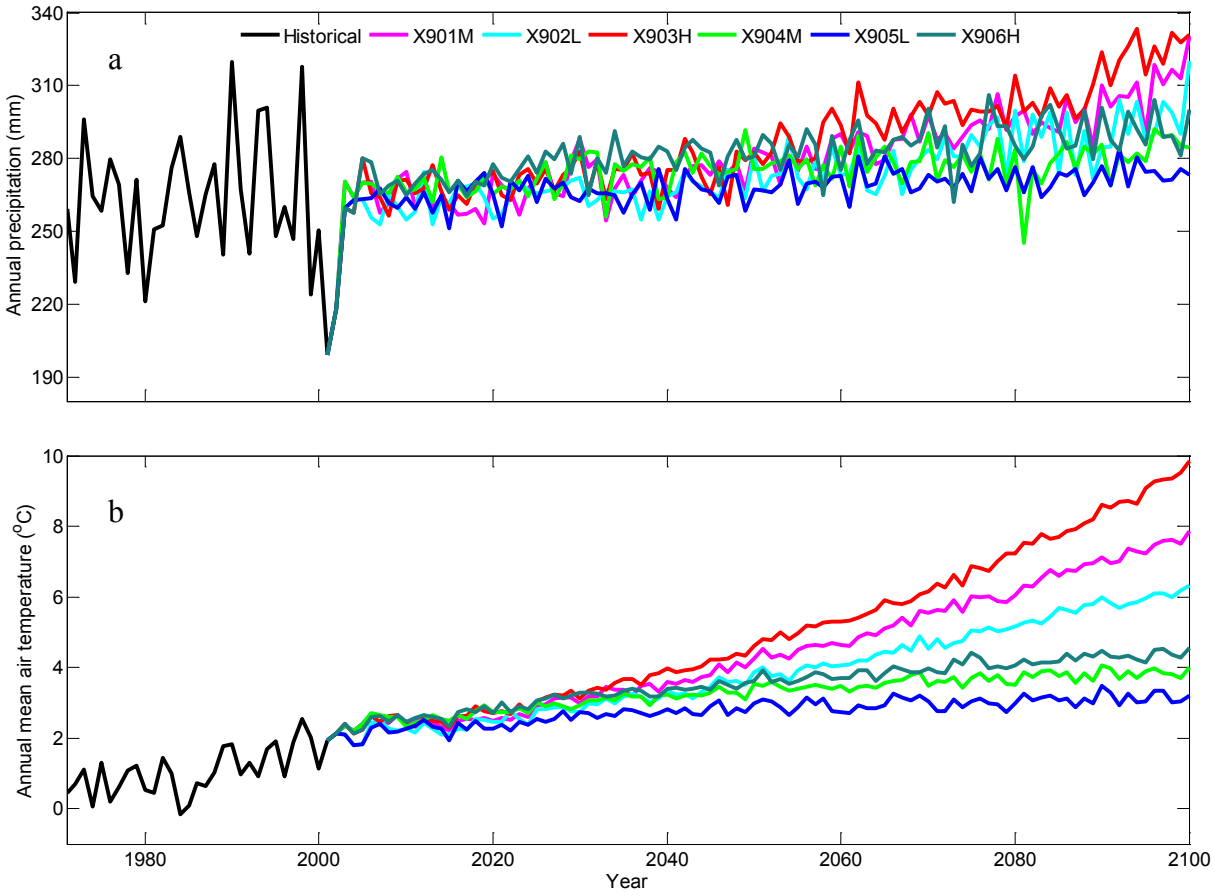

Figure 3.1 Climate variation of the Mongolia plateau during the period of 1971-2100 in X901M, X902L, X903H, X904M, X905L, and X906H: (a) annual precipitation, and (b) annual mean air temperature.

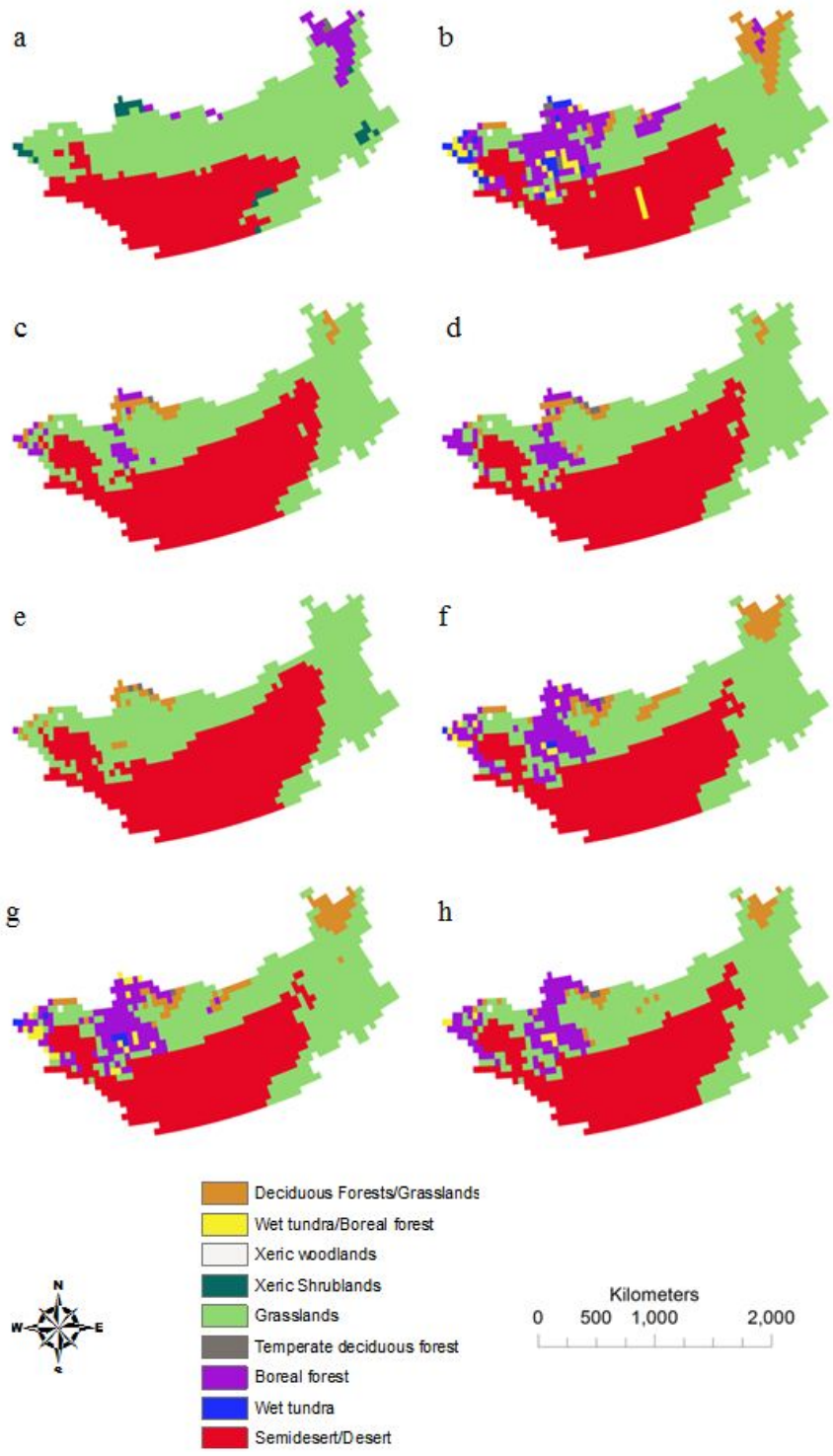

Figure 3.2 Land cover of Mongolia plateau from (a) MODIS land cover data of 2001, and from SibClim simulation of (b) 2000, (c) 2100 in X901M, (d) 2100 in X902L, (e) 2100 in X903H, (f) 2100 in X904M, (g) 2100 in X905L, and (h) 2100 in X906H.

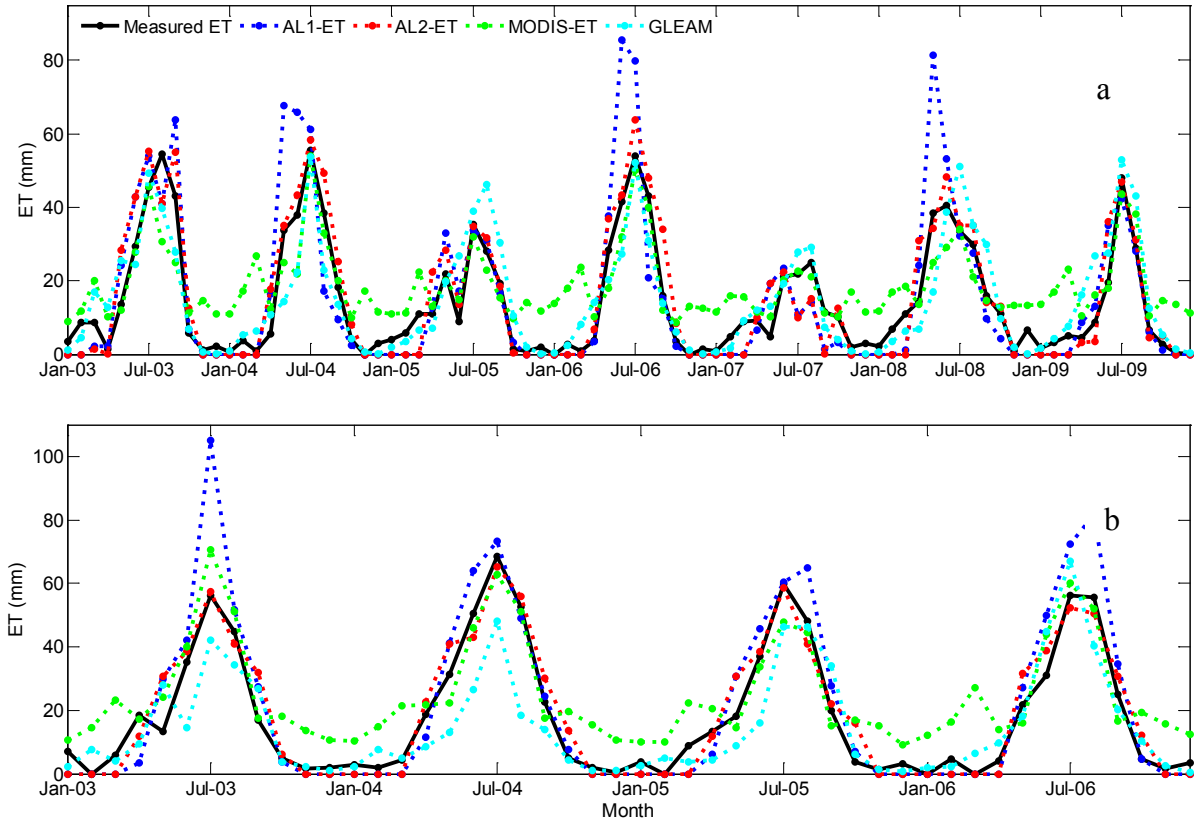

Figure 3.3 Comparison between measured *ET*, AL1-ET, AL2-ET, MODIS-ET and GLEAM at: (a) KBU site, and (b) SKT site.

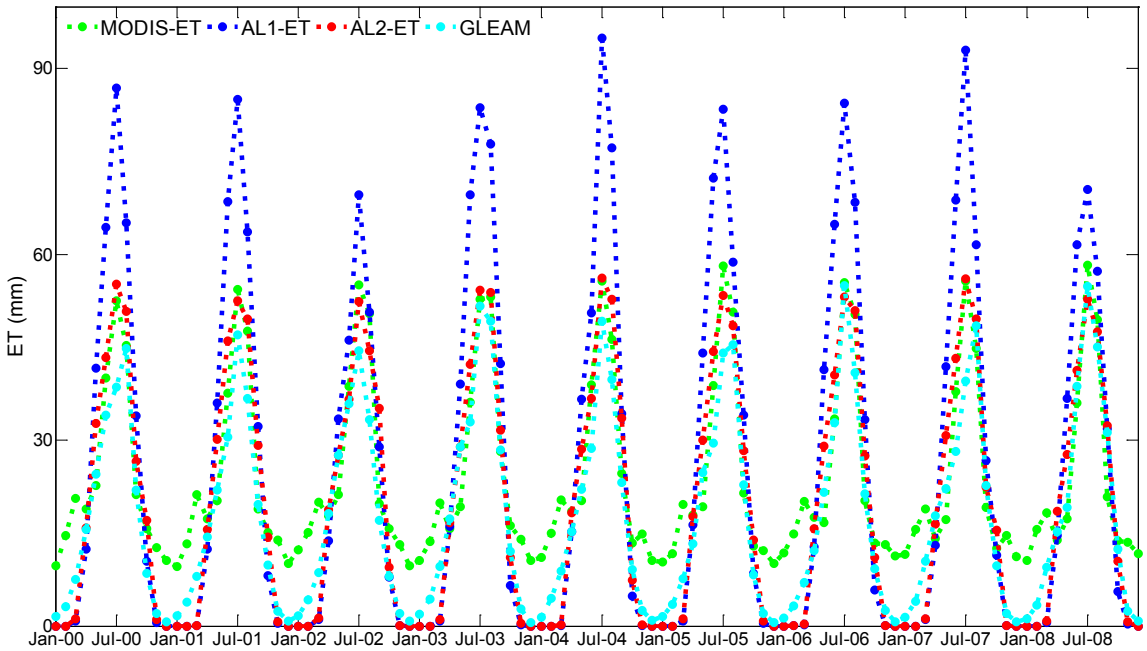

Figure 3.4 Comparison among regional MODIS-ET, AL1-ET, AL2-ET and GLEAM during 2000-2008.

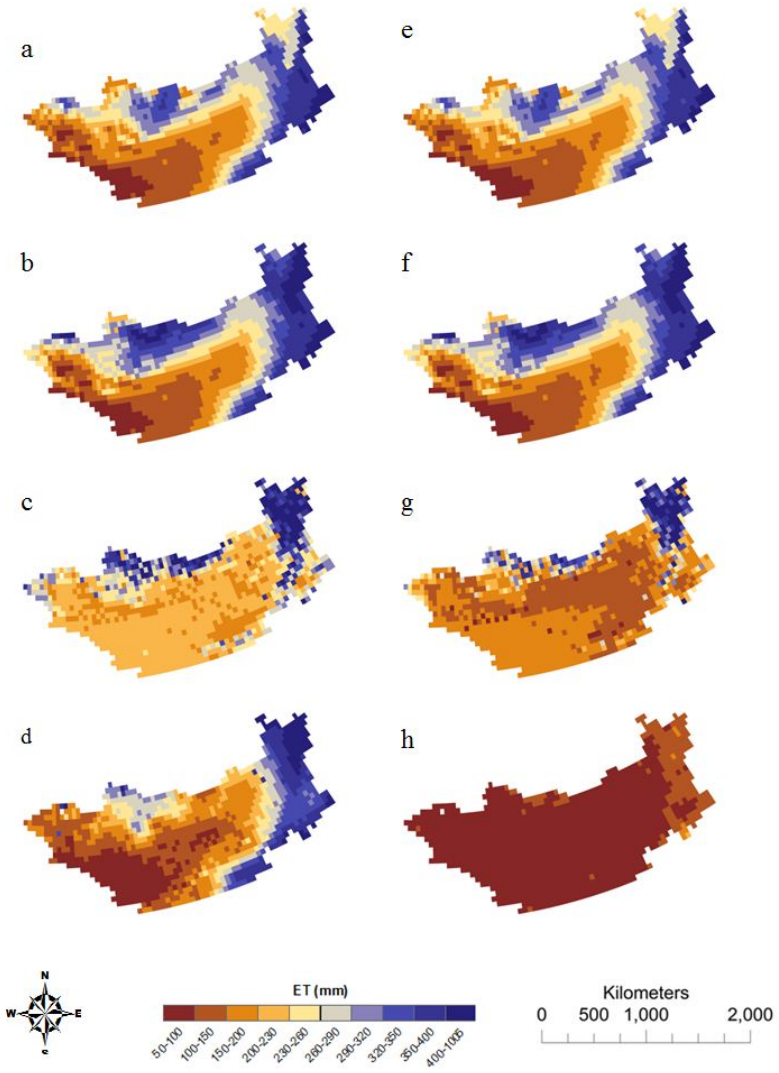

Figure 3.5 Spatial pattern of average annual *ET* over 2000-2008 derived from (a) AL2, (b) AL1, (c)MODIS, and (d) GLEAM , and average growing season *ET* over 2000-2008 derived from (e) AL2, (f) AL1, (g) MODIS, and (h) average annual PM-Mu ET over 2000-2007 in Vinukollu et al. (2011).

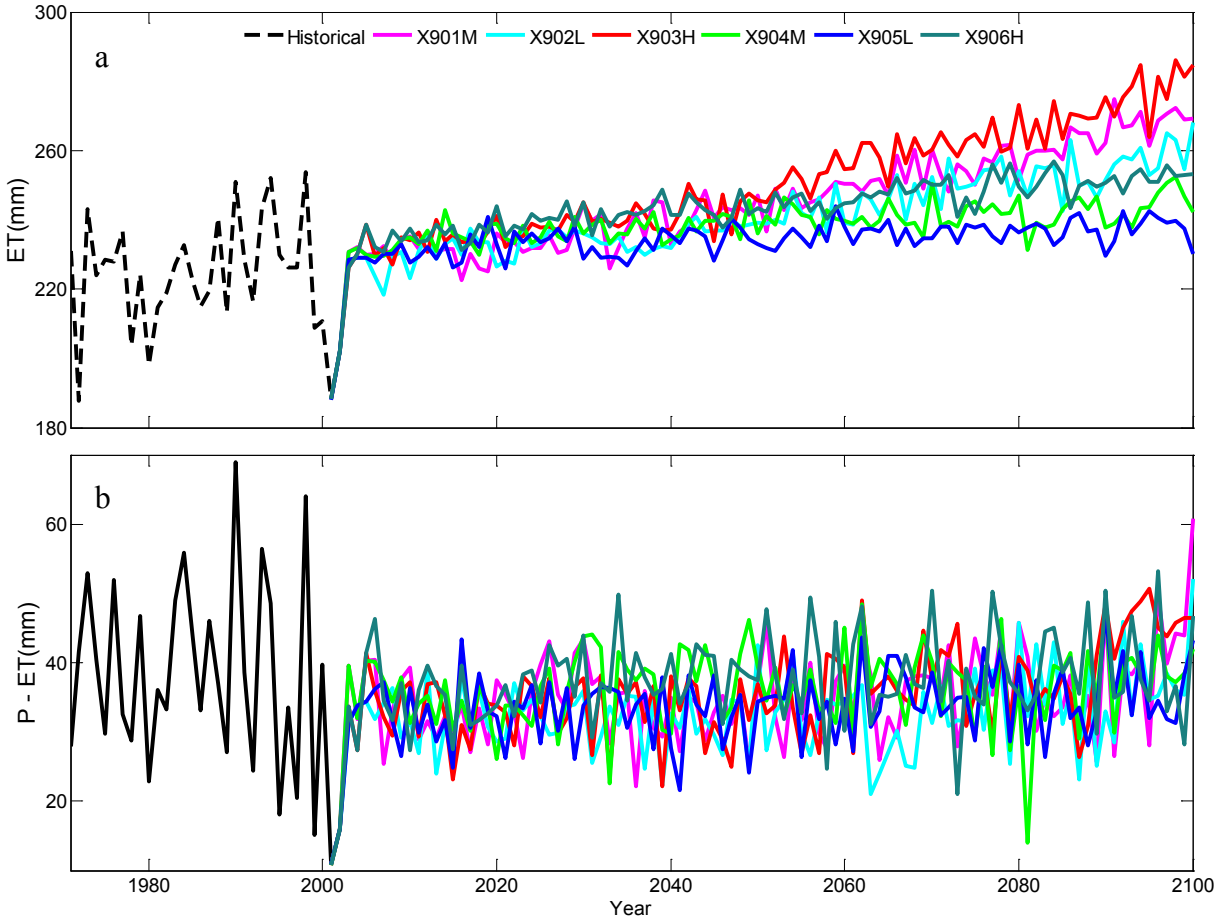

Figure 3.6 *ET* and *P-ET* variations over 1971-2100 under VEG1 in X901M, X902L, X903H, X904M, X905L, and X906H : (a) annual regional AL2-ET, and (b) annual regional *P-ET*.

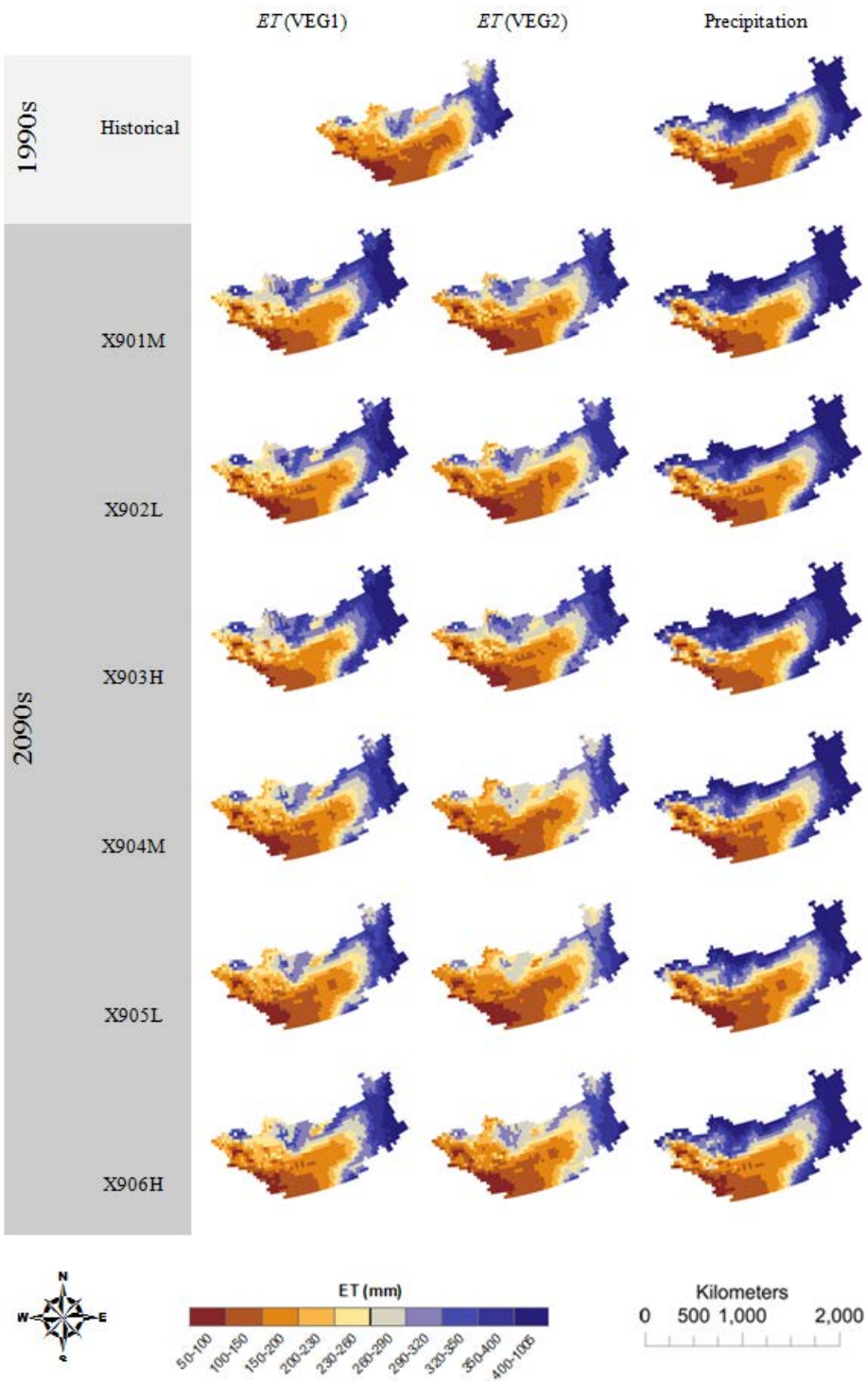

Figure 3.7 Spatial patterns of average annual AL2-ET (under VEG1 and VEG2) and precipitation over the 1990s and the 2090s in X901M, X902L, X903H, X904M, X905L, and X906H.

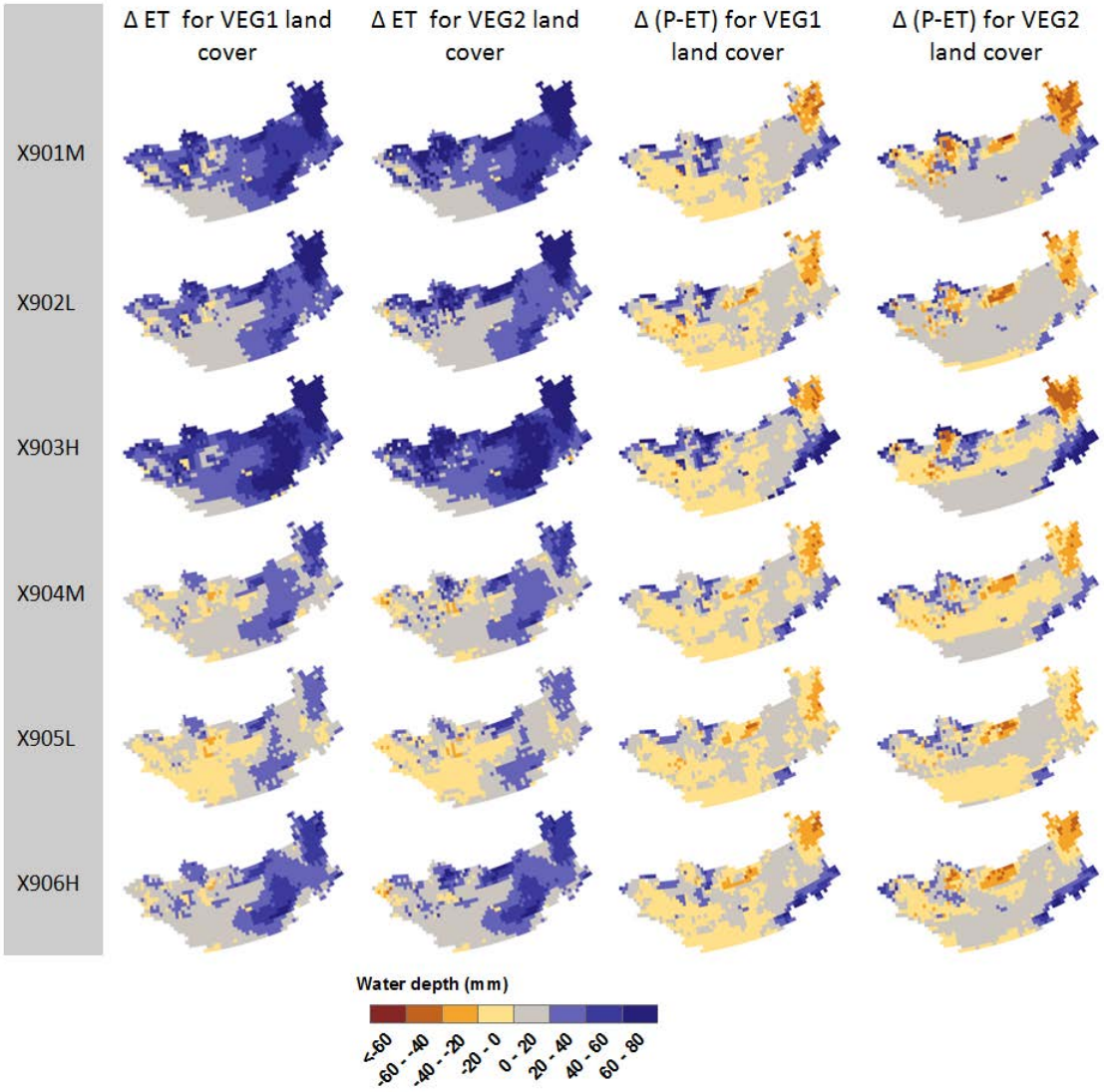

Figure 3.8 Spatial patterns of changes in average annual AL2-ET and net precipitation from the 1990s to the 2090s, using VEG1 and VEG2 land covers and X901M, X902L, X903H, X904M, X905L, and X906H climate scenarios.

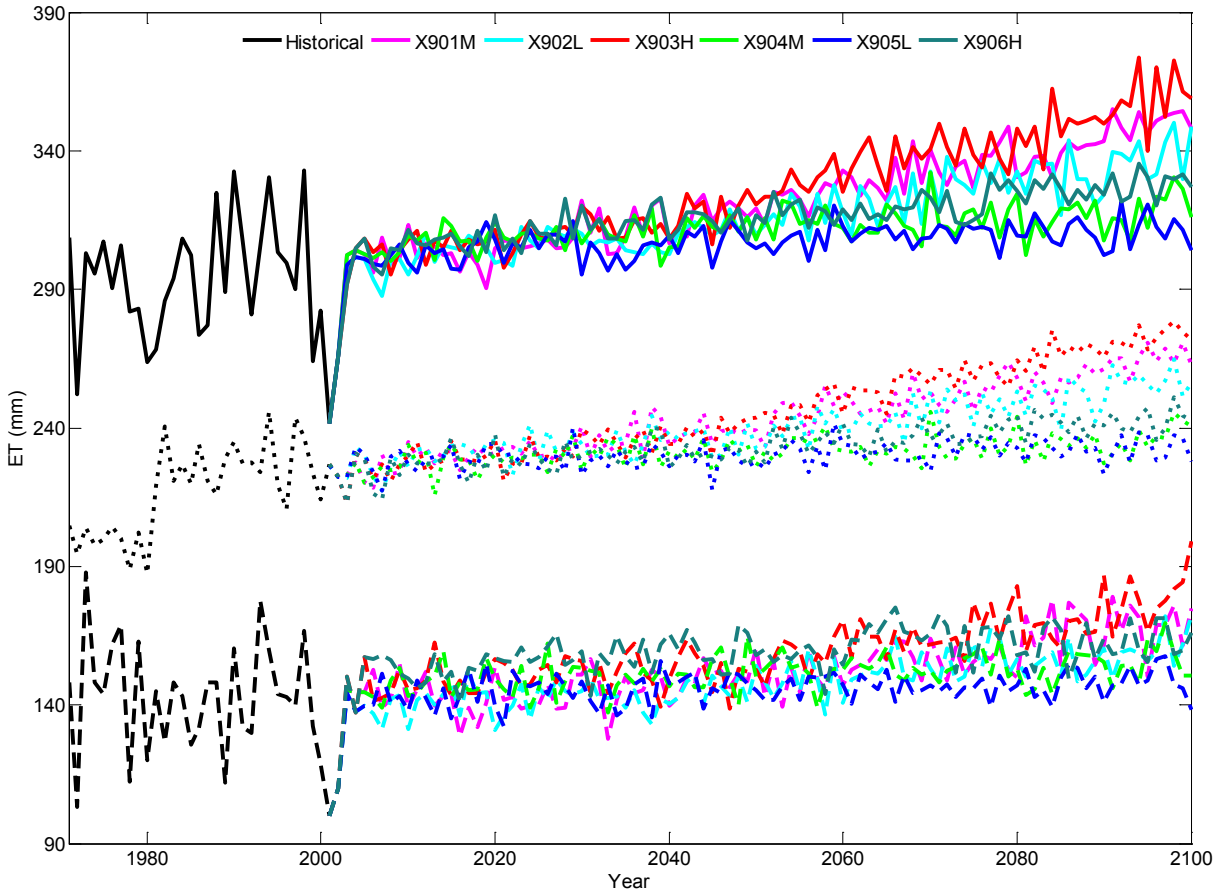

Figure 3.9 Annual regional grassland *ET*, boreal forest *ET*, and semidesert/desert *ET* variation over the period of 1971-2100 in X901M, X902L, X903H, X904M, X905L, and X906H under VEG1 (grassland *ET* - solid line; boreal forest *ET* - dotted line; semidesert/desert *ET* - dashed line).

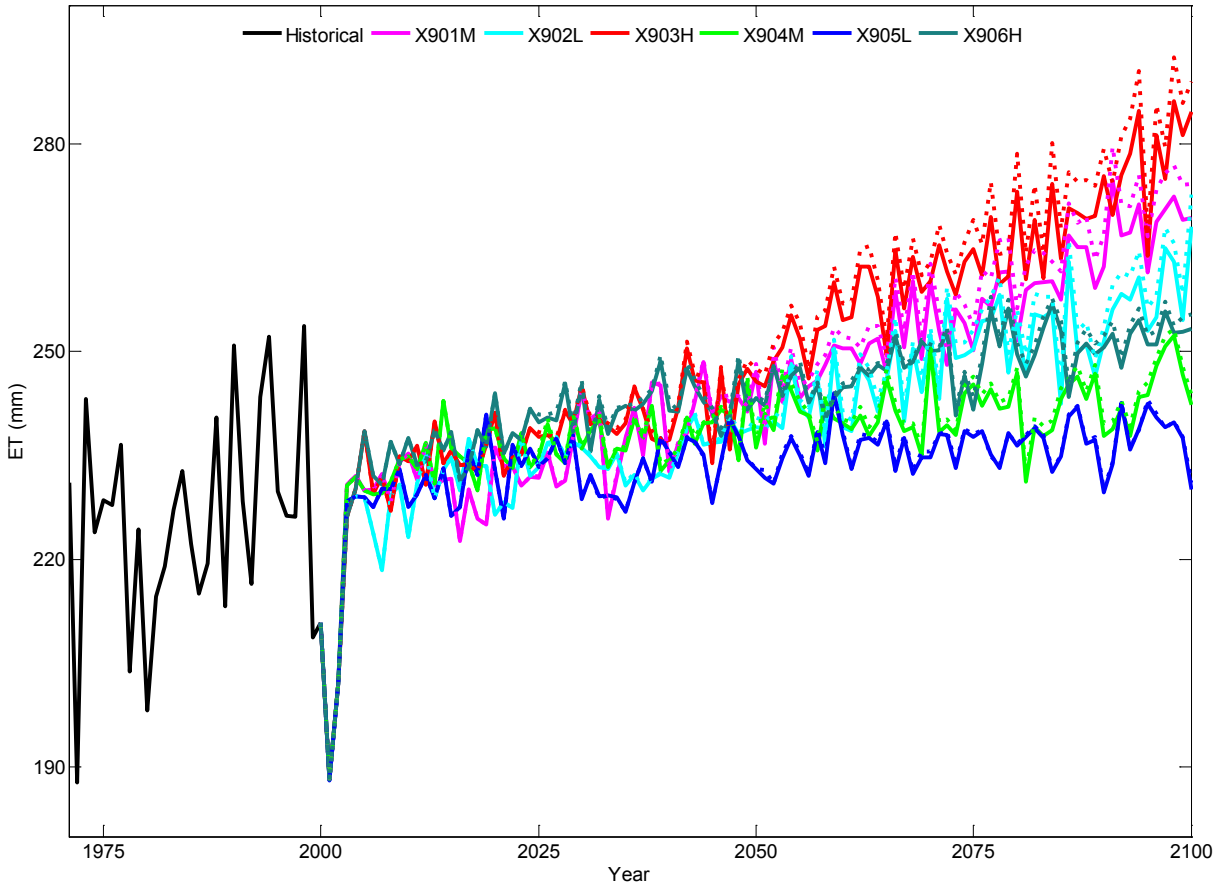

Figure 3.10 Annual regional *ET* variations over the period 1971-2100 under VEG1 and VEG2 (VEG1- solid line; VEG2 - dotted line) in X901M, X902L, X903H, X904M, X905L, and X906H.

Table 3.1 Values of major parameters attained through parameterization or estimation from reference. SD: semidesert/desert; WT: wet tundra; BF: boreal forest; TF: temperate forests; GR: grasslands.

Parameter	**SD**	**WT**	**BF**	**TF**	**GR**	**References**
β (hpa)	2.0	2.0	1.50	1.5	2.1	Mu. et al. (2007, 2011) and Fisher et al. (2008)
SLA (m^2/g C)	0.05	0.05	0.02	0.025	0.05	Milner et al.(2003), White et al. (2000), Poorter et al. (1998) and Garnier et al.(1997)
C_L (m/s)	0.005	0.004	0.0032	0.003	0.005	Mu. et al. (2007, 2011) and Cleugh et al. (2007)

Table 3.2 Comparison of accuracies among AL1-ET, AL2-ET, MODIS-ET and GLEAM estimates at the EC sites of SKT and KBU, a and b under each ET estimate category stand for whole measurement period and growing seasons, respectively . Low values of RMSE and higher values of NS indicate better accuracy.

	SKT								KBU							
	AL1-ET		AL2-ET		MODIS-ET		GLEAM		AL1-ET		AL2-ET		MODIS-ET		GLEAM	
	a	b	a	b	a	b	a	b	a	b	a	b	a	b	a	b
RMSE (mm mon^{-1})	10.99	14.05	6.30	7.67	10.65	8.16	9.27	10.93	11.86	15.56	6.70	7.58	9.04	7.84	7.14	9.17
NS	0.71	0.51	0.91	0.89	0.73	0.82	0.76	0.62	0.42	0.13	0.82	0.76	0.62	0.73	0.78	0.68

Table 3.3 Range (mm) and increasing trends (mm yr^{-2}) of regional annual AL2-ET, AL1-ET, and precipitation of Mongolia in the 21st century in X901M, X902L, X903H, X904M, X905L, and X906H under VEG1

	AL2-ET		Precipitation	
	Range	Trend	Range	Trend
X901M	188-275	0.47	199-330	0.38
X902L	188-268	0.38	199-320	0.28
X903H	188-286	0.55	199-334	0.48
X904M	188-252	0.17	199-292	0.18
X905L	188-244	0.11	199-284	0.12
X906H	188-257	0.25	199-306	0.28

Note: for all the trend analyses, $P < 0.001$.

Table 3.4 Range (mm) and increasing trends (mm yr^{-2}) of annual grassland *ET*, boreal forest *ET*, and semidesert/desert *ET* of Mongolia in the 21st century in X901M, X902L, X903H, X904M, X905L, and X906H

	Grass		Boreal Forest		Semidesert/desert	
	Range	Trend	Range	Trend	Range	Trend
X901M	242-355	0.60	218-270	0.26	100-179	0.34
X902L	242-350	0.48	217-264	0.20	100-172	0.28
X903H	242-374	0.67	213-278	0.29	100-199	0.38
X904M	242-332	0.20	215-246	0.10	100-170	0.15
X905L	242-322	0.17	213-242	0.06	100-158	0.10
X906H	242-335	0.32	213-251	0.13	100-175	0.19

Note: for all the trend analyses, $P < 0.001$.

CHAPTER 4. RESPONSE OF EVAPOTRANSPIRATION AND WATER AVAILABILITY TO THE CHANGING CLIMATE IN NORTHERN EURASIA[3]

4.1 Abstract

Northern Eurasian ecosystems play an important role in the global climate system. Northern Eurasia (NE) has experienced dramatic climate changes during the last half of the 20th century and to present. To date, how evapotranspiration (*ET*) and water availability (*P–ET*, P: precipitation) had changed in response to the climatic change in this region has not been well evaluated. This study uses an improved version of the Terrestrial Ecosystem Model (TEM) that explicitly considers *ET* from uplands, wetlands, water bodies and snow cover to examine temporal and spatial variations in *ET,* water availability and river discharge in NE for the period 1948–2009. The average *ET* over NE increased during the study period at a rate of 0.13 mm yr^{-1} yr^{-1}. Over this time, water availability augmented in the western part of the region, but decreased in the eastern part. The consideration of snow sublimation substantially improved the *ET* estimates and highlighted the importance of snow in the hydrometeorology of NE. We also find that the modified TEM estimates of water availability in NE watersheds are in good

[3] Liu, Y., Zhuang, Q., Pan, Z., Miralles, D., Tchebakova, N., Kicklighter, D., Chen., J., Sirin, A., He, Y., Zhou, G., Melillo, J. (2014), Responses of evapotranspiration and water availability to the changing climate in Northern Eurasia, *Climatic Change* 1-15 DOI 10.1007/s10584-014-1234-9

agreement with corresponding measurements of historical river discharge before 1970. However, a systematic underestimation of river discharge occurs after 1970 indicates that other water sources or dynamics not considered by the model (e.g., melting glaciers, permafrost thawing and fires) may also be important for the hydrology of the region.

4.2 Introduction

Evapotranspiration (*ET*) is a key component of the Earth system. It links the Earth surface energy balance with its water balance and affects the biogeochemical exchanges between the biosphere and atmosphere (Dolman and de Jeu 2010; Wang and Dickinson 2012). *ET* conveys about half of the solar energy absorbed by the land back to the atmosphere as latent heat flux (Stephens et al. 2012). Because water vapor is the dominant greenhouse gas in the atmosphere (Held et al. 2000), *ET* is thus critical in regulating the Earth's energy balance and therefore its temperature. In addition, *ET* returns more than 60% of annual precipitation (*P*) back to the atmosphere, constraining the water availability over the continents (Vörösmarty et al. 1998; Miralles et al. 2011a; Kumar et al. 2014), and providing climate feedbacks via precipitation recycling (Seneviratne et al., 2010).

There is a growing consensus that water availability is becoming a more crucial limiting factor for economic development (Vörösmarty et al. 2010).With an increasing human population, the rapidly rising demand for water is causing this resource to become progressively scarce. Climatic change may exacerbate this water limitation, as future warming is expected to raise the rates of *ET* leading to further drying of the land surface

(Huntington, 2006; Douville et al. 2012), particularly in regions already suffering from water scarcity (Dorigo et al. 2012).

To date, *ET* is deemed as one of the most difficult components of the hydrological cycle to quantify accurately (Dolman and De Jeu 2010), partially because a large number of environmental (e.g., soil moisture, plant phenology, soil properties) and climatic factors (e.g., solar radiation, temperature, humidity, wind speed) affect the process (e.g., Monteith, 1965). Understanding historical changes in *ET* would enable a better quantification of the future availability of water across the continents, which in turn, may help to better manage water resources via irrigation scheduling, drought detection and assessment and so forth. Recently developed methodologies that up-scale *in situ* measurements (Jung et al. 2010; Xiao et al. 2012) or combine satellite-based data (Fisher et al. 2008; Miralles et al. 2011a,b; Mu et al. 2011) provide new opportunities to estimate *ET* over large regions for the limited time period of observational records. These spatially explicit estimates can also be used to benchmark land surface models (Mueller et al. 2013), which in turn, can estimate changes in regional hydrology for longer time period in the past or project these changes into the future.

Ecosystems in Northern Eurasia (NE) play an important role in the global climate system due to their high sensitivity to climatic change and the vast land area (Fig. 4.1) that they cover (Adam et al. 2008; Groisman et al. 2010). NE accounts for 19% of the Earth's land surface, 59% of the terrestrial land north of 40°N, about 70% of the Earth's boreal forests, and more than two-thirds of the Earth's permafrost (NEESPI 2004). While it is widely accepted that the Earth's temperature has increased globally in recent decades, this increase has been more rapid in NE (Groisman et al. 2009; IPCC 2013). A significant

portion of the total terrestrial freshwater flux to the Arctic Ocean is generated in this region (Frey 2003); increases in this freshwater flux may potentially weaken the North Atlantic thermohaline circulation and slow CO_2 transport to the deep ocean (Peterson et al. 2002; ACIA 2005). Despite this crucial role, little is known about how past changes in climate have affected the terrestrial water cycle in the region.

This study uses an improved version of a process-based biogeochemistry model, the Terrestrial Ecosystem Model (TEM 5.0; Zhuang et al. 2010), to gain new insights into the dynamics of the terrestrial water cycle in NE. TEM is a process-based biogeochemistry model that uses spatially referenced data on climate, soils, land cover, and elevation to simulate C, N, and water fluxes and pools in terrestrial ecosystems (e.g., Zhuang et al. 2010; Liu et al. 2013). With a long time series of forcing data, TEM estimates allow a longer-term (1948–2009) analysis of *ET* and water availability (*P–ET*) than the one based on satellite-based *ET* datasets only. The *ET* algorithms in the previous version of TEM (Zhuang et al. 2010 – hereafter referred to as TEM-AL1) do not consider the effects of land cover heterogeneity on *ET* estimation, which are particularly important when modeling *ET* and are not well addressed by many of the currently existing *ET* estimation schemes (Mengelkamp et al. 2006; Mueller et al. 2013). In addition, the atmospheric evaporative demand (AED) in TEM-AL1 is represented by the Jensen-Haise formula (Jensen and Haise, 1963) and is only affected by variations in climate. This formula is reported to overestimate AED during the summer (Feddes and Lenselink 1994) so that *ET* is also overestimated by TEM-AL1 (Liu et al. 2013). To address these limitations, we developed new *ET* algorithms for TEM – hereafter referred to as TEM-AL2 – to improve the simulation of *ET* in high latitude ecosystems (see Section 4.3.2).

In Section 4.3 of this study, we: (a) describe the improvements to the TEM *ET* algorithms, (b) parameterize the improved TEM using data from eddy-covariance (EC) towers, and (c) evaluate *ET* estimates from the improved TEM by comparisons against satellite-based *ET* products. Section 4.4 focuses on the analysis of the historical changes in *ET*, with special emphasis on the implications of these changes for the availability of water resources in NE.

4.3 Methods

4.3.1 Overview

In a recent study (Liu et al. 2013), we found that the Penman-Monteith approach incorporating physiological and aerodynamic constraints on AED provided better estimates of ET across the Mongolian Plateau than TEM-AL1, which is based on empirical relations of ET with solar radiation and air temperature described by Jensen and Haise (1963). However, in Liu et al. (2013), ET was estimated from transpiration and soil surface evaporation in only uplands (i.e. upland ecosystems). Here, we further modify the TEM ET algorithms to estimate: 1) transpiration separately for uplands and wetlands; 2) evaporation separately for uplands, wetlands, and water bodies; and 3) snow sublimation. We refer to the new algorithms as TEM-AL2. These modifications aim at improving the representation of the interactions between the terrestrial energy and water budgets and to increase their realism in high-latitude regions. The different ET components are aggregated to grid cell scale (hereafter ETa) weighted by the fraction of each land cover per grid cell (see Eq. 4.1 and 4.2 in Section 4.3.2). The fraction coverages of uplands, wetlands and water bodies are assumed to be static within each

grid cell and sum to 1, but these land cover types may be totally or partially covered by snow during some part of the year. The fractional snow cover varies monthly and is represented with seasonal snow cover climatology (see Section 4.3.3.2). Then regional ET is estimated by calculating area-weighted average of ETa across all grid cells in NE. Finally, regional estimates of ET are examined for temporal trends.

To calibrate the TEM-AL2 and evaluate its performance relative to the TEM-AL1 version, ET measurements from 13 EC sites in the NE are used (http://www.asianflux.com, http://gaia.agraria.unitus.it/, Table 4.1, Fig. 4.3a). In addition, two satellite-based ET products – the MODIS product (Mu et al. 2011, hereafter MODIS-ET) and GLEAM (Global Land-surface Evaporation: the Amsterdam Methodology, Miralles et al. 2011a,b) – are also compared to EC data to evaluate their validity at the site level relative to TEM. These satellite products along with the mean of the LandFlux-EVAL merged ET systhesis datasets (hereafter EVAL) by Mueller et al. (2013), and the PM-Mu ET estimates by Vinukollu et al. (2011) are used to evaluate the spatiotemporal variability of the regional TEM-AL2 ET estimates in Section 4.3.6. EVAL and PM-Mu ET estimates are not compared with EC data because of differences in the timing of the ET estimates and the EC measurements. In this study, we use the Mann-Kendall trend test (Hamed and Rao, 1998) to determine significant time-series trends.

4.3.2 Modification of ET algorithms

In this study, we continue our revision of TEM-AL1 based on Liu et al. (2013) by incorporating separate algorithms and parameterizations to derive monthly ET (or evaporation) from uplands, wetlands, water bodies and snow cover. ET from uplands

includes transpiration from plant canopies, evaporation from wet canopies, saturated and moist soil surfaces. Although the same algorithms are used in wetlands as in uplands, ET is assumed to be not limited by water in wetlands (see e.g. Mohamed et al. 2012). For water bodies, evaporation is estimated based on algorithms described by Penman (1948, 1956). Snow sublimation is estimated based on algorithms described by Zhuang et al. (2002). Because we assume that any snow is uniformly distributed within a grid cell, the effects of snow dynamics on ET from a particular land cover type or plant function type (PFT) in a grid cell is determined as follows:

$$ET_i = (1 - p_s) \times ET_{i0} + p_s \times ET_s \quad (4.1)$$

where ETi0 represents monthly ET from the fraction of the ith land cover or PFT within each grid cell not covered by snow; ETs is snow sublimation; ps is the fraction of a grid cell covered by snow; and ETi is the ET from the ith land cover or PFT both covered and uncovered by snow within a grid cell. Fractional snow cover is relatively low during summer and high during winter. The total ET of each grid cell (ETa) is then calculated by aggregating the ET estimates for both snow-free and snow-covered uplands, wetlands and water:

$$ET_a = p_u \times ET_u + p_t \times ET_t + p_w \times ET_w \quad (4.2)$$

where pu, pt, and pw represent the fractions of uplands, wetlands and water bodies within each grid cell, respectively (i.e., the sum of pu, pt and pw is 1). ETu, ETt, and ETw represent the ETi (see Eq. 4.1) from the uplands, wetlands and water bodies for the corresponding grid cell, respectively.

The algorithms for TEM-AL1 and TEM-AL2 used in this study have been listed in Table 4.2. Our new algorithms for estimating ET for upland ecosystems are similar to those by Mu et al. (2011). However, there are several differences between these two methods. First, ET estimates by Mu et al. (2011) are not constrained by soil moisture, whereas TEM-AL2 uses the available soil water as determined by the TEM soil water balance (Liu et al. 2013). Second, the fraction of vegetation cover (Fc) in Mu et al. (2011) is represented by MODIS FPAR (MOD15A2), whereas TEM-AL2 uses the internal Fc from the TEM's LAI module (Liu et al. 2013). Third, we use the method in Allen et al. (2008) to estimate the soil heat flux, whereas Mu et al. (2011) adopted the methods in Jacobsen and Hansen (1999). Fourth, The TEM-AL2 uses the Shuttleworth (1992) method for estimating net emissivity between the atmosphere and the ground (ε'):

$$\varepsilon' = a_e + b_e\sqrt{e_d} \tag{4.3}$$

where ed is vapor pressure (kPa), and ae and be are coefficients, where ae lies in the range 0.34 to 0.44 and be in the range -0.14 and -0.25. Mu et al. (2011) estimated ε' using the methods of Idso and Jachson (1969). The relative sensitivity of soil moisture constraint factor to vapor pressure deficit (i.e β, see Fisher et al. 2008), is parameterized to be biome-specific in TEM-AL2 instead of using a fixed value for all biomes as in Mu et al. (2011). Finally, the mean potential stomatal conductance per unit leaf area (CL) is parameterized for each biome in TEM-AL2 and the value is different from that in Mu et al. (2011).

Methods for calculating ET in upland ecosystems are also used here to estimate the ET from wetlands. However, it is assumed that ET is unconstrained by available

water in wetland soils (Mohamed et al. 2012) while moisture availability limits ET in upland ecosystems.

For water bodies, the Penman equation (1948, 1956) is introduced to estimate evaporation:

$$\lambda E = \frac{\Delta(R_n - G) + \gamma E_a}{\Delta + \gamma} \times 86400 \times MD \quad (4.4)$$

where λE (J m-2 mon-1) is the flux of latent heat, Rn (W m-2) is the net radiation, G (W m-2) is the monthly change of energy storage in the water body, λ (J kg-1) is the latent heat of evaporation, γ (Pa k-1) is the psychometric constant, Δ is the slope of the saturation vapor pressure curve (Pa k-1), and MD is the number of days during a particular month, and Ea accounts for an empirical wind function and is expressed as:

$$E_a = 6.43 \times (a_w + b_w \times u_z) \times (e_s - e_a) \quad (4.5)$$

where aw and bw are empirical wind function coefficients, es (Pa) and ea (Pa) are the saturated and actual vapor pressure in the air, respectively, and uz (m s-1) is wind speed at the z height, Penman (1963) proposed aw = 0.5 and bw = 0.54 for open water for z = 2 m.

The G is estimated as described by Jensen (2010) and Jensen et al. (2005):

$$G = 0.5 \times R_{sn} - 0.8 \times R_{nl}, \quad \text{for day of year} < 180 \quad (4.6a)$$

$$G = 0.5 \times R_{sn} - 1.3 \times R_{nl}, \quad \text{for day of year} > 180 \quad (4.6b)$$

where R_{sn} is net solar radiation, and R_{nl} is long-wave radiation.

4.3.3 Data

4.3.3.1 Climate data

Input data on air temperature (T), precipitation (P), cloudiness (C), vapor pressure (V), wind speed (u), atmospheric CO2 concentrations, land cover type, albedo, elevation, and soil texture are needed to estimate ET using the TEM-AL2. Surface incoming shortwave radiation (R) is estimated from the TEM by using latitude, date, and cloudiness (Pan et al. 1996). Soil texture, elevation and land cover data vary spatially over the study region and are assumed to remain unchanged throughout 1948–2009, whereas other inputs vary over time and space. In this study, all simulations are conducted at a spatial resolution of 0.5° latitude × 0.5° longitude.

Gridded historical time series of monthly T, P, C, and V from the Climate Research Unit of the University of East Anglia (CRU TS3.10, the precipitation dataset is the corrected version v3.10.01; Harris et al. 2013) are used. The CRU dataset has been selected for this study because its accuracy stands out from a variety of widely-used forcing datasets in the NE region (Liu et al. 2014, in review; Simmons et al. 2004). For u we use monthly climatology data during 1961–1990 from CRU, due to the unavailability of historical time series. In addition, the spatial resolution of these wind data is degraded from 10' to 0.5° by averaging values of 10' cells within each 0.5° cell, to be consistent with the other forcing datasets.

The climate datasets used in the study, CRU TS 3.10 (Harris et al. 2013), are evaluated through comparisons with the time series of meteorological data from the European Climate Assessment & Dataset (ECA&D), the National Meteorological

Information Center of China Administration (NMICCA), and the EC tower sites within the NE domain (Table 4.3). Observed relative humidity (RH) and T are used to derive vapor pressure (Allen 1998) to compare against CRU vapor pressure. In addition, the corresponding climatologies of all CRU forcing data except wind speed are compared against the climatologies extracted from measurements collected at 86 meteorological stations during 1966-1970 across Russia (Reference Book on Climate of the USSR). Overall, our assessment indicates that the CRU data compares generally well with the ground measurements. An average absolute mean percentage difference (MPD) below 16% across all stations for each climate variable (except for C, Table 4.4) suggests a good representation of the regional climate conditions. Uncertainties in the CRU data come from the sparseness of ground measurements and the scaling errors associated with comparing site data to grid cell data organized at a spatial resolution of 0.5o latitude × 0.5o longitude. Weather data from only a small number of weather stations are involved in the interpolation of CRU data (Jones, 2012) so that spatial heterogeneity of weather will result in bias in the CRU data.

4.3.3.2 Ancillary input data

Data on soil texture, elevation, historical climate and atmospheric CO2 concentrations from 1948 through 2009 are collected from several sources. The soil texture data are from the Food and Agriculture Organization/Civil Service Reform Committee (FAO/CSRC) digitization of the FAO-UNESCO (1971) soil map (Zobler 1986). Elevation data are from the Shuttle Radar Topography Mission (Farr et al 2007).

The annual global atmospheric CO2 concentration data are acquired from atmospheric observations (Keeling et al 2005).

The distribution of plant functional types (PFTs) over the domain is derived from the International Geosphere-Biosphere Program (IGBP) Data and Information System (DIS) DISCover Database (Belward et al. 1999; Loveland et al. 2000), and reclassified into the TEM vegetation classification scheme at a spatial resolution of 0.5o × 0.5o (Melillo et al. 1993). The distributions of wetland and water bodies are extracted from the Global Lakes and Wetlands Database (GLWD – Lehner and Döll 2004). Lakes, reservoirs and rivers in the GLWD are reclassified into water bodies. Marshes, floodplains, coastal wetlands, saline wetlands, bogs, fens and mires in this NE region are reclassified into tundra wetland used in the TEM vegetation classification scheme (Melillo, 1993). The fraction coverages of wetlands and water bodies within each 0.5°×0.5° grid cell are derived based on their distribution in GLWD, and the remaining fraction is attributed to uplands. Then the fraction coverages of uplands, wetlands and water bodies sum to 1 and they are assumed to be unchanged throughout 1948-2009. The PFT map of the NE domain and the fraction cover of upland ecosystems, wetlands and water bodies, and six major river watersheds in the NE domain (Kolyma, Lena, Yenisei, Ob, Pechora, and Northern Dvina) are presented in Fig. 4.1. This map is assumed to be unchanged throughout 1948–2009. The MODIS Snow Cover Monthly data (MOD10CM) from 2000 through 2012 are also used, and snow cover of the same month in each year is averaged, so as to develop seasonal snow cover climatology for each grid cell. The seasonal snow cover variation of each grid cell is assumed to remain unchanged from 1948 through 2009 and is represented by the above seasonal snow cover climatology.

For snow dynamics, we use a seasonal climatology of snow cover derived from MODIS Snow Cover monthly data (MOD10CM) from 2000–2012, due to unavailability of snow cover time series covering the entire period 1948–2009. Thus, our analyses do not capture the signal of warming-induced reduction of snow cover over the most recent decades (ACIA, 2005). Despite this limitation, the introduction of seasonal snow coverage is an effort to increase the realism of the model representation of the NE region, where snow prevails during several months per year.

MODIS albedo data (MCD43C3) for 2005 is used to determine the mean monthly albedo of each PFT (Jin 2003a, b; Salomon et al. 2006). It is assumed that the albedo remained unchanged during 1948–2009 due to the unavailability of time series data. The monthly albedo of each PFT is then used as PFT-specific parameters.

4.3.3.3 Data for model evaluation

EC data are used to calibrate the TEM-AL2 ET algorithms and evaluate the performance of the TEM-AL1 algorithms and satellite products. Data of latent heat fluxes, air temperature, precipitation, relative humidity, and incoming shortwave radiation are collected from 13 sites (Table 4.1). An Artificial Neural Network method (Papale 2003) is used to fill any gaps in the data caused by system failure or data rejection. The half-hourly air temperature, relative humidity, latent heat flux, and incoming shortwave radiation are averaged, and the half-hourly precipitation is summed to get monthly values. In addition, monthly ET estimates from MODIS (Mu et al. 2011) and from GLEAM are used for comparisons to site-level ET estimates by the TEM.

Gridded ET estimates extracted from the global results of PM-Mu ET in Vinukollu et al. (2011), the EVAL (Mueller, 2013), MODIS-ET, and GLEAM are also used to evaluate the spatial magnitude and variability of the TEM-AL2 estimates across the NE domain. Both PM-Mu ET (Vinukollu et al. 2011) and MODIS-ET (Mu et al. 2011) are based on modifications of the Penman-Monteith approach by Mu et al. (2007). On the other hand, GLEAM uses a Priestley-Taylor approach with evaporative constraints based on satellite-derived soil moisture and vegetation water content (Miralles et al. 2011a, b). The dataset by the LandFlux-EVAL initiative consists of a merger of 14 different ET datasets and the mean of the merged datasets is used in this study (Mueller et al. 2013).

4.3.4 Model parameterization

Many parameters involved in the TEM-AL2 are defined from literature values (e.g., Shuttleworth 1992, ASCE 1996, Mu et al. 2007, 2011). However, some parameters such as the relative sensitivity of soil moisture to vapor pressure deficit (β), specific leaf area (SLA), mean potential stomatal conductance per unit leaf area (CL), and coefficients for calculating the net emissivity between the atmosphere and the ground (ae, be) for each PFT need to be calibrated using EC measured evaporation fluxes. For ecosystems that have more than one EC site, we conduct "leave-one-out" cross validation (Zhang 1993) to yield one set of parameter combinations by PFT.

4.3.5 Site-level evaluation

Comparisons of site-level estimates of ET from TEM-AL1 and TEM-AL2 against measured ET at the 13 EC sites demonstrate that the calibrated TEM-AL2 (Fig. 4.2) systematically outperforms the TEM-AL1. The parameterization of TEM-AL2 to latent

heat flux data measured at EC sites for various PFTs allows consideration of effects of different land characteristics on AED, and subsequently ET, whereas TEM-AL1 considers only changes in climate conditions when estimating AED. TEM-AL2 ET captures the seasonality of the measured ET well at all sites (Fig. 4.2). The ratio of ET to precipitation (i.e., ET/P) from TEM-AL2 ET is very close to that measured at the EC sites (Table 4.1). An average root mean square difference (RMSD) of 8.54 mm mon-1, Nash–Sutcliffe model efficiency coefficient (NS) of 0.81, mean percent difference (MPD) of 8.96%, and Pearson correlation coefficient (r) of 0.95 across all sites (Table 4.5) indicate that the TEM-AL2 ET compares reasonably well with field measurements. In contrast, TEM-AL1 overestimates ET during summer for the majority of the locations, mostly due to the overestimation of AED in summer (Liu et al. 2013). After calibration, TEM-AL2 ET estimates are also closer to the EC measurements than MODIS-ET (average RMSD, NS and r of 15.26 mm mon-1, 0.51, and 0.90, respectively) and GLEAM (average RMSD, NS and r are 12.86 mm mon-1, 0.62 and 0.91, respectively). Generally MODIS overestimates ET in summer relative to EC measurements (Fig. 4.2), while GLEAM matches the seasonal patterns of measurements well at most sites although it overestimates the ET during the summer at the xeric shrublands site (Ivotuk) and the tundra wetland site (SEFaj).

4.3.6 Evaluation of the spatiotemporal variability of ET

All of the aforementioned satellite-based products (MODIS-ET, GLEAM, EVAL, PM-Mu ET), TEM-AL1 and TEM-AL2 report ET estimates for upland ecosystems, whereas only TEM-AL2 and GLEAM account for ET (or evaporation) from snow, water

bodies and wetlands. For consistency, we use the TEM-AL2 ET estimates for only upland ecosystems in the assessment of their spatial distribution by comparison to TEM-AL1 ET and the above mentioned satellite products.

Overall, the average ET estimated by TEM-AL2 for NE is 270.1 mm yr-1 during 2000-2009, slightly lower than the 298.5 mm yr-1 estimated by GLEAM and the 303.3 mm yr-1 estimated by EVAL, and much lower than the 341.4 mm yr-1 estimated by TEM-AL1. In contrast, the PM-Mu ET estimates by Vinukollu et al. (2011) are substantially lower than the other ET estimates in NE (Fig 4.3), which is consistent with the evaluation by Vinukollu et al. (2011) that showed a sizeable negative bias in that product. The high TEM-AL1 ET estimate is mainly due to the overestimation of ET in summer months (the difference between TEM-AL1 ET and TEM-AL2 ET decreases from 28.4% to 9.5% when ET from JJA is not considered). The spatial distribution of TEM-AL2 ET matches well with that of GLEAM, EVAL and MODIS-ET (Fig. 4.3), with r values ranging from 0.79 to 0.92 (Fig. 4.4).

The seasonal variability of TEM-AL2 ET shows good agreement with EVAL and GLEAM (Fig. 4.5), as reflected by the RMSD (4.7 mm mon-1 for EVAL, 5.77 mm mon-1 for GLEAM) and the MPD during the growing season (May-Sep., 8.71% for EVAL, 10.73% for GLEAM). TEM-AL1 ET and PM-Mu ET show different seasonalities from TEM-AL2 ET (Table 4.6). With respect to TEM-AL1 ET, the difference is primarily due to the above-mentioned overestimation of ET in summer. In the case of PM-Mu-ET, the difference is most likely due to the large negative bias in summer as indicated by Vinukollu et al. (2011).

The general agreement between the calibrated TEM-AL2 ET and the ET estimates from satellite-based products provides extra confidence in the ability of TEM-AL2 to estimate spatial and temporal variations in ET across NE. In the following sections, TEM-AL2 is used to examine how recent changes in climate in NE have influenced ET, water availability (P-ET) and river discharge in NE between 1948 and 2009.

4.4 Results

4.4.1 Variation of ET in NE for 1948–2009

The ET varies greatly among uplands, wetlands and water bodies. The highest ET rates occur in water bodies (776-802 mm yr-1), followed by wetlands (241-281 mm yr-1) and uplands (231-267 mm yr-1). The variation of ET among land covers is not just caused by the different algorithms and parameters used to estimate ET for each cover type or moisture supply, but also differences in climatic conditions. The mean incoming solar radiation (R) for water bodies is estimated as 29.37 W m-2 higher than for uplands and 48.66 W m-2 higher than for wetlands. The mean annual T experienced over water bodies is about 4°C higher than for uplands and 9°C higher than for wetlands, while the mean VPD for water bodies is 2.83 hPa higher than for uplands and 3.81 hPa higher than for wetlands. These differences in climatic conditions occur because most water bodies are located in the southern edge of NE (Fig. 4.1d) whereas most wetlands are located in the northern parts of NE (Fig. 4.1c). In addition, the albedo of water bodies is also lower than that of uplands (see Shuttleworth, 1992), which leads to more available energy for evaporation. These climatic differences, the unlimited availability of water and the use of

different ET algorithms for open-water evaporation (see Section 4.3.2 and Table 4.2) explain why the ET from water bodies is ~3 times that of uplands and wetlands. These open-water ET estimates are comparable to previous estimates from the adjacent Caspian Sea and Black Sea (Froehlich 2010; Romanou et al. 2010). On the other hand, the difference in ET between uplands and wetlands is small, due to the positive effects on ET of a larger T and R in uplands being offset by the constraint of soil-water limitations.

Within the uplands, ET varies among the different plant functional types (Fig. 4.6): temperate coniferous forests (402.8 mm yr-1), temperate deciduous forests (388.9 mm yr-1), grasslands (289.6 mm yr-1), xeric woodlands (276.8 mm yr-1), boreal forest (232.2 mm yr-1), wet tundra (187.2 mm yr-1), xeric shrublands (175.9 mm yr-1) and alpine tundra/polar desert (129.8 mm yr-1). Again, this is largely explained by the differences in climate experienced by the different PFTs (Table 4.7), with higher ET in areas of higher energy (i.e., R, T) and moisture supply (i.e., P). While ET in the northern NE is mainly limited by energy, ET in the southern NE seems more constrained by moisture supply. For example, xeric shrublands in the southern landscapes receive large amounts of energy (high T and R), but low P such that ET is limited by moisture availability. In contrast, alpine tundra/polar deserts receive relatively more P, but small amount of energy (low T and R) such that ET is mainly limited by energy.

The (area-weighted) ETa over NE presents a small increasing trend of 0.13 mm yr-2 ($p < 0.05$) from 1948 to 2009 (Fig. 4.7). The average ETa/P ratio of 63.6% is comparable to global ratios reported in previous studies (e.g., Vörösmarty et al. 1998; Miralles et al. 2011a). All three land covers show small but statistically significant ($p < 0.05$) positive trends in ET (0.09 mm yr-2 for uplands, 0.26 mm yr-2 for wetlands and

0.12 mm yr-2 for water bodies). These changes are consistent with the slight increases in T over this period ($p < 0.05$): 0.03 °C yr-1 for the uplands, 0.02 °C yr-1 for the wetlands and 0.03 °C yr-1 for the water bodies. No significant trends were detected for P, R and C. The increase in T leads to an increase in vapor pressure deficit (VPD, Fig. 4.7), also an increase in the slope of saturation vapor pressure curve (Δ), a decrease in aerodynamic resistance by promoting turbulences in the surface layer, and a decrease in the stomatal resistance by elevating the minimum air temperature. All these processes are accounted for in our representation of ET in TEM-AL2 (Table 4.2). These temperature-related changes result in an increase of ET. The ET increased for all PFTs in the NE domain – except for xeric woodlands. Boreal forests are the main contributor to ET increase due to the largest area percentage (30.8%) and the highest increasing trend (0.15 mm yr-1 yr-1).

Across NE, the general spatial pattern of ETa does not change significantly over time (Fig. 4.8a). The ETa gradient from the north to mid-latitudes of the domain is almost unchanged from the 1950s to 2000s, with the highest ETa in the southwest, the southeast and the south-central, where temperate forests and water bodies are abundant. In contrast, although magnitudes of local temporal changes in ETa (i.e. ΔETa) are small relative to ETa, the spatial pattern of ΔETa differs across the region (Fig. 4.8b). The large increases of ETa in the southwest and the large decreases of ETa in the southeast are consistent with the corresponding changes of precipitation in these areas (also see John et al. 2013). Meanwhile, ETa presents an overall increasing trend across the NE except the south and north central part (Fig. 4.9). The trend pattern of ETa generally matches well with that of T and P, and it is a consequence of trade-off between individual effects of climate variables (e.g., P, T, R and VPD) on ETa. For example, in the southeast, where P is

declining and T is increasing, ETa presents a declining trend as the negative effects of limited water supply on ETa overshadows the promotion of ETa by warming.

4.4.2 Implications of ET variation for water availability

Changes in ET over time and space may lead to a regional intensification or weakening of the water cycle (Hungtington 2006; Bates et al. 2008), with direct implications for the recycling of precipitation, generation of runoff and ground water recharge. Overall, P–ETa in the southern part is lower than that in the north (Fig. 4.8a), as P is lower and ETa rates are larger due to warmer climate conditions and more radiation in the south.

Changes in P–ETa (i.e. Δ(P–ETa)) for 1948–1999 vary across the NE domain (Fig. 4.8b), but no significant trends ($p>0.05$) are identified for the entire domain (Fig. 4.7). The western part of the domain experiences a mild increase in P–ETa whereas negative trends occur in the east. These results are consistent with observational studies that the climatic conditions in the western part of the high latitudinal NE domain became more humid during the 20th century, whereas drier weather conditions prevailed east of the Ural Mountains (Groisman et al. 2010; John et al. 2013). The opposite trends in P–ETa in the eastern and the western parts of the region offset each other, such that there is no significant trend in the regional water availability over the study period. However, the spatial pattern of P–ETa remains nearly unchanged from the 1950s through the 2000s.

Changes in water availability are related to changes in runoff and river discharge. Our simulations indicate that the annual mean volumetric soil moisture varied little from year to year in the NE and does not show a significant long-term trend. These changes in

soil water storage over the long periods of this study are insignificant compared to the volumes of P and ETa. As subsurface flow out of the NE watersheds is also considered to be negligible, then most of the available water will runoff from the watershed and contribute to river discharge. TEM-AL2 estimates of P–ETa are analyzed for the six largest river watersheds in NE: Kolyma, Lena, Yenisei, Ob, Pechora and Northern Dvina (Fig. 4.1). These six Eurasian arctic rivers drain about two-thirds of the Eurasian arctic landmass (Peterson et al. 2002). The runoff for each watershed is estimated by aggregating the grid cell level estimates of P–ETa across the watershed area. Subsequently, runoff estimates from the six watersheds are aggregated to obtain the total river discharge for the six watersheds for the period 1948-1999. Aggregated values are compared to river discharge gauge measurements from the Global Runoff Data Centre (GRDC) and those by Peterson et al. (2002).

The estimates of aggregated river discharge for the six largest watersheds in NE from TEM-AL2 are much closer to the aggregated discharge measurements from the GRDC and Peterson et al. (2002) than those from TEM-AL1 (Fig. 4.10). Taking the mean discharge from the GRDC and Peterson et al. (2002) as reference, the errors associated with TEM-AL2 (RMSD = 126.23 km3 yr-1, MPD = -4.02%) are much lower than those of TEM-AL1 (RMSD = 527.74 km3 yr-1, MPD = -28.5%). Most of the underestimation of discharge by TEM-AL1 has to do with the overestimation of TEM-AL1 ET (Section 4.3.5). Therefore, improvements in the estimation of ET by TEM-AL2 also lead to more realistic estimates of long-term river discharge.

To better understand why TEM-AL2 substantially outperforms TEM-AL1, we conducted a simulation experiment using four grid cells that represent all possible land

cover compositions in the NE (Table 4.8). These four grid cells at quite different locations across NE have been randomly chosen (Fig. 4.3a). Three grid cells are dominated by either uplands, wetlands, or water bodies, respectively, and the fourth grid cell has mixed land cover types. For each grid cell, we conduct a TEM-AL1 simulation and five TEM-AL2 simulations assuming different land cover compositions and snow scenarios: 1) the prescribed fraction coverage of uplands, wetlands and water bodies in the cell with snow dynamics; 2) the same prescribed fraction coverage as 1) but assuming no snow; 3) assuming 100% uplands without snow; 4) assuming 100% wetlands without snow; and 5) assuming 100% water bodies without snow. The ET estimates from these 5 scenarios are hereafter referred to as ETa, ETa0, ETu0, ETt0 and ETw0, respectively, to be consistent with previous notations. The TEM-AL1 ET is much higher than ETa across all 4 cells. These results indicate that the use of the Penman-Monteith based equation that has been calibrated to various land cover characteristics in the region will estimate a lower ET, more available water and consequently a higher runoff than the Jensen-Haise formulation. Moreover, ETa is systematically lower than ETa0 across the 4 cells. Consequently, P–ETa will be much higher and more runoff will occur. This highlights the role of snow on limiting ET in the NE region. In addition, differences among ETu0, ETt0 and ETw0 in each grid cell emphasize the effects of land cover heterogeneity on ET estimation and imply that the omission of wetlands and water bodies might cause ET to be underestimated in NE.

The estimation of ET and runoff in NE has been substantially improved by taking into consideration the influence of land cover characteristics and heterogeneity on AED and ET. Most current ET estimation schemes, however, do not explicitly consider the

detailed ET processes examined in this study (Mengelkamp et al. 2006; Mueller et al. 2013) and may lead to large bias in ET and runoff. This is especially significant for the NE region as snow, wetlands and water bodies play important roles in the hydrological processes (ACIC, 2005). Although snow sublimation accounts for a small portion of the total ET (mostly <8%, Fig. 4.11), consideration of snow dynamics limits the magnitude of total ET and improves the realism of ET representation in NE where snow prevails during several months in a year.

Unlike previous studies (e.g., Groisman et al. 2010; Peterson et al. 2002), no significantly positive trends in river discharge in the NE have been simulated by the TEM. The consistent underestimation of aggregated discharge after 1970 implies that there might be some other water sources or water dynamics that increase river discharge that are not being considered, such as the melting of glaciers, the thawing of permafrost, inter-basin transfer, land-use change and fire disturbances (Adam et al. 2007, 2008; McClelland et al. 2004). In addition, biases in ET estimation will also lead to systematic biases in estimating river discharge. Our ET estimation may be biased by the lack of consideration of CO2 effects on stomatal conductance, the use of a seasonal climatology for wind speed and snow cover, the assumption of unlimited water supply for ET in wetlands, and the assumption of a constant land cover.

4.5 Conclusions

The ET response to the changing climate in the NE and its implications for water availability and river discharge from 1948 through 2009 have been explored using an improved version of the TEM that incorporates more ET processes (i.e., canopy

interception loss, evaporation from wet land surfaces, evaporation from water bodies and wetlands, and snow sublimation) and considers the influence of a heterogeneous land cover on ET. Comparisons of model results to in situ measurements of ET and satellite products demonstrate that the improved algorithms captures the spatiotemporal changes of ET in NE substantially better than the previous version of TEM, which did not consider the influence of land characteristics on atmospheric evaporative demand (AED). Our results suggest that ET has increased during our study period as a consequence of the concurrent slight rise in air temperature.

Improvements in the estimation of ET have caused more water to be available for runoff, which has also led to improvements in model estimates of river discharge. These improvements mainly result from a reduced AED estimate by the new algorithms and the influence of snow cover on limiting ET. Consideration of wetlands and water bodies in the landscape leads to higher ET estimates in the NE than if the presence of these wet land covers is ignored. Finally, our analyses indicate that latent heat fluxes measured at eddy-covariance flux sites provide useful information for improving the simulation of regional hydrometeorology by land surface models.

4.6 Acknowledgements

This research is supported by the NASA Land Use and Land Cover Change program (NASA- NNX09AI26G, NN-H-04-Z-YS-005-N, and NNX09AM55G), the Department of Energy (DE-FG02-08ER64599), the National Science Foundation (NSF-1028291 and NSF- 0919331), the NSF Carbon and Water in the Earth Program (NSF-0630319), and the Dynamics of Coupled Natural and Human Systems (CNH) Program of the NSF (#1313761).. We also acknowledge the Global Runoff Data Centre for provision of the gauge station data. Runoff data in Peterson et al. (2002) were obtained from the R-ArcticNet database. A special acknowledgment is made here to Prof. Eric Wood for his generous provision of the ET datasets of Vinukollu et al. (2011), and to Dr. Brigitte Mueller and Dr. Martin Hirsci for the provision of the LandFlux-EVAL dataset of Mueller et al. (2013). Diego Miralles acknowledges the support by the European Space Agency WACMOS-ET project (4000106711/12/I-NB).

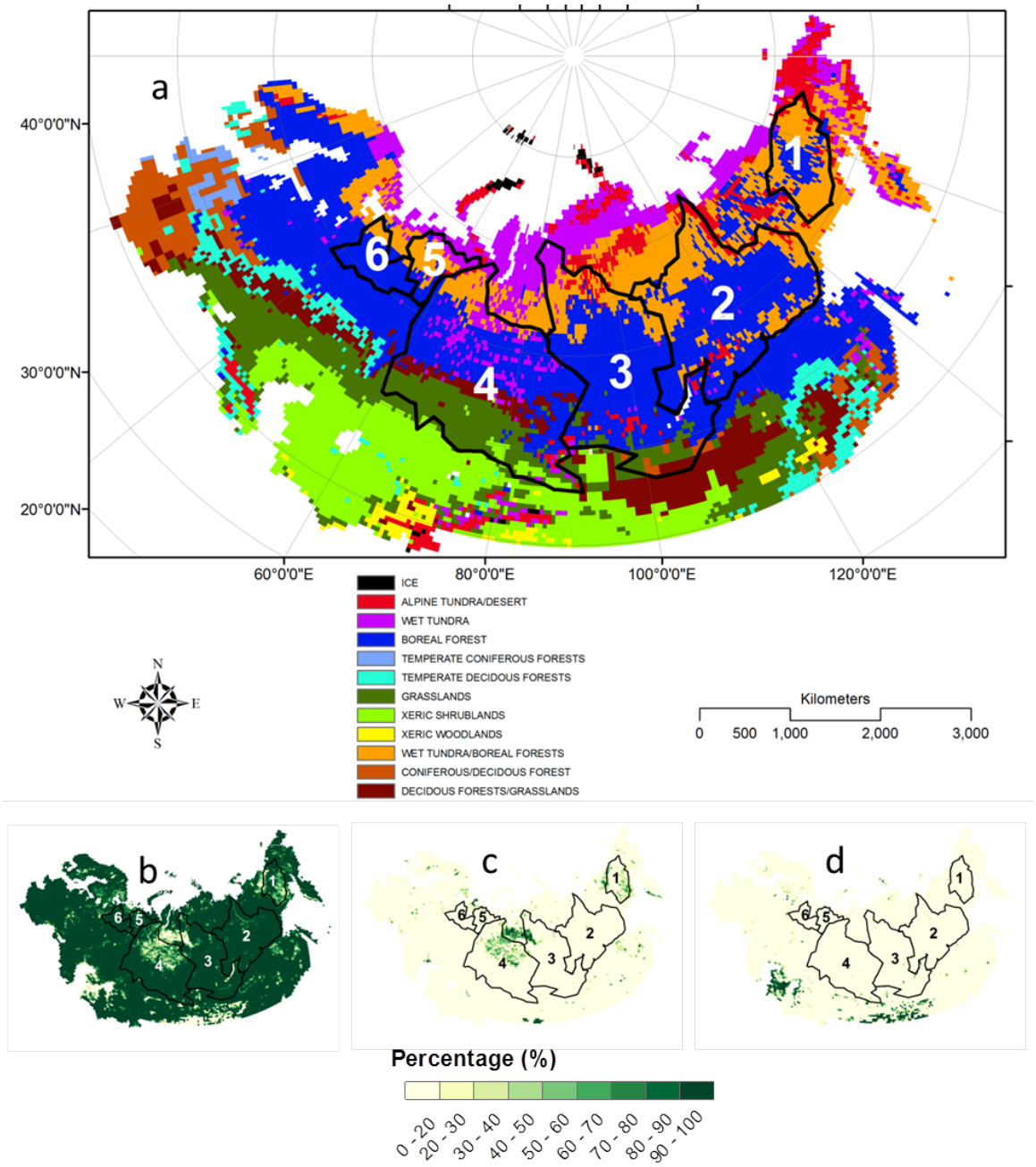

Figure 4.1 Distribution of plant functional types in NE domain (a), and fractional coverage of upland ecosystems (b), wetlands (c) and water bodies (d). The boundaries of six major river watersheds in the NE domain are delineated, 1 , 2, 3, 4, 5 and 6 within the boundaries stand for Kolyma, Lena, Yenisei, Ob, Pechora and Northern Dvina watershed, respectively.

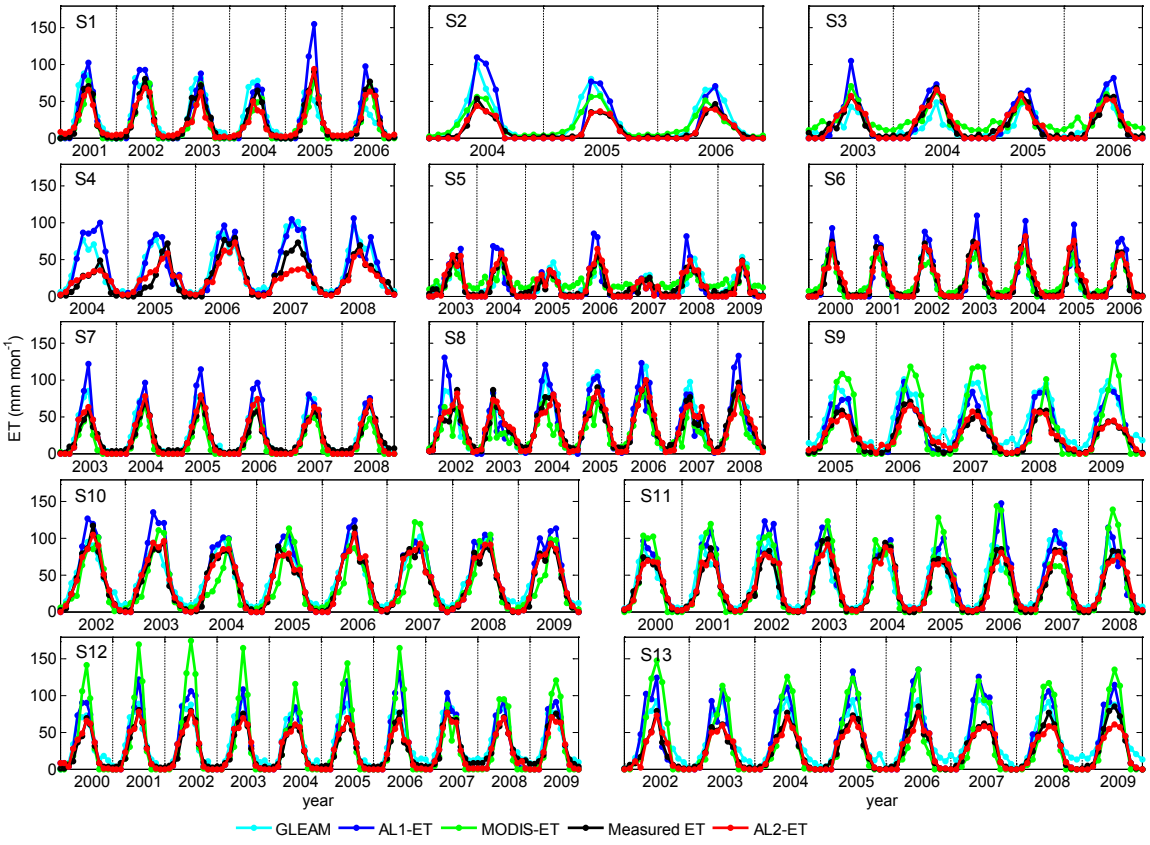

Figure 4.2 Comparison between measured ET, AL1-ET, AL2-ET, MODIS-ET and GLEAM at 13 EC sites. Site codes (S1-S13) are corresponding to those in Table 4.1.

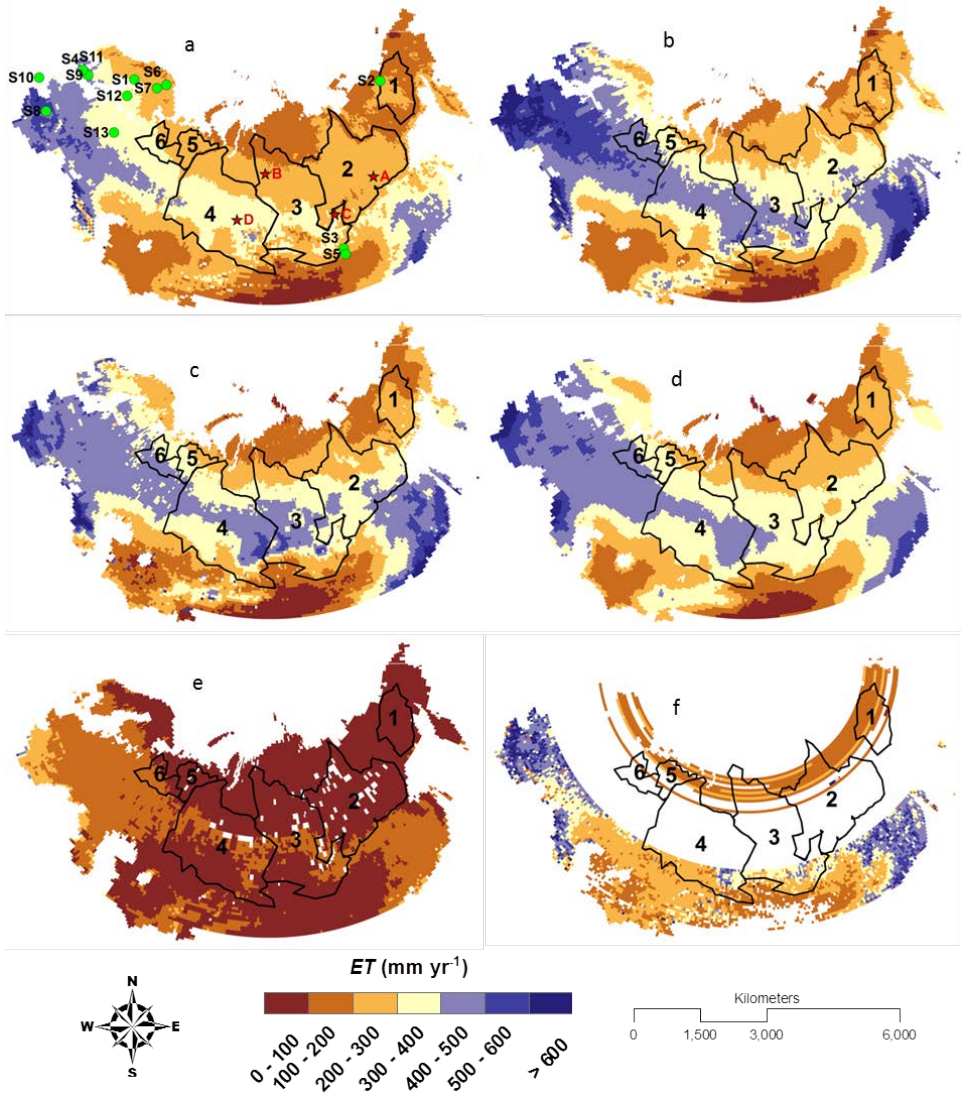

Figure 4.3 Spatial patterns of average annual *ET* for uplands in the NE estimated by TEM and several satellite products: a) TEM-AL1 *ET* during 2000–2009, b) TEM-AL2 *ET* during 2000–2009, c) GLEAM (Global Land-surface Evaporation: the Amsterdam Methodology) during 2000–2009, d) the mean of LandFlux-EVAL merged synthesis product during 2000–2005, e) PM-Mu *ET* during 2000–2007 in Vinukollu et al. (2011) and f) MODIS-ET during 2000–2009. Areas with missing values or filled values are blanks on the map. The boundaries of six major river watersheds in the NE are delineated; 1, 2, 3, 4, 5 and 6 stand for Kolyma, Lena, Yenisei, Ob, Pechora and Northern Dvina watershed, respectively. The 13 EC sites and the four grid cells used for the simulation experiment are also shown on a), where EC site codes (S1-S13) and cell codes (A-D) correspond to those in Table 4.1 and Table 4.8, respectively. Note that the boundaries and numbers remain the same for all maps in this study.

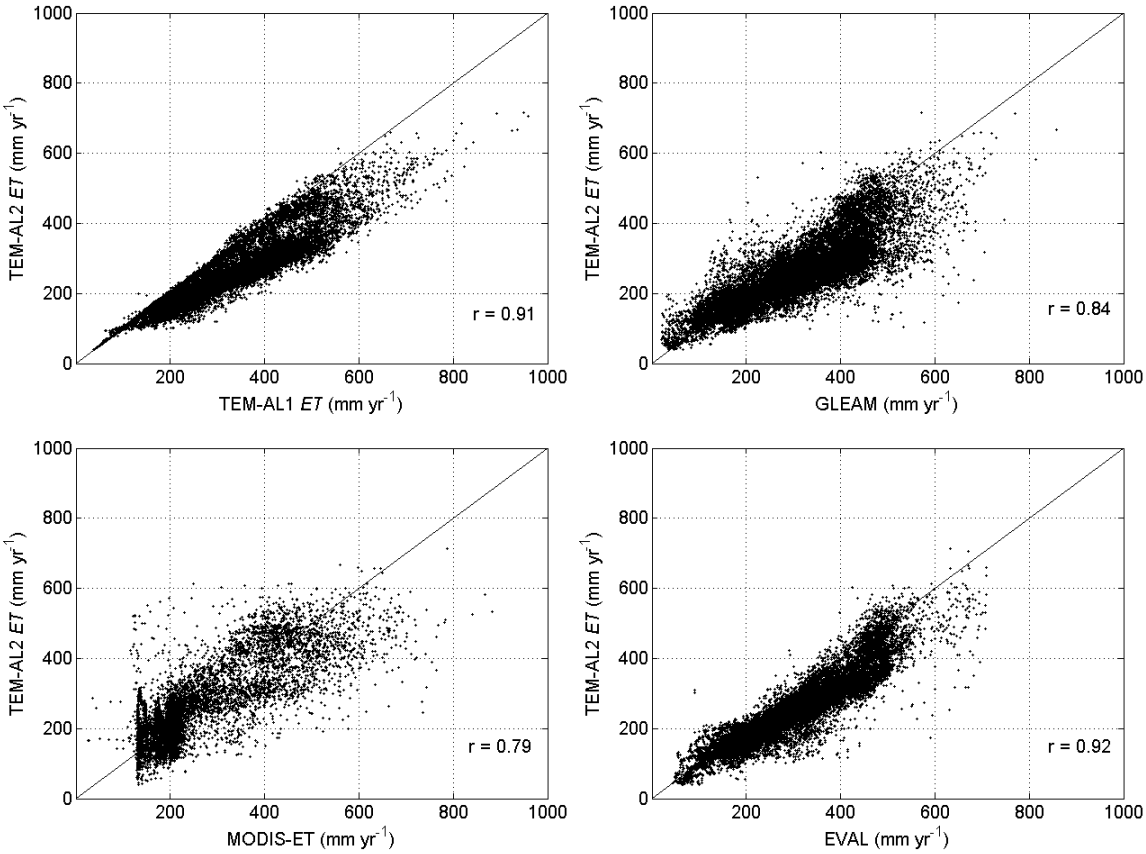

Figure 4.4 Comparison of annual TEM-AL2 *ET* with TEM-AL1 *ET*, GLEAM, MODIS-*ET* and EVAL, Pearson correlation coefficients (r) are listed. Note that *ET* estimates used here are the same as those listed in Figure 4.3.

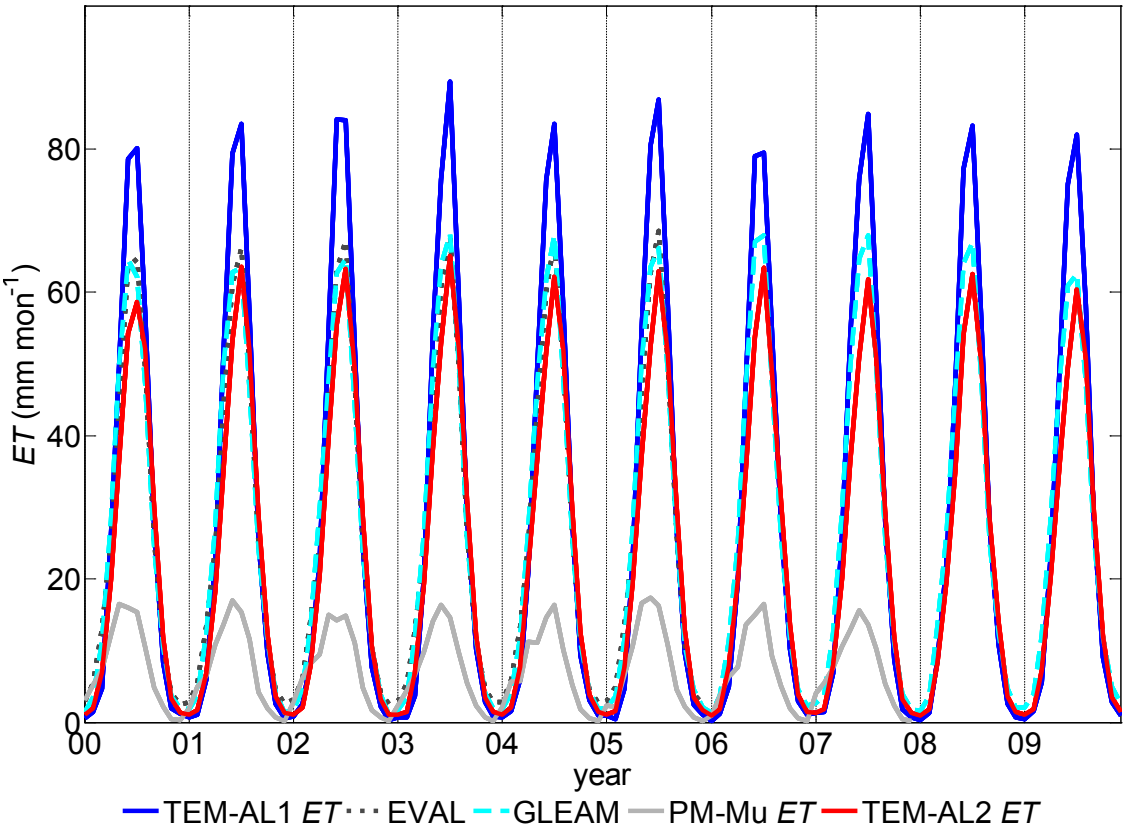

Figure 4.5 Comparisons among seasonal estimates of TEM-AL1 *ET*, EVAL, GLEAM, PM-Mu *ET* and TEM-AL2 *ET* in NE during 2000-2009. MODIS-ET is not involved in this comparison because its *ET* estimates are either filled values or missing values for ~54% of the domain.

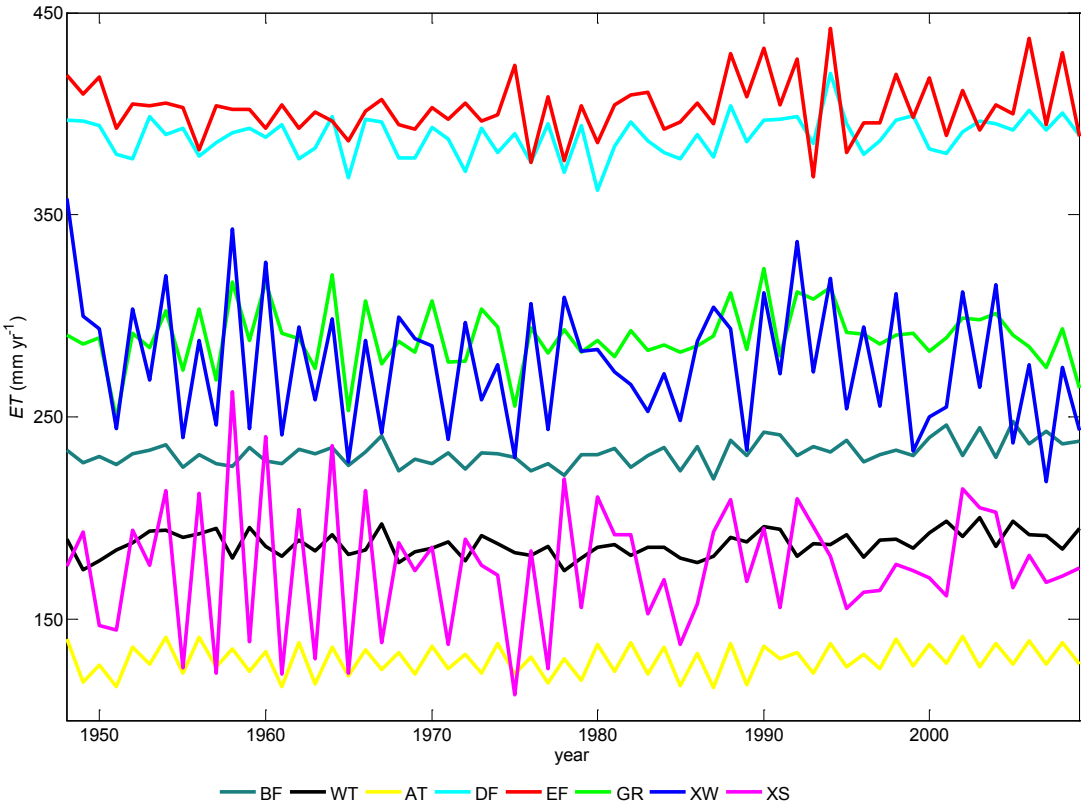

Figure 4.6 Comparison of annual *ET* estimates among different PFTs from 1948 to 2009. BR: boreal forest; WT: wet tundra; AT: alpine tundra/polar desert; DF: temperate deciduous forests; EF: temperate coniferous forests; GR: grasslands; XW: xeric woodlands; XS: xeric shrublands.

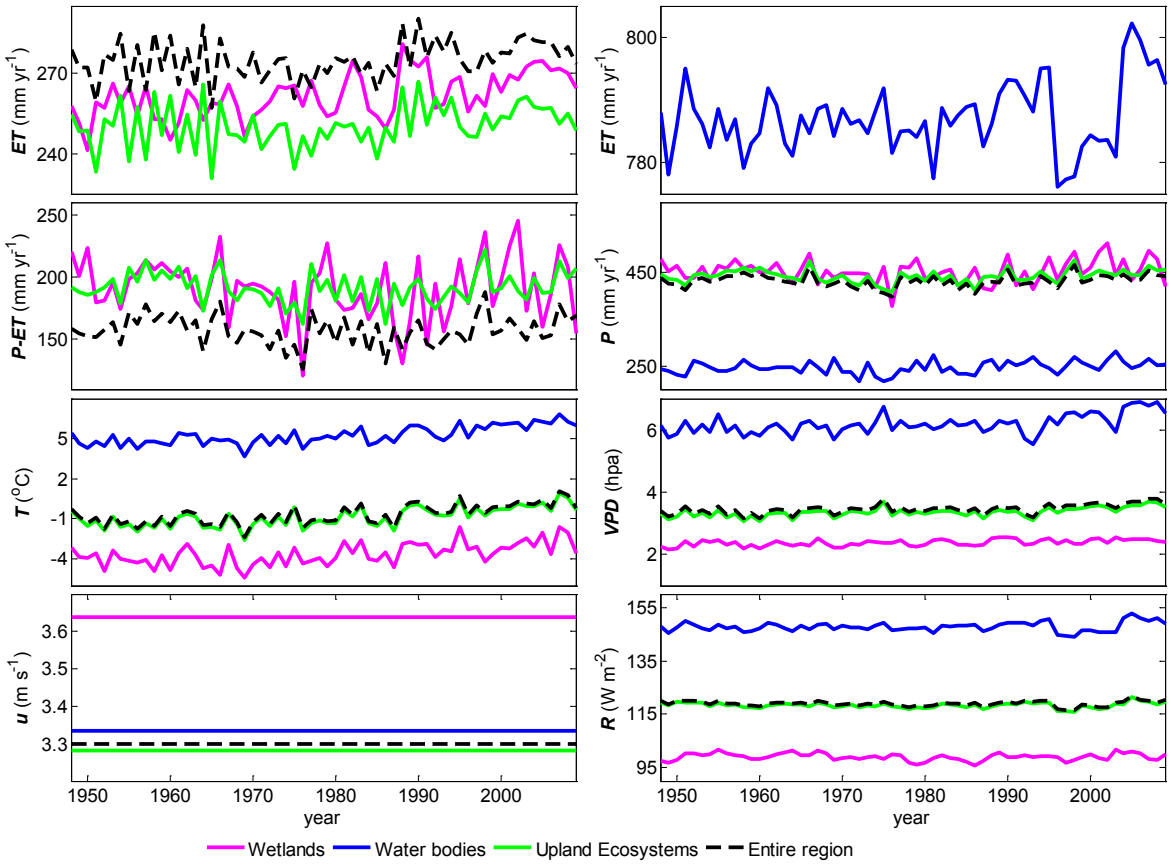

Figure 4.7 Inter-annual variability of *ET*, *P–ET* and selected climate variables for the entire NE region, and for the various land covers (uplands, wetlands and water bodies) within NE.

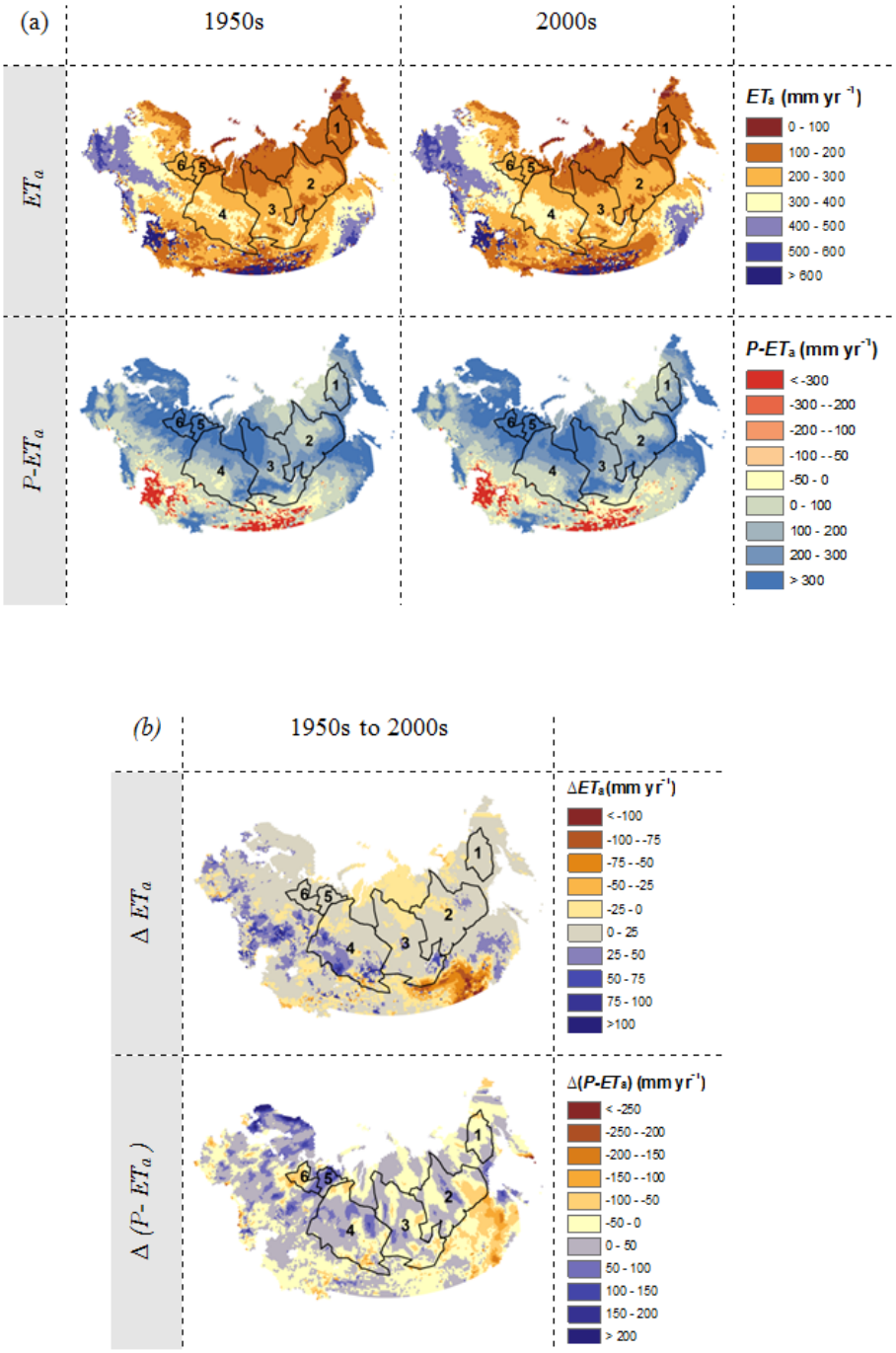

Figure 4.8 Average spatial patterns for (a) the aggregated *ET* (i.e. ET_a) and $P–ET_a$ in the 1950s and the 2000s, and (b) change of ET_a (i.e., $\Delta\ ET_a$) and change of $P–ET_a$ (i.e., $\Delta(P–ET_a)$) from the 1950s to the 2000s

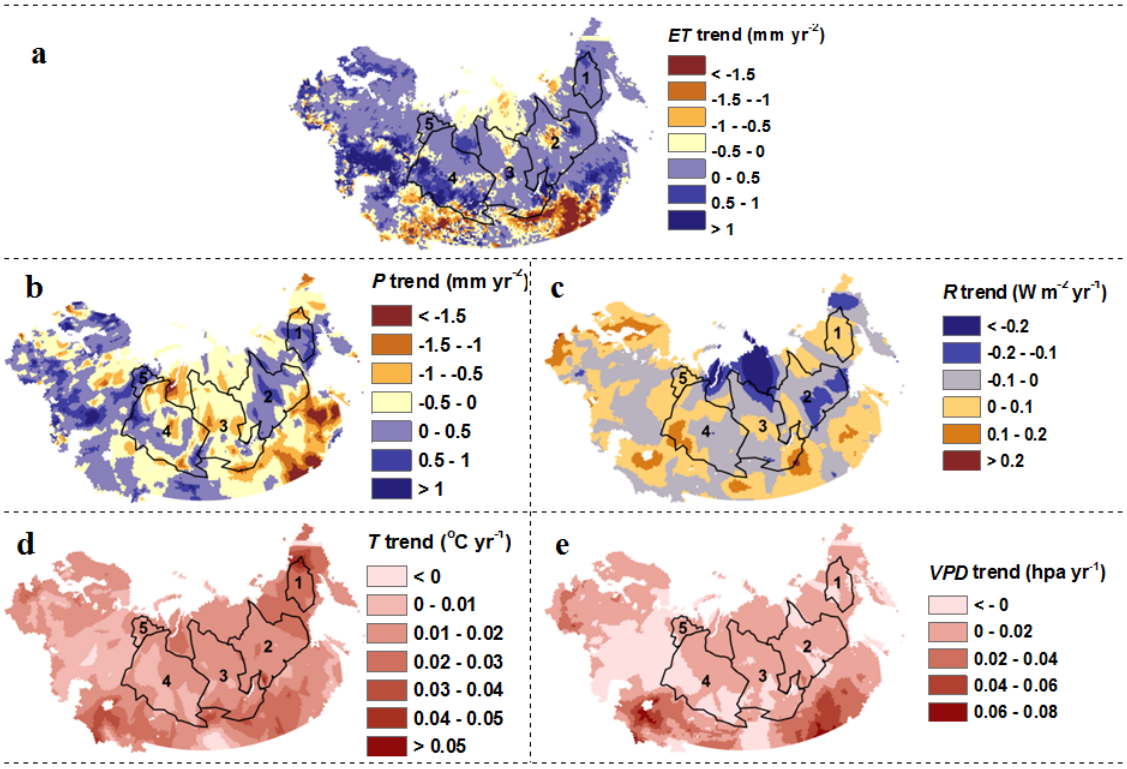

Figure 4.9 Spatial variability of trends in ET_a and climate variables during 1948-2009 across NE: a) ET_a, b) precipitation (P), c) incoming solar radiation (R), d) air temperature (T), and e) vapor pressure deficit (VPD).

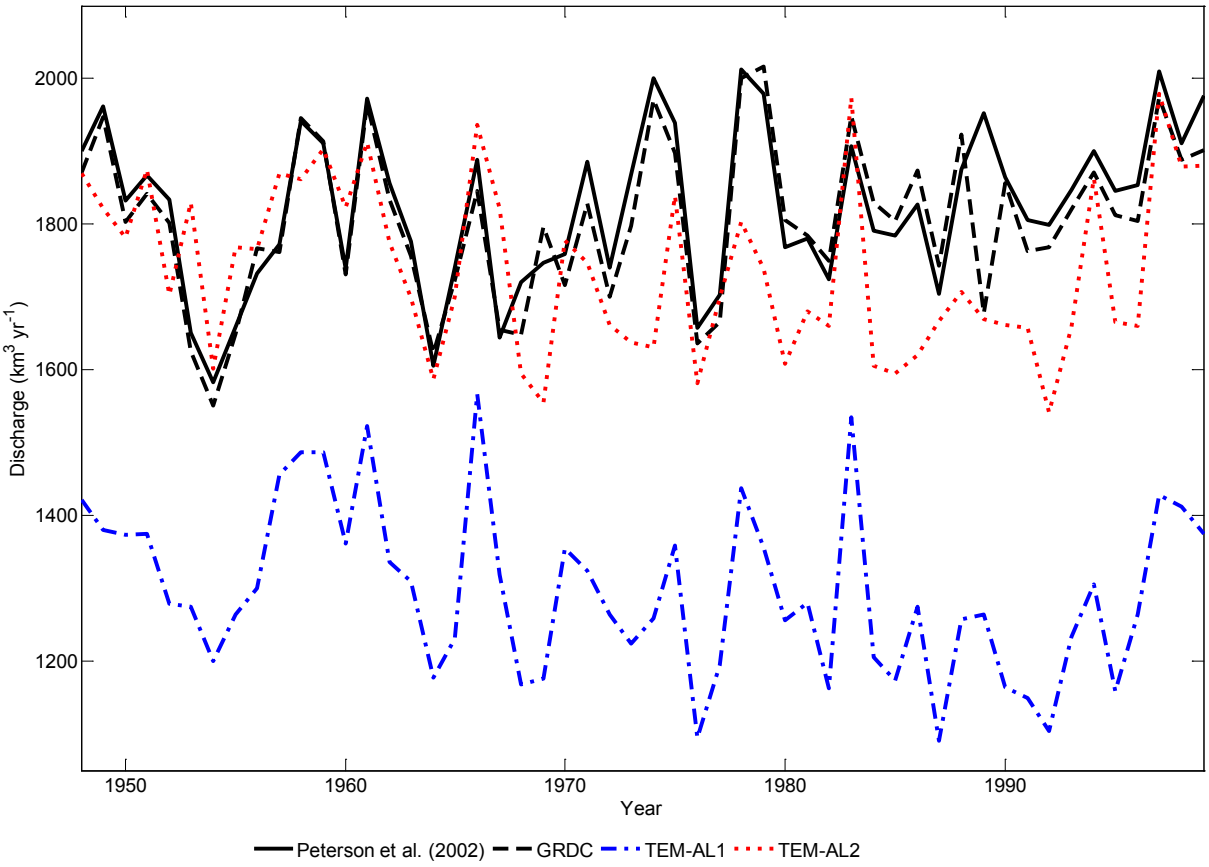

Figure 4.10 Discharge from the six largest watersheds in the NE during 1948–1999 as estimated by TEM and previous studies.

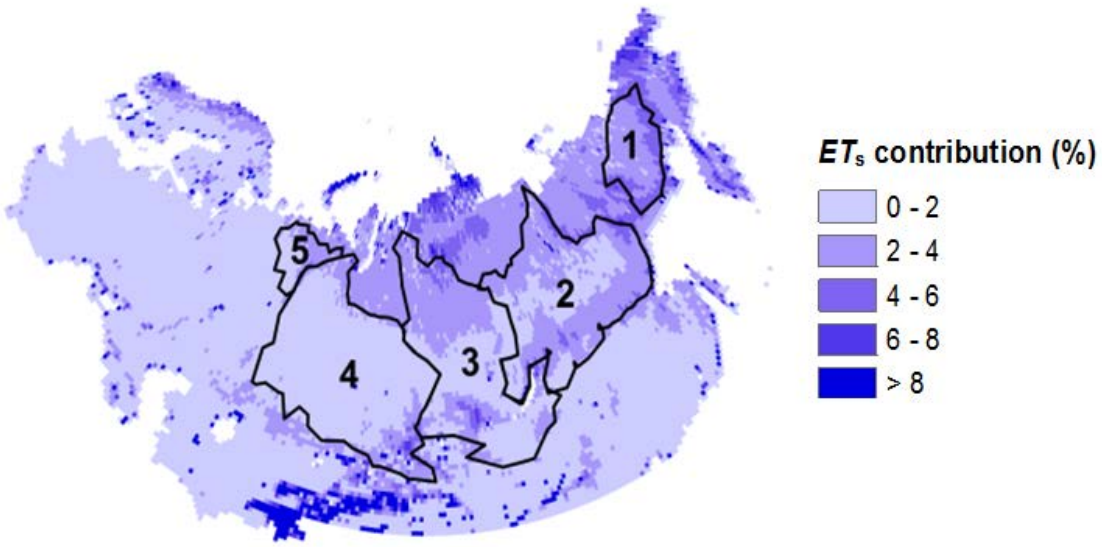

Figure 4.11 Spatial variability of long-term average contribution of snow sublimation (ET_s) to total ET (ET_a) during 1948-2009 across NE.

Table 4.1 Site information for the eddy-covariance (EC) towers used in the parameterization of TEM-AL2.

PFT	Site name	Site code	Location	Measurement period	Average ET (mm yr^{-1})	ET range (mm yr^{-1})	Average *ET/P*	Average TEM-AL2 *ET/P*
Tundra wetland	SEDeg	S1	19.56° E,64.18°N	2001-2006	245.78	193.13-311.82	55.8%	55.8%
Xeric shrublands	Ivotuk	S2	155.75° W,68.48° N	2004-2006	186.38	162.61-227.28	75.9%	63.5%
Boreal forest	SKT	S3	108.7° E,48.3° N	2003-2006	220.83	202.36-255.8	84.9%	88.5%
Grasslands	DKLva	S4	12.08° E,55.68° N	2004-2008	330.97	210.95-469.78	56.7%	51.3%
Grasslands	KBU	S5	108.7° E,47.2° N	2003-2009	181.39	133.81-227.44	90.5%	93.4%
Tundra wetland	FIKaa	S6	27.29° E, 69.14° N	2000-2006	241.4	183.01-285.43	54.4%	58.3%
Coniferous forest	FISod	S7	26.64° E,67.36° N	2003-2008	241.1	222.59-268.13	70.9%	73.4%
Grasslands	HUBug	S8	19.60° E,46.69° N	2002-2008	460.3	380.25-521.81	88.7%	88.2%
Tundra wetland	SEFaj	S9	13.55° E,56.27° N	2005-2009	242.95	216.16-295.72	35.8%	32.8%
Grasslands	ATNeu	S10	11.32° E,47.11° N	2002-2009	474.66	435.47-522.93	67.4%	69.6%
Deciduous forest	DKSor	S11	11.64° E,55.49° N	2000-2008	410.33	358.72-469.06	57.8%	59.6%
Coniferous forest	FIHyy	S12	24.29° E,61.85° N	2000-2009	310.85	253.04-365.16	65.8%	64%
Coniferous forest	RUFyo	S13	32.92° E,56.46° N	2002-2009	303.66	234.42-390.62	59.2%	57.7%

Note: The Ivotuk site is located in Alaska, which is out of the NE domain. It is used in this study is because its location is close to the NE domain, and there is no EC site located in the domain that allows for the parameterization of Xeric shrublands. Average *ET* and the range of *ET* at each site are derived from measurements. Average *ET/P* stands for the average ratio of measured *ET* to precipitation during the measurement period of each site, average TEM-AL2 *ET/P* represents the average ratio of TEM-AL2 *ET* to precipitation during same time period.

Table 4.2 Equations and key parameters used in TEM-AL2 and TEM-AL1. SWB indicates that ET is constrained by soil water balance. In TEM-AL1, ET is derived from potential evapotranspiration (PET) in conjunction with a water balance model (WBM, Vörösmarty et al. 1998; Liu et al. 2013). PET represents the atmospheric evaporative demand (AED), which is not constrained by land characteristics. However, the supply of water for ET in the WBM does depend on biome-specific rooting depths.

TEM-AL2							
Land cover	*ET* processes		equations	variables	key parameters	SWB	references
uplands	transpiration		$\lambda E_{trans} = \frac{(s \times A \times F_c + \rho \times C_p \times VPD \times F_c / r_a) \times (1 - Fwet)}{s + \gamma \times (1 + r_s / r_a)} \times 86400 \times MD$	E_{trans}: transpiration from vegetation canopy (mm mon^{-1}) λ: latent heat of vaporization (J kg^{-1}) s: slope of the saturation vapor pressure curve (Pa K^{-1}) A: available energy (w m^{-2}) F_c: vegetation coverage ρ: air density(kg m^{-3}) C_p: specific heat capacity of air (J kg^{-1} K^{-1}) VPD: vapor pressure deficit (Pa) r_a: aerodynamic resistance r_s: surface resistance Fwet: water cover fraction of land surface γ: psychometric constant (Pa K^{-1}) MD: number of days per month	SLA: specific leaf area C_L: mean potential stomatal conductance per unit leaf area gl_bl: leaf-scale boundary layer conductance a_e: coefficients for calculating net emissivity between the atmosphere and the ground b_e: coefficients for calculating net emissivity between the atmosphere and the ground	Y	Mu et al. (2011); Liu et al. (2013)
	soil evaporation	moist surface	$\lambda E_{moist\_soil} = \frac{(s \times A_{soil} + \rho \times C_p \times VPD \times (1 - F_c) / r_a) \times (1 - Fwet)}{s + \gamma \times r_{tot} / r_a} \times 86400 \times MD \times (\frac{RH}{100})^{VPD}$	E_{moist_soil}: evaporation from moist soil surface (mm mon^{-1}) Asoil: available energy allocated to soil surface (w m^{-2}) r_{tot}: sum of surface resistance and the aerodynamic resistance for vapor transport others are the same as above			
		wet surface	$\lambda E_{wet\_soil} = \frac{(s \times A_{soil} + \rho \times C_p \times VPD \times (1 - F_c) / r_a) \times Fwet}{s + \gamma \times r_{tot} / r_a} \times 86400 \times MD$	E_{wet_soil}: evaporation from wet soil surface others are the same as above			
	canopy interception loss		$\lambda E_{can} = \frac{(s \times A \times F_c + \rho \times C_p \times VPD \times F_c / r_a) \times (1 - Fwet)}{s + \frac{P_a \times C_p \times r_s}{\lambda \times \varepsilon \times r_a}} \times 86400 \times MD$	E_{can}: transpiration from vegetation canopy (mm mon^{-1}) Pa: air pressure (Pa) ε: molecular weight ratio of water to dry air others are the same as above			
wetlands	same as upland		same as uplands	same as uplands	same as uplands	N	Mohamed et al.(2012)
water bodies	evaporation		$\lambda E_{water} = \frac{s \times (R_n - G) + \gamma \times E_a}{s + \gamma} \times 86400 \times MD$	E_{water}: evaporation from water surface (mm mon^{-1}) R_n: net radiation (mm mon^{-1}) E_a: bulk aerodynamic term G: heat flux in the water others are the same as above	NA	N	Penman (1948, 1956)
snow	sublimation		$\lambda E_{sub} = \frac{RA \times 1000}{\lambda_w + K} \times MD$	E_{sub}: sublimation from snow covered surface (mm mon^{-1}) RA: incoming shortwave radiation (MJ m^{-2} d^{-1}) K: latent heat fusion (MJ mm^{-2} d^{-1}) λ_w: latent heat of vaporization of water (MJ mm^{-2} d^{-1})	NA	N	Zhuang et al. (2002)
TEM-AL1							
Land cover	*ET* processes		equations	variables	key parameters	SWB	references
uplands	atmospheric evaporative demand		$PET = [(0.014 \times (1.8 \times T + 32) - 0.37)] \times R_s \times 0.016742 \times MD$	PET: potential evapotranspiration (mm mon-1) T: air temperature (°C) MD: number of days per month R_s: incoming shortwave radiation (Cal cm^{-2} d^{-1})	NA	Y	Zhuang et al. (2002); Liu et al. (2013)
wetlands	NA		NA	NA	NA	NA	NA
water bodies	NA		NA	NA	NA	NA	NA
snow	NA		NA	NA	NA	NA	NA

Table 4.3 Observed data at meteorological stations and eddy-covariance (EC) sites used to assess the CRU TS3.1 dataset (*T* = air temperature, *P* = precipitation, *V* = vapor pressure, *R* = incoming solar radiation, *C* = cloudiness, *RH* = relative humidity, *u* = wind speed). Time series data at different temporal resolutions are resampled to a monthly resolution. ECA&D: European Climate Assessment & Dataset, NMICCA: National Meteorological Information Center of China Administration.

Spatial domain	Datasets	Time span	Temporal resolution	Number of stations	Data source
Europe	*T*	1948–2009	Daily	1637	ECA&D
Europe	*P*	1948–2009	Daily	2718	ECA&D
Europe	*RH*	1948–2009	Daily	192	ECA&D
Europe	*C*	1948–2009	Daily	500	ECA&D
Europe	u	1979–2008	Daily	92	ECA&D
China	*P, T, RH*	1981-2009	monthly	175	NMICCA
NE	*P, T, V, R*	2000-2009	Half hour	12	http://www.asianflux.com, http://gaia.agraria.unitus.it/
Russia	*P,T, V, C*	1966-1970	Multi-year monthly average	86	Reference books on climate of the USSR

Table 4.4 Evaluation of the CRU TS3.1 climate variables (*T* = air temperature, *P* = precipitation, *V* = vapor pressure, *R* = incoming solar radiation, *C* = cloudiness) against observations. For the time series data, values represent the average RMSD and absolute MPD across all meteorological stations and EC sites. For the climatology, values represent the average RMSD and absolute MPD across all the 86 meteorological stations in Russia. RMSD: root mean square difference, MPD: mean percent difference.

	Time series data		**Climatology**	
	Mean RMSD	Mean absolute MPD	Mean RMSD	Mean absolute MPD
T	1.31 (°C mon^{-1})	8.30%	1.45 (°C mon^{-1})	7.82%
P	12.12 (mm mon^{-1})	15.7%	12.27 (mm mon^{-1})	14.94%
V	0.8 (hPa)	8.95%	0.92 (hPa)	12.06%
R	11.28 (W m^{-2})	10.47%	N/A	N/A
C	9.99 (%)	6.74%	15.25 (%)	25.1%

Table 4.5 RMSD, NS, MPD and r for different *ET* products at each EC site. Here a, b, c and d stand for TEM-AL1 *ET*, TEM-AL2 *ET*, MODIS-ET and GLEAM, respectively. RMSD: root mean square difference, MPD: mean percent difference, NS: the Nash–Sutcliffe model efficiency coefficient, and r: Pearson correlation coefficient.

	RMSD (mm mon^{-1})				NS				MPD				r			
	a	b	c	d	a	b	c	d	a	b	c	d	a	b	c	d
ATNeu	13.9	8.5	18.7	11.5	0.8	0.9	0.7	0.9	17.9%	7.8%	-10.1%	16.1%	0.96	0.99	0.86	0.96
DKLva	16.6	11.2	18.4	13.4	0.2	0.7	0.2	0.2	37.8%	-11.5%	N/A	23.4%	0.81	0.92	N/A	0.82
DKSor	15.9	8.6	18.6	15.1	0.7	0.9	0.7	0.8	23.9%	9.3%	13.2%	16.5%	0.95	0.97	0.93	0.91
FIHyy	16.	7.2	27.6	12.9	0.6	0.9	0.2	0.7	39.7%	13.4%	18.4%	18.9%	0.96	0.98	0.92	0.94
FIKaa	9.8	8.7	9.8	7.5	0.9	0.9	0.9	0.9	12.4%	7.9%	-4.5%	-8.4%	0.93	0.94	0.93	0.96
FISod	15.8	9.6	8.6	10.8	0.4	0.8	0.8	0.7	30.7%	13.3%	-14.1%	17.9%	0.95	0.97	0.95	0.95
HUBug	19.4	13.2	15.9	13.6	0.5	0.5	0.7	0.7	10.6%	13.1%	-20.7%	9.3%	0.87	0.91	0.86	0.92
IVOtuk	19.7	4.5	11.1	10.5	0.7	0.9	0.5	0.1	31.8%	2.3%	25.6%	25.8%	0.94	0.96	0.87	0.91
RUFyo	22.2	8.6	16.9	15.9	0.3	0.9	0.1	0.6	49.7%	3.4%	16.0%	21.7%	0.95	0.95	0.92	0.95
SEDeg	14.0	8.5	8.7	15.0	0.7	0.9	0.9	0.7	30.0%	-9.9%	-10.9%	25.7%	0.96	0.96	0.95	0.86
SEFaj	16.1	10.2	25.7	25.0	0.4	0.5	0.1	0.1	37.0%	11.4%	64.8%	29.9%	0.93	0.96	0.87	0.92
SKT	10.	6.1	10.3	9.1	0.7	0.9	0.8	0.8	18.6%	5.7%	10.1%	12.3%	0.95	0.96	0.91	0.86
KBU	11.3	6.2	8.7	7.1	0.5	0.9	0.7	0.8	14.9%	6.3%	14.2%	13.3%	0.87	0.94	0.84	0.89

Table 4.6 Seasonality differences between other *ET* products and TEM-AL2 *ET*. RMSD: root mean square difference, MPD: mean percent difference.

	RMSD (mm mon^{-1})	**MPD (growing season)**
EVAL	4.7	8.71%
GLEAM	5.77	10.73%
TEM-AL1 *ET*	10.77	20.3%
PM-Mu *ET*	20.52	-69.72%

Table 4.7 Mean annual climate conditions (*P* = precipitation, *T* = air temperature, *R* = incoming solar radiation, *VPD* = vapor pressure deficit, *u* = wind speed) for different PFTs during 1948–2009. BR: boreal forest; WT: wet tundra; AT: alpine tundra/polar desert; DF: temperate deciduous forests; EF: temperate coniferous forests; GR: grasslands; XW: xeric woodlands; XS: xeric shrublands.

	P **(mm yr^{-1})**		***T*** **(℃)**		***R*****(W m^{-2})**		***VPD*** **(hPa)**		***u*** **(m s^{-1})**
	Range	Mean	Range	Mean	Range	Mean	Range	Mean	Mean
BF	444.4-548.2	498.9	-6.4 - -2.7	-4.5	197.5-205.5	201.2	2.0-2.2	2.1	3.0
WT	376.8-487.7	434.6	-9.8 - -6.1	-8.1	170.8-181.9	176.4	1.4-1.8	1.6	3.8
AT	354.0-440.5	397.0	-12.1- -8.9	-10.8	194.6-206.9	200.4	1.9-2.2	2.1	3.7
DF	488.9-615.1	549.5	3.4-6.7	5.0	279.1-297.9	289.1	3.4-4.4	3.7	3.3
EF	585.2-797.7	693.3	5.4-8.4	6.9	258.1-289.5	273.7	2.8-3.9	3.2	3.4
GR	311.9-421.6	368.7	1.7-5.5	3.6	297.1-313.7	303.7	3.9-5.2	4.5	3.4
XW	250.7-546.4	355.2	7.8-10.9	9.4	343.6-363.6	355.1	7.2-9.7	8.4	2.6
XS	130.3-242.8	177.6	7.2-10.5	8.9	333.9-356.7	343.3	7.0-9.1	7.9	3.3

Table 4.8 Influence of land cover on *ET* (mm yr^{-1}) and *P–ET* (mm yr^{-1}) at four experimental grid cells. p_u, p_t, p_w, p_{s1} and p_{s2} represent the fractions of uplands, wetlands, water bodies, and snow for the growing season and the non-growing season within each grid cell, respectively. TEM-AL1 *ET* stands for *ET* derived from the previous version of TEM (TEM-AL1), and ET_a and ET_{a0} stand for *ET* aggregated over all land cover types in a grid cell with and without consideration of snow dynamics, respectively. ET_{u0}, ET_{t0}, ET_{w0} stands for *ET* from a grid cell assuming it is covered by 100% uplands, 100% wetlands and 100%water bodies, respectively. Note that all *ET* terms below other than TEM-AL1 *ET* are derived from TEM-AL2.

cell	location	p_u , p_t , p_w	p_{s1} , p_{s2}	TEM-AL1 *ET*	ET_a	ET_{a0}	ET_{u0}	ET_{t0}	ET_{w0}	*P*–(TEM-AL1 *ET*)	$P–ET_a$
A	125.5° E, 58°N	100%, 0%, 0%	19.8%, 97.3%	326.3	173.9	221.8	221.8	242.5	338.5	252.8	405.3
B	88° E, 64.5°N	0%, 99.8%, 0.2%	21.8%, 96.9%	316.4	181.3	228.3	224.9	228.1	313.7	265.2	400.3
C	109.5° E, 55°N	8.6%, 0%, 91.4%	18.1%, 90.7%	374.2	338.4	416.9	307.1	313.5	427.2	1.6	37.4
D	80° E, 55.5°N	70.5%, 6.5%, 23%	0.4%, 74.5%	354.9	342.4	365.4	321.7	370.6	498.2	84.5	77.0

CHAPTER 5 IMPACT OF FORCING DATA UNCERTAINTY ON THE ESTIMATION OF EVAPOTRANSPIRATION IN NORTHERN EURASIA[4]

5.1 Abstract

The ecosystems in Northern Eurasia (NE) play an important role in the global water cycle and the climate system. While evapotranspiration (ET) is a critical variable to understand this role, ET over this region remains largely unstudied. Using an improved version of the Terrestrial Ecosystem Model, we examine the impact that uncertainties in climate forcing data have on the estimation of ET for the period 1979–2008 (based on five widely used datasets), and explore the dominant climatic drivers on ET dynamics in NE. Estimates of regional-average ET vary in the range of 263.5–369.3 mm yr-1 depending on the choice of forcing data, a range of variability that corresponds to as much as 31% of the mean ET. On the other hand, the long-term average spatial patterns of ET across the region are generally consistent for all forcing datasets. Our ET estimates in NE are largely affected by uncertainties in precipitation (P), air temperature (T), incoming shortwave radiation (R) and vapor pressure deficit (VPD). During the growing season, the correlations between ET and each forcing variable indicate that T is the

[4] Liu, Y., Zhuang, Q., Miralles, D., Pan, Z., Tchebakova, N., Kicklighter, D., Zhu, Q., He, Y., Chen, J., Tchebakova, N., Sirin, A., Niyogi, D., Melillo, J. Impact of forcing data uncertainty on the estimation of evapotranspiration in Northern Eurasia, *J Geophys Res:Atmos* in review

dominant factor in the north and P in the south. For the non-growing season, the dynamics of ET are mainly explained by R and VPD. Unsurprisingly, the uncertainties in ET-forcings propagate as well to estimates of the volume of water available for runoff (P-ET). While CRU dataset appears as a better choice of forcing via our assessment, the quality of forcing data remains a major challenge to accurately quantify the regional water balance in NE.

5.2 Introduction

Evapotranspiration (ET) is an essential physical process that governs the energy, water and carbon cycling between land and atmosphere (Dolman and de Jeu 2010; Wang and Dickinson 2012). Direct measurements of ET only exist at local scales, making the accurate estimation of this flux a necessary task to improve the regional-scale management of water resources, and to reduce the uncertainty in the predictions of how the global water cycle will respond to the changing climate. However, ET estimation is complicated by a large number of biogeophysical (e.g., soil moisture, plant physiology, soil properties) and climatic (e.g., radiation, temperature, humidity, wind speed) factors affecting this natural process (Monteith 1965; Niyogi et al. 2009; Dolman and De Jeu 2010). Nevertheless, recent years have seen the development of process-based numerical models that represent the key physical and biogeochemical interactions driving ET: hydrological models (e.g., Vörösmarty et al. 1998), dynamic vegetation models (e.g., Lund-Potsdam-Jena, Gerten et al. 2004), land surface models (e.g., Liang et al. 1994; Niu et al. 2011), or simple algorithms designed to work with satellite Earth observations as input (Mueller et al. 2013; Mallick et al. 2014). These numerical models enable the

estimation of ET at regional or global scales, at various spatial and temporal resolutions, and with different degrees of accuracy.

The accuracy in ET estimates from numerical models depends on (a) the accuracy in the climate data used to force the models, (b) the realism of the model representations of the physical and biogeochemical processes that occur in nature, and (c) the spatiotemporal scale of the ET estimate. Previous studies have investigated these sources of uncertainty. For example, Douville (1998) examined the sensitivity of ET to the changes in land surface parameters, precipitation forcing and run-off representation using a land surface model; Oki et al. (2006) uncovered large discrepancies of ET estimates among a range of land surface models; Rawlins et al. (2006) investigated the effects of different forcing data and methods for the estimation of ET in Western Arctic; both Livneh and Lettenmaier (2012) and Fergusson et al. (2011) reported how a lack of water budget constraints on remote sensing ET estimates may lead to overestimation of ET. Along with others, these studies highlighted the need of combining high-quality forcing data with sound model representation for the accurate estimation of ET. Meanwhile, the uncertainty in the estimation of ET will also respond to forcing and model uncertainties distinctly in different regions of the world, due to the global heterogeneity in physical and biogeochemical conditions and that the dominant ET drivers may change accordingly from region to region (Mengelkamp et al. 2006; Beyrich and Mengelkamp, 2006; Miralles et al. 2011a). Nonetheless, the particular impact of climate forcing data uncertainties on the estimation of ET at large scales has not been extensively studied, regardless of its importance in skill development for current models to estimate the variability of regional and continental-scale water balances.

This study still focuses on the territory of Northern Eurasia (NE), a critical region for Earth's climate due to its vast area (see Fig. 4.1), its high sensitivity to global warming (Serreze et al. 2000; IPCC, 2007), and its significant feedbacks on the global climate system (Adam and Lettenmaier 2008; Groisman et al. 2010). Despite its critical role in climate, the large-scale hydrology of NE remains largely unstudied, especially from the perspective of ET. Here we use an improved version of a process-based biogeochemistry model, the Terrestrial Ecosystem Model (TEM 5.0; Zhuang et al. 2010; Liu et al. 2013, 2014), to estimate ET based on a range of current climate datasets as forcing. This study aims to investigate the plausible ET dynamics in NE during 1979–2008, the range of variability in ET estimates that responds to uncertainties in forcing data, and the regional changes in the sensitivity of ET to different climatic drivers. The overreaching goal is to shed light on the appropriateness of currently existing climate forcing data in quantifying the terrestrial water cycle in NE.

5.3 Methods

5.3.1 Approach

We use an improved version of TEM – developed in Chapter 4 – that explicitly considers ET from heterogeneous land cover type: uplands, wetlands, water bodies and snow cover, where ET from uplands and wetlands includes transpiration from plant canopies, evaporation from wet canopies, moist and saturated soil surfaces (Liu et al. 2014). The choice of TEM for our study over other existing models is justified for two reasons. First, Most ET estimation schemes (see Mengelkamp et al. 2006; Mueller et al. 2013) do not explicitly consider some of the detailed ET processes incorporated in the

current version of TEM (e.g., snow sublimation), whose consideration has shown to improve the model realism in high-latitudes (Liu et al. 2014). Second, site-level comparisons against EC data indicate that the ET derived from the latest TEM version (hereafter called TEM-ET) driven by measured meteorological data at the EC sites has high credibility in reproducing the observations in comparison to a range of widely-used ET products (see Liu et al. 2014). Note that for the purpose of this study we focus on the aggregated ET over all land cover types, instead of each separate ET component (e.g. transpiration, snow sublimation, etc.). A detailed description of the latest TEM version that is used here can be found in Liu et al. (2014).

The TEM model has been run for 1979–2008 using a set of five different climate forcings as indicated in Section 5.3.2. Regional annual estimates from two global satellite-based ET products – the mean of the LandFlux-EVAL merged datasets by Mueller et al. (2013), hereafter referred to as EVAL, and GLEAM (Global Land-surface Evaporation: the Amsterdam Methodology, Miralles et al. 2011a,b) are used for comparison and to check the plausibility of the range of the five TEM-ET estimates. Since the primary objective of this study is to examine forcing-induced ET estimation uncertainty using TEM – rather than inter-comparing different models to investigate their disparities – only TEM is involved in the simulations with five different forcing datasets. Additionally, runoff measurements for the six largest watersheds in NE from Peterson et al. (2002) and the Global Runoff Data Center (GRDC) are used to evaluate the forcing-induced uncertainties in estimates of P–ET (i.e., a proxy for the volume of water available for runoff – see e.g., Miralles et al. 2011b). Finally, to identify the dominant

drivers of ET in NE, correlations between ET estimates and each forcing variable are calculated and contrasted through an analysis based on Budyko curves (Budyko 1974).

5.3.2 Data

Climatic data for monthly air temperature (T), precipitation (P), either incoming shortwave radiation (R) or cloudiness (C), vapor pressure(V) and wind speed (u), and other ancillary inputs including atmospheric CO2 concentrations, soil texture, elevation and land cover are needed to drive TEM to estimate ET. Climatic inputs vary over time and space, whereas soil texture, elevation and land cover data only vary spatially and are assumed to be static throughout 1979–2008.. All simulations are conducted at a spatial resolution of 0.5° latitude × 0.5° longitude. Five widely used climate datasets are used to force TEM and estimate ET for NE: (1) the Climate Research Unit (CRU) TS3.1 (with the P dataset being the corrected version v3.10.01) of the University of East Anglia (Harris et al. 2013), (2) the European Centre for Medium-Range Weather Forecasts (ECMWF) ERA-Interim Reanalysis (Dee et al. 2011), (3) the National Aeronautics and Space Administration Modern Era Retrospective-Analysis for Research and Applications (MERRA) (Rienecker et al. 2011), (4) the National Centers for Environmental Prediction/National Center for Atmospheric Research (NCEP/NCAR) reanalysis (Kistler et al. 2001), and (5) the Global Meteorological Forcing Dataset for land surface modeling by Princeton University (PU) (Sheffield et al. 2006).

Input climate data include monthly average T, P, R or C, V and u. In the case of CRU TS3.1 dataset, only a monthly climatology is available for u (mean of all the same months of the year for 1961–1990, New et al. (1998)), and R is estimated based on

latitude, date, and CRU cloudiness following Pan et al. (1996). All forcing climate data are resampled at 0.5º spatial resolution by using the inverse distance weighting method (Shepard, 1968). We use the same ancillary data, including soil texture, elevation, land cover, albedo, snow cover and atmospheric CO2 concentrations, as those in Chapter 4.

5.4 Results and Discussion

5.4.1 Temporal and spatial uncertainties in forcing data

Grid cell data from the five forcing datasets are evaluated against the observed meteorological data from the European Climate Assessment & Dataset (ECA&D), the National Meteorological Information Center of China Meteorological Administration (CMA), and EC towers within the NE domain (Table 4.3). The temporal variability of the climate forcing variables differs substantially among the datasets (Fig. 5.1). Overall, ERA-Interim shows the highest T, VPD and u, NCEP/NCAR has the highest P and R, while CRU shows the lowest values of P, T and R. In MERRA, u is systematically lower. However, systematic errors aside, the temporal dynamics of T, VPD and u are remarkably similar for all five forcing datasets, while P and R show larger differences, with correlation coefficients (r) between different datasets ranging from 0.25–0.90 for P, and even lower (-0.11–0.45) for R (see also Fig. 5.1b). In terms of long-term (1979-2008) average spatial variability over the study region, the different forcing datasets agree better with each other than temporal variability. The large differences in the spatial distribution from forcing to forcing only occur for u (Fig. 5.2).

Comparison against in situ measurements reveals an overall better quality of the CRU TS3.1 dataset (Table 5.1), with the best statistics of all five datasets for T, P and

relative humidity (RH) (derived from T and V after Andrews 2010). Conversely, ERA-Interim shows the highest average root mean square error (RMSE) for T, NCEP/NCAR for P, and MERRA for RH and u. ERA-Interim shows the lowest average RMSE for u. At the same time, MERRA displays the lowest correlation with measurements for the majority of climate variables (T, P, RH and u). Nonetheless, it must be noted that the scale mismatch between the gridded forcing datasets and the in-situ measurements may inherently reflect in the results of this validation.

For most variables, the standard deviation (σ) of the forcing data ensemble is larger than the σ of that particular variable for each forcing dataset (Table 5.2). This holds both for temporal and spatial σ, suggesting that the uncertainties in the forcings may be higher than the dynamic range of these variables. Especially, the mean temporal σ of the forcing ensemble for R and u is up to 25 and 17 times the σ of the individual R and u time series, respectively. Also notable is the spatial σ of P in NCEP/NCAR, which is much greater than that of the multi-forcing ensemble, suggesting an unrealistically high spatial variability of P in NCEP/NCAR; this is consistent with the large RMSE mentioned above and reported in Table 5.1.

5.4.2 Temporal uncertainties in ET

The temporal variability of the regional-average ET (i.e., area-weighted ET across all grid cells in NE) show that the annual ET vary substantially depending on the forcing dataset (Fig. 5.1a), from higher to lower: ETERA, ETNCEP, ETPU, ETMERRA, ETCRU (subscripts indicate the forcing used in the derivation of the ET via TEM). While the highest (ETERA) ranges between 338.4–369.3 mm yr-1, the lowest (ETCRU) ranges

between 263.5–290.3 mm yr-1. These differences between ETERA and ETCRU are therefore in the order of 31% of the mean magnitude of the flux, indicating the potential of forcing data to induce systematic errors in the ET estimates. Moreover, the mean temporal σ of ET product ensemble over 1979–2008 is more than three times the temporal σ of each ET product itself (Table 5.2), highlighting the importance of this forcing-induced uncertainty in comparison to the real magnitude of the signal. Nonetheless, the discrepancy in the ET estimates from each forcing set is systematic (Fig. 5.1a); systematic errors aside, an agreement in the temporal dynamics of the resulting ET from each of the forcing sets still exists.

The satellite-based ET product GLEAM reports a spatiotemporal average of 299.5 mm yr-1 for NE during 1980–2008, while EVAL reports a value of 311.3 mm yr-1 during 1989–2005 (Fig. 5.1a). ETPU is the product that matches best with these absolute averages from GLEAM and EVAL. Note that comparison to the GLEAM and EVAL products is not necessarily a measure of accuracy because these datasets can also show considerable uncertainties in our study region as recently reported in Liu et al. (2014).

Seasonal dynamics of the five ET products are generally similar (Fig. 5.1c), and compare well to those of EVAL (r =0.95-0.99) and GLEAM (r =0.93-0.98), although differences still exist in the summer. The largest differences among the five ET products occur during summertime (Fig. 5.1c), when solar radiation is at its maximum and evaporative stress is frequent (thus uncertainties in P forcing can become crucial). The forcing datasets also show the largest discrepancies in the summer, with an average inter-forcing spread of P, T, R, VPD and u of up to 40.2 mm mon-1, 4.5°C, 227.9 W m-2, 7.2 hPa and 2.3 m s-1, respectively (Fig. 5.1c). These inter-forcing differences will inevitably

result in large differences in the subsequent ET estimates. As an example, in summertime, ETCRU shows the lowest average values due to the lowest P, T and R, while ETERA shows the highest values as a consequence of the high T, P, VPD and u.

5.4.3 Spatial uncertainties in ET

The spatial variability of ET seems more consistent from product to product, with a common gradient from north to mid-latitudes, and with the highest ET located over the southwestern temperate forests where energy and water supply are abundant (Fig. 4.1). The assumption of static land cover throughout 1979-2008, as well as general agreement in the representation of spatial variability across forcings (Fig. 5.2, see also Section 5.4.1), likely contributes to the overall consistent spatial variability across different ET products. Nonetheless, the inter-product spatial σ is also larger than the mean spatial σ of each ET product, except for ETERA (Table 5.2), stressing the importance of forcing-induced uncertainty in the estimation of ET. The overall higher and lower values for ETERA and ETCRU, respectively, occur across the entire domain, likely due to the systematically higher T, VPD and u in ERA-Interim and systematically lower R and T in the CRU.

The ET for the north and the south of NE vary greatly among the ET products (Table 5.3, Figure 5.3). Here we use the southern extent of the Taiga zone as the boundary between the north and the south of NE. However, comparison between ET/forcing in the north and the south is generally consistent across all ET products/forcings (e.g., ETsouth > ETnorth for ETCRU, and this is also the case for ETERA, ETNCEP, ETMERRA and ETPU). Other than land cover variations across the north and the south (Fig. 4.1), the differences in climate conditions appear responsible for

the spatial difference of ET rates. Overall, high ET occurs in area with high energy (i.e., T, R, u) or water supply (i.e., P). The south has more favorable energy conditions (i.e., higher R, T) and more water bodies that would potentially reduce stress for ET – another reason for higher ET in the south than the north. Note that ETCRU, ETERA and ETPU are higher than corresponding P in the south, because there are abundant water bodies where evaporation is assumed to be not limited by water supply and evaporation from water bodies tends to be ~3 folds of that from uplands (Liu et al. 2014). On the other hand, the north of NE has lower T, R and VPD so that ET is limited by energy and tends to be lower.

5.4.4 Temporal uncertainties of P-ET

TEM simulations indicate that the annual mean volumetric soil moisture varied little from year to year in the NE, this enables the use of P-ET as a surrogate for the volume of water available for runoff. For each forcing dataset, estimates of P-ET from the six largest watersheds in the NE (Fig. 4.1) are aggregated to obtain the total runoff for the six watersheds during 1979–1999 – the P from the corresponding forcing dataset has been used in combination with the ET resulting from forcing the TEM with the meteorology of that dataset. These aggregated P-ET estimates are then compared to river discharge measurements from the GRDC and those by Peterson et al. (2002). As expected, the annual P-ET estimates tend to be closer to discharge measurements at annually than at monthly scales, due to the fact that the underlying assumptions in this comparison (negligible changes in soil water storage and no travel time of rainfall to the river outlet) are only valid when considering longer time-scales.

The average inter-product spread for the P-ET estimates amounts to 2140.1 km3 yr-1. Once again, CRU estimates compare better to the mean in situ river discharge from the GRDC and Peterson et al. (2002) (Fig. 5.4). The validation statistics (RMSE and mean percentage error, MPE) for the P-ET estimates driven by the five datasets are: 164.25 km3 yr-1 and -5.43% for CRU; 405.35 km3 yr-1 and 19.77% for ERA-Interim; 492.63 km3 yr-1 and -25.32% for PU; 843.71 km3 yr-1 and 41.62% for MERRA; and 1647.34 km3 yr-1 and 87.88% for NCEP/NCAR. The P-ET estimates based on NCEP/NCAR show a systematic overestimation, in agreement with the positive bias in P illustrated in Fig. 5.1. Meanwhile, different P-ET products present contrasting trends: those derived from MERRA and ERA-Interim present a significant decreasing trend ($p<0.01$), which is contrary to previous findings in Peterson et al. (2002), suggesting that the choice of climate forcing is crucial for the hydrological modeling of the region.

5.4.5 Dominant factors in determining ET across the NE

Pearson's correlation coefficients (r) between the five TEM-ET products and corresponding climate forcing unanimously indicate that, during the growing season (May-Sep.; Groisman et al. 2003; Parmentier et al. 2011), ET is primarily constrained by T (and R) in the north but P in the south (Fig. 5.5a). The correlation between T and R is high in the north (average r varies between 0.68–0.91 for the five forcing datasets), suggesting that large portion of the correlation between ET and T can be explained by the dependency of T (and ET) on R. The variability of the ET estimates during the non-growing season is generally dominated by R (Fig. 5.5b), mostly due to the dependency of snow sublimation on R as represented by the TEM (Coughlan and Running 1997; Liu et

al. 2014). For the CRU and ERA-Interim datasets, ET shows the highest correlation with VPD in the southwest during the non-growing season (note however that the correlations between VPD and R in this area are also high).

Budyko curves (Budyko 1974) derived from the five sets of ET data further confirm the above results (Fig. 5.6). In the south, most grid cells in all five datasets consistently display ratios of potential ET to P (i.e., PET/P) greater than 1, suggesting that ET in this region is limited by the supply of water. On the other hand, PET/P is less than 1 in most grid cells of the north, suggesting an energy limitation. The inter-product consistency in the spatial variability of the dominant ET drivers shown in Fig. 5.5 and 5.6 – despite the apparent differences amongst the different forcing datasets (Fig. 5.1, 5.2, 5.3) – indicates the important role played by the static ancillary datasets of soil properties and land use, and especially the importance of the ET algorithms and parameterizations in defining the sensitivity of the model output (ET) to the different forcing variables.

5.5 Conclusions

Using the latest version of the TEM (Liu et al. 2014), the uncertainties in climate forcing data, and how they propagate to the uncertainty in ET and P-ET estimates, as well as the dominant climatic factors of ET are investigated for Northern Eurasia (NE) during 1979–2008. Validation results reveal systematic errors in a range of commonly-used forcing datasets, and these errors propagate to the TEM ET estimates, especially in summertime. The P-ET estimates present a large spread and systematic errors when compared to discharge measurements from the six largest watersheds in NE, in particular for some of the forcing datasets (e.g., NCEP/NCAR).

While uncertainties in the forcing data do not alter substantially the average spatial distribution of the TEM ET estimates – which is largely affected by the land cover distribution and the specific cover-type model parameterizations – the long-term average magnitude and temporal variability show a great dependence on the choice of forcing dataset. Nonetheless, independent of the forcing dataset, the climatic variables that dominate ET temporal variability remain the same from product to product. For all data sets, air temperature appears as the most important driver of ET in the north of NE and precipitation in the south during the growing season. For the rest of the year, solar radiation and vapor pressure deficit appear more important. Water limitations in the south indicate the need for accurate precipitation data and suggest that ET models that are based on energy terms alone (that exclude surface energy balance models. e.g., Thornthwaite 1948, Turc 1961, Hamon 1963, Priestley and Taylor 1972) are not appropriate for the estimation of ET in the region.

Several limitations in the study may include: (1) our TEM-ET estimation does not consider the effects of CO2 on stomatal conductance or soil water stress in wetlands; (2) we have used climatological wind speed data in CRU TS3.1 due to unavailability of monthly time series; (3) the uncertainty due to the scale mismatch between the coarser forcing data and finer ET processes has not been separately assessed; and (4) the land cover has been assumed to remain unchanged during the entire study period, despite the increasing frequency of forest fires and other land use practices in the NE in recent years (McClelland et al. 2004).

Nonetheless, this study unequivocally highlights important disagreements among broadly-used climate forcing datasets in NE, and provides evidence of the propagation of

these uncertainties in the estimation of hydrological fluxes and in particular ET. Thus this study underscores the needs of high-quality input forcing data to model the large-scale hydrology of NE. From our assessment, the CRU forcing presents an overall better quality on its evaluation against in situ measurements, and yields the lowest bias in the P-ET estimates when compared to river discharge records. Results also suggest the need for a thorough validation of the estimates of air temperature from ERA-Interim reanalysis in NE, and the precipitation and radiation data from the NCEP/NCAR reanalysis, due to their apparent deficiencies as manifested in our study.

5.6 Acknowledgements

This research is supported by the NASA Land Use and Land Cover Change program (NASA- NNX09AI26G, NN-H-04-Z-YS-005-N and NNX09AM55G), the Department of Energy (DE-FG02-08ER64599), the National Science Foundation (NSF-1028291 and NSF-0919331), and the NSF Carbon and Water in the Earth Program (NSF-0630319). We acknowledge the Global Runoff Data Centre for provision of the gauge station data. Runoff data in Peterson et al. (2002) were obtained from the R-ArcticNet database. A special acknowledgment is made to Brigitte Mueller and Martin Hirschi for the provision of the LandFlux-EVAL dataset in Mueller et al. (2013). Eddy covariance data are obtained for free from http://www.asianflux.com and http://gaia.agraria.unitus.it/. Observed data at meteorological stations are obtained from European Climate Assessment & Dataset and the National Meteorological Information Center of China Meteorological Administration for free. Forcing climate data are from different sources for free which has been indicated in Section 5.3.2.

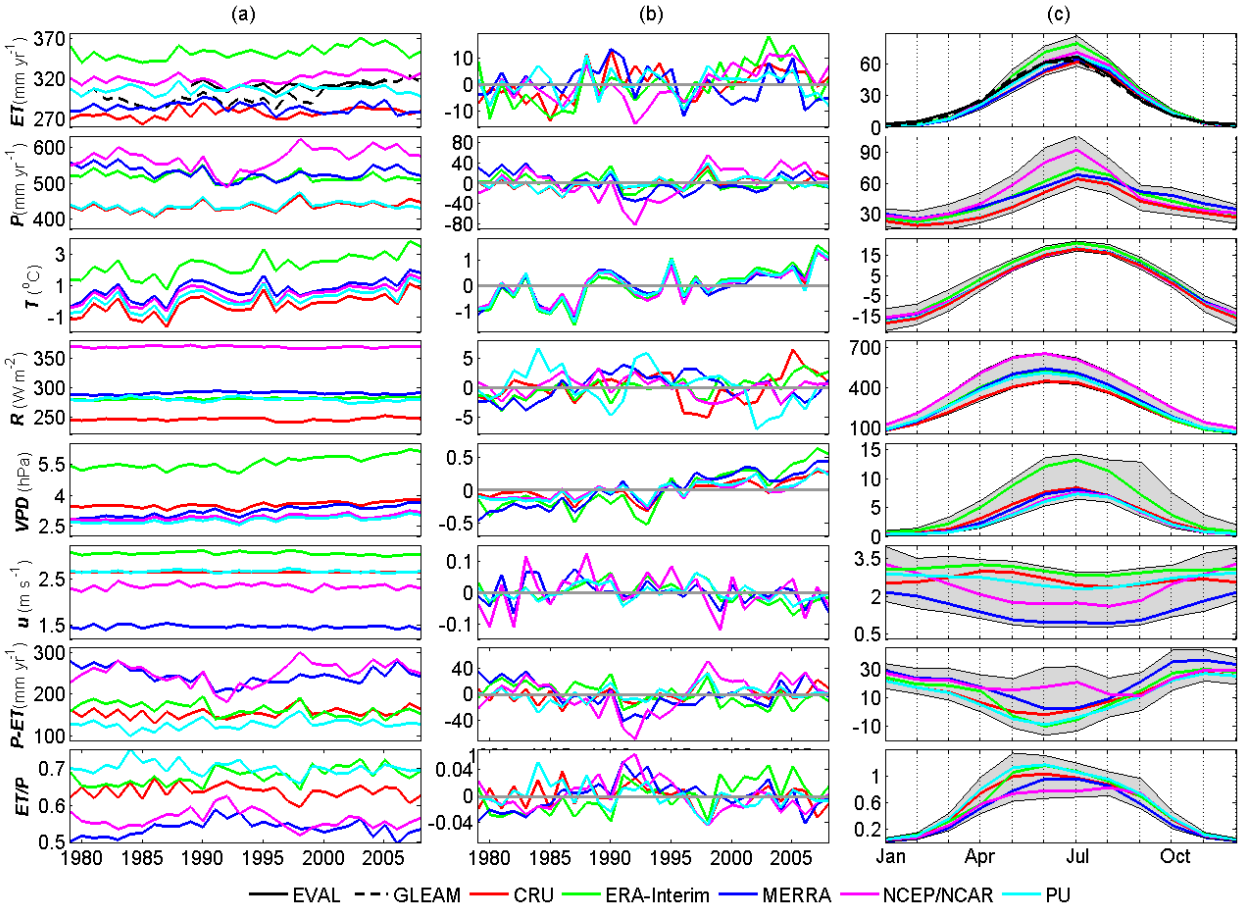

Figure 5.1 Temporal variability of the regional *TEM-ET* and forcing variables in the NE (a) Inter-annual variability, (b) annual anomaly, and (c) climatological seasonality (calculated by averaging all the same months of the year for 1979–2008). The shaded area stands for the spread of the monthly values (the difference between the largest and lowest values for the same months of the year over 1979–2008).

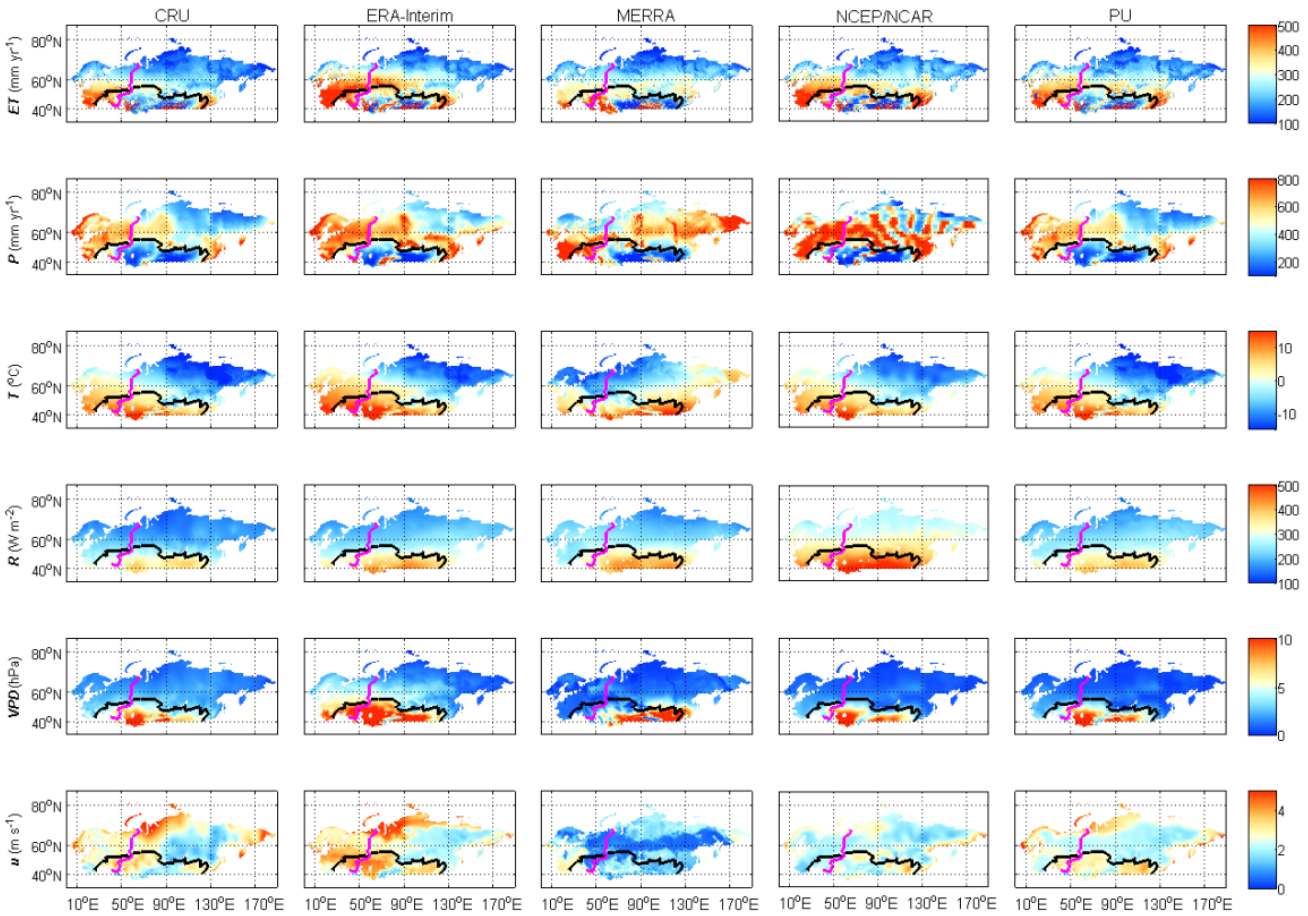

Figure 5.2 Spatial variability of the *TEM-ET* and forcing variables in the NE, here average annual values during 1979–2008 are presented. The black line on the map represents the boundary between the north and south (south extent of the Taiga zone), and the pink line is the boundary between Asia NE and Europe NE, and these lines stand for the same throughout this study.

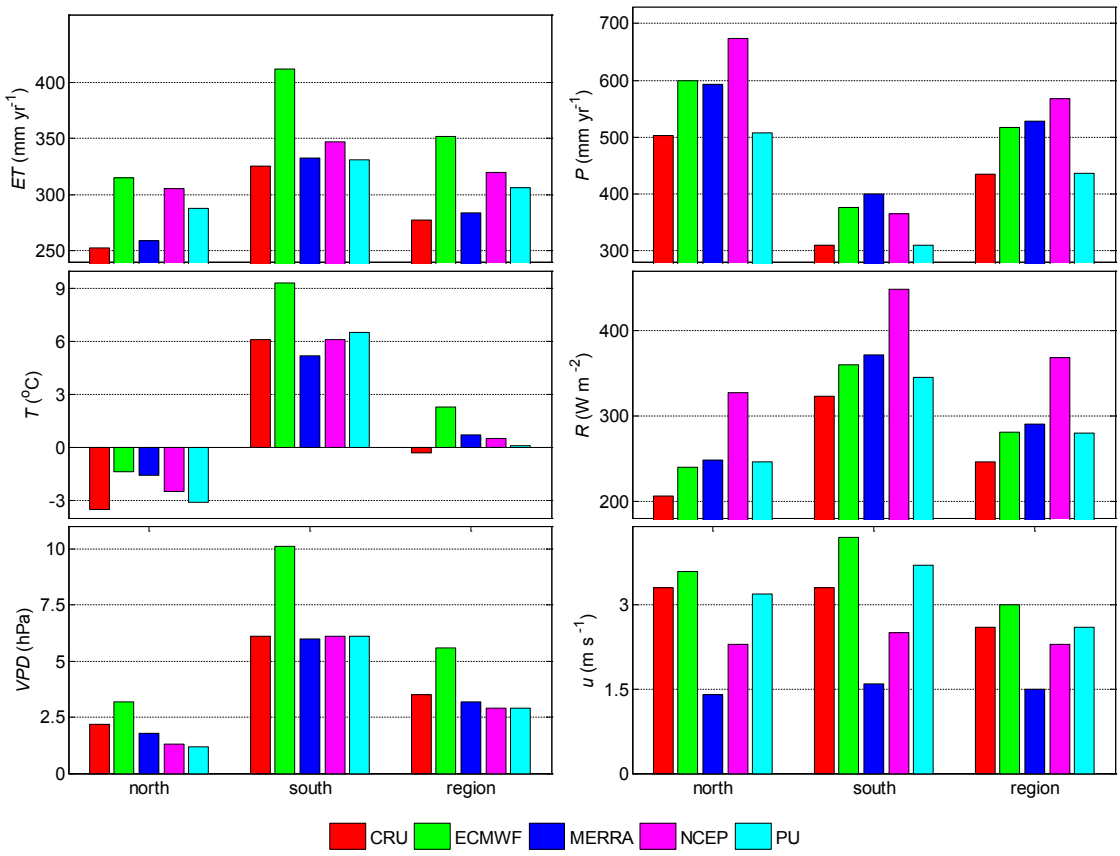

Figure 5.3 Comparison of the *TEM-ET* and climate forcing across different landscapes in the NE. Here "north", "south" and "region" at the bottom of the plot stand for the north and the south of NE and the entire NE region, respectively.

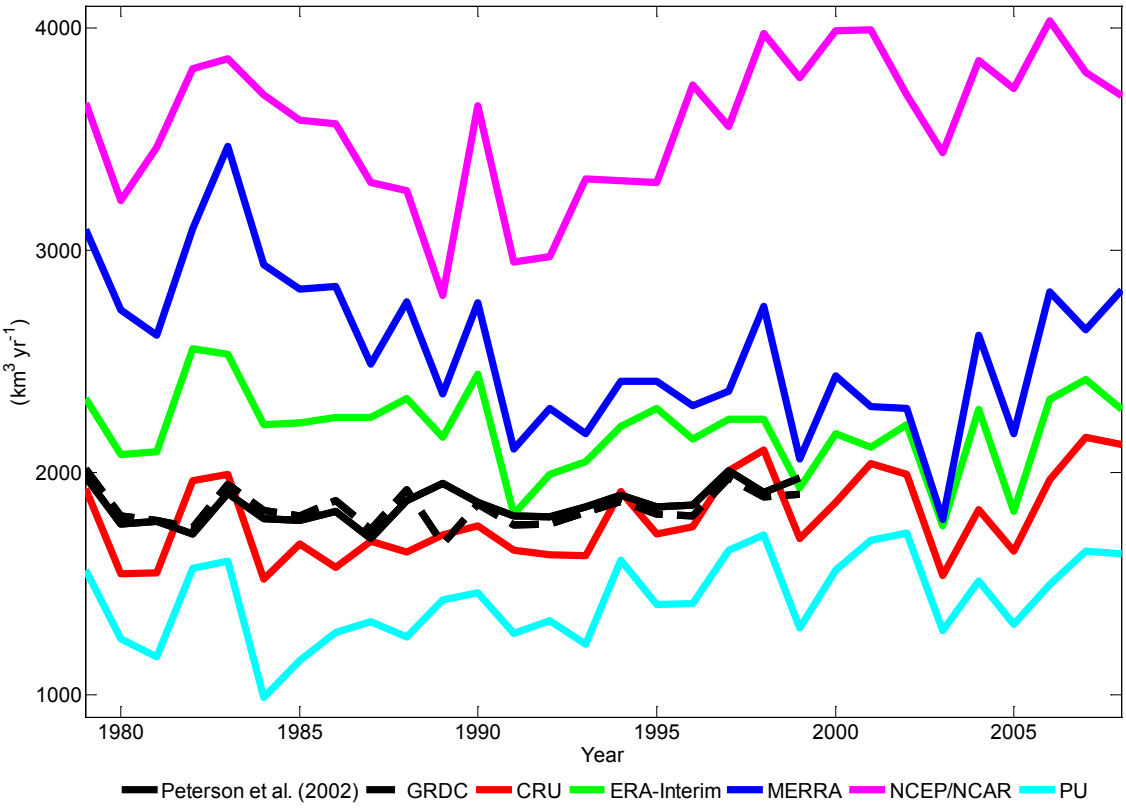

Figure 5.4 Comparison of TEM *P-ET* estimates driven by the five forcing datasets with the runoff measurements in Peterson et al. (2002) and GRDC in the NE region.

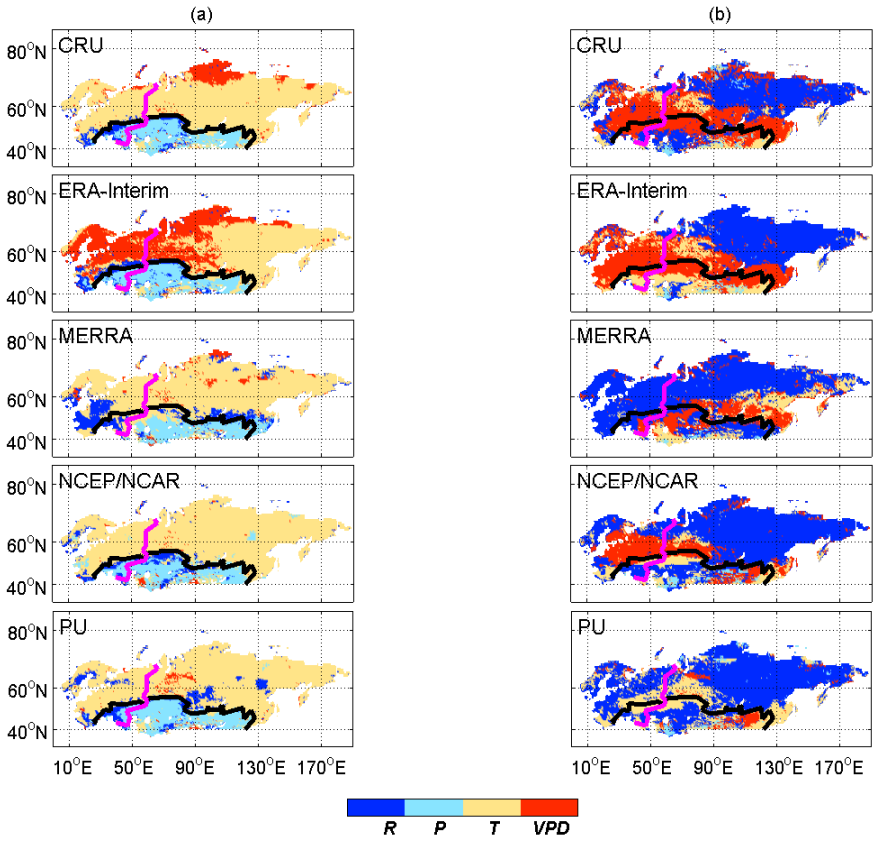

Figure 5.5 Spatial patterns of climate variables that show the highest Pearson correlation with *TEM-ET* estimates ($p<0.05$) during (a) the growing season, (b) non-growing season. Correlations are based on monthly time series for 1979–2008.

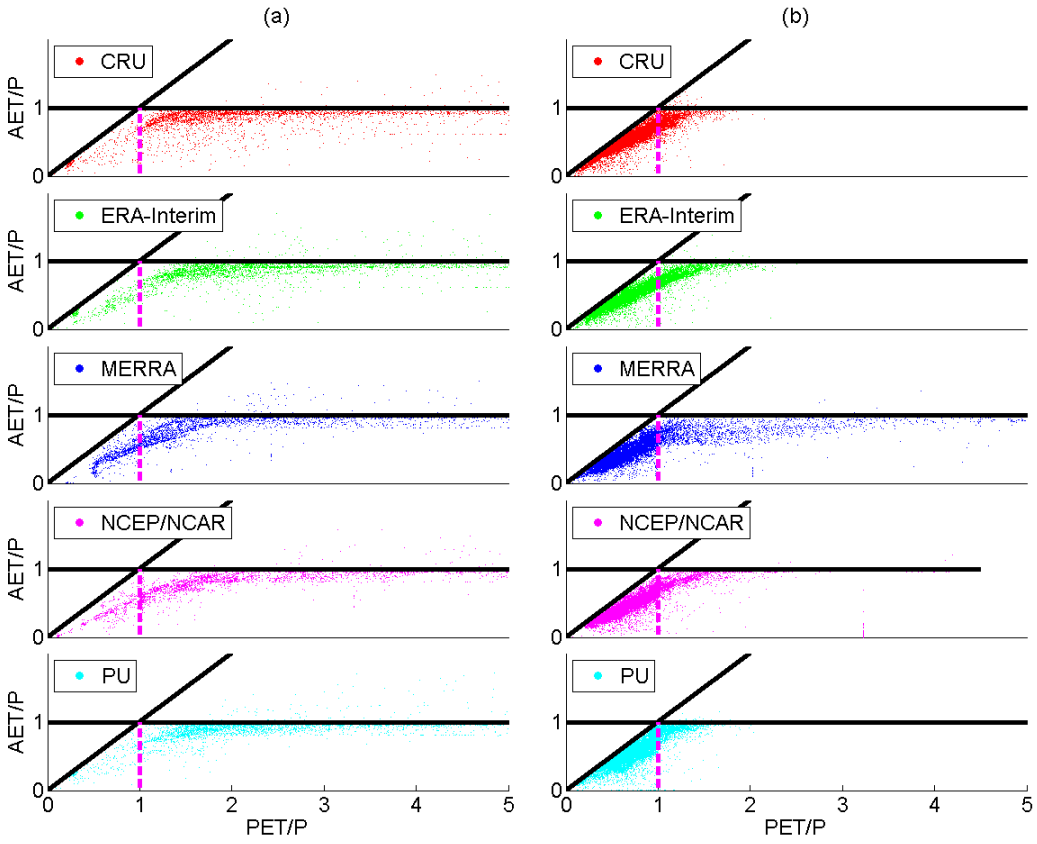

Figure 5.6 Budyko curves derived using TEM estimates and the five forcing datasets for the (a) south, (b) north. Each point represents a different grid cell.

Table 5.1 Evaluation of the forcing data (*T* = air temperature, *P* = precipitation, *RH* = relative humidity, *C* = cloudiness, *u* = wind speed) against observations at meteorological stations and EC sites. The values represent the average RMSE, average absolute MPE and average r across all meteorological stations and EC sites. The RMSE units for *T*, *P* and *u* are °C, mm yr^{-1} and m s^{-1}, respectively.

	CRU			**ERA-Interim**			**MERRA**			**NECP/NCAR**			**PU**		
	RMSE	MPE	r	RMSE	MPE	r	RMSE	MPE	r	RMSE	MPE	r	RMSE	MPE	r
T	1.28	9.2%	0.99	2.2	14.2%	0.98	1.91	22.7%	0.91	1.66	12.9%	0.98	1.31	8.1%	0.98
P	11.9	16.8%	0.84	14.1	22.1%	0.82	14.5	27.8%	0.31	20.2	36.1%	0.66	13.4	18.7%	0.81
RH	8.2%	4.5%	0.68	11.5%	12.5%	0.79	15.8%	17.8%	0.11	10.7%	12%	0.55	14.4%	12.3%	0.25
u	N/A	N/A	N/A	1.3	37.4%	0.67	1.9	48.3%	0.11	1.6	33.2%	0.35	1.49	34.3	0.51
C	10.5%	3.5%	0.63	N/A	N/A	N/A	N/A	N/A	N/A	N/A	N/A	N/A	N/A	N/A	N/A

Note: statistics for *u* are not available for CRU because CRU does not have monthly time series data, and statistics for *C* are only available for CRU is because *R* is collected instead of *C* for the other four datasets. Here R is not assessed due to shortage of *in-situ* measurements.

Table 5.2 Standard deviation (σ) of different *ET* products and forcings over 1979–2008. σ1: mean temporal σ of the ensemble of *ET* products/forcings; σ2: mean spatial σ of the ensemble of *ET* products/forcings; σ3: temporal σ of individual *ET* product/forcing; σ4: spatial σ of individual *ET* product/forcing. Note that for σ2 and σ4, average annual *ET* product/forcing over 1979–2008 is used for mean spatial σ calculation, which corresponds to Figure 5.2. The units for *ET*, *P*, *T*, *R*, *VPD* and *u* are mm yr^{-1}, mm yr^{-1}, °C, W m^{-2}, hPa and m s^{-1}, respectively.

			CRU		**ERA-Interim**		**MERRA**		**NCEP/NCAR**		**PU**	
	σ1	σ2	σ3	σ4	σ3	σ4	σ3	σ4	σ3	σ4	σ3	σ4
ET	26.9	165.2	6.08	143.59	7.98	212.34	6.19	135.03	6.45	159.85	5.19	155.82
P	54.1	250.9	12.8	212.0	13.5	220.78	19.08	252.97	29.84	311.52	12.83	212.46
T	0.87	8.1	0.64	8.38	0.7	8.97	0.61	7.19	0.59	7.24	0.64	8.38
R	40.7	81.1	2.52	69.33	1.80	72.10	2.22	75.01	1.62	73.16	3.24	61.29
VPD	1.02	3.28	0.14	2.26	0.30	4.30	0.25	3.30	0.14	2.73	0.14	2.78
u	0.52	0.92	0.00	0.86	0.03	0.89	0.04	0.72	0.06	0.49	0.03	0.65

Table 5.3 Average *TEM-ET* and climate forcing across the north, the south and entire NE during 1979–2008. The units of *ET*, *R*, *P*, *T*, *VPD* and *u* are mm yr^{-1}, W m^{-2}, mm yr^{-1}, °C, hPa and m s^{-1}, respectively.

	Variable	CRU	ERA-Interim	MERRA	NCEP/NCAR	PU
north	*ET*	252.1	314.9	258.7	305.4	287.5
	R	205.5	239.7	247.9	327.1	245.6
	P	502.9	599.2	593.6	673.4	507.5
	T	-3.5	-1.4	-1.6	-2.5	-3.1
	VPD	2.2	3.2	1.8	1.3	1.2
	u	3.3	3.6	1.4	2.3	3.2
south	*ET*	325.5	421.9	332.8	346.9	341.5
	R	322.9	360.3	371.1	448.6	344.6
	P	300.0	355.7	400.3	364.9	297.1
	T	6.1	9.3	5.2	6.1	6.5
	VPD	6.1	10.1	6.0	6.1	6.1
	u	3.3	4.2	1.6	2.5	3.7
entire NE	*ET*	277.1	351.4	283.9	319.6	305.9
	R	245.5	280.8	289.9	368.5	279.4
	P	433.7	516.2	527.8	568.3	435.8
	T	-0.3	2.3	0.7	0.5	0.1
	VPD	3.5	5.6	3.2	2.9	2.9
	u	2.6	3.0	1.5	2.3	2.6

CHAPTER 6 SUMMARY AND FUTURE OUTLOOK

6.1 Summary

My dissertation research mainly investigates the impacts of climate change and agricultural activities on the changes of water cycling in the critical area – Northern Eurasia (NE). A series of studies have been conducted to contribute to better understanding of those impacts. I have been applying a combination of modeling, in-situ observations and remote sensing data, uncertainty analysis and model-data fusion to fulfill the research tasks. Corresponding to research tasks in Section 1.3.1, here I summarize the main findings of this dissertation research:

1. The fact that soil moisture and discharge decline in the past three decades in Northern China (NC) has been unraveled with robust field observations. Agricultural activities play an important role in the evolution of the decline in this region. Intensification of agricultural activities including increase in fertilizer use, prevalence of water-expensive crops and cropland expansion have aggravated the decline in this region.

2. Replacing Jensen-Haise formulation (energy terms alone) with the Penman-Monteith based approach for representation of atmospheric evaporative demand has substantially improved model performance in estimating *ET*. Regional annual *ET* keeps

increasing across different climate change scenarios on the Mongolia Plateau during the 21st century. Meanwhile, the available water for human use will not change significantly during the 21st century in this region. In addition, climate change is more important than climate-induced land cover change in determining regional *ET*.

3. Incorporation of detailed *ET* processes (canopy interception loss, *ET*/evaporation from wet land surfaces, water bodies and wetlands, and snow sublimation) in the TEM substantially improved the accuracy of the estimation of *ET* and runoff. Consideration of snow sublimation limits the magnitude of total *ET* and greatly improves the realism of *ET* representation in NE where snow prevails during several months of a year. While the average *ET* over NE increased during the 1948-2009, water availability augmented in the western part of the region, but decreased in the eastern part.

4. Estimates of regional *ET* vary greatly depending on the choice of forcing data, while spatial variability of *ET* appears more consistent. Uncertainties in *ET* forcings propagate as well to the estimates of runoff. Independent of the forcing dataset, the climatic variables that dominate *ET* temporal variability remain the same among all TEM *ET* products – the north is energy-limited and the south is water-limited. While CRU dataset appears as a better choice of forcing via our assessment, the quality of forcing data remains a major challenge for accurate quantification of regional water balance in NE.

6.2 Limitations

Across this dissertation research, it is unavoidable that there might be some limitations. The limitations are due to unavailability of data, insufficient understanding of

the interactions between land, atmosphere and human, and complexity in model representation and so on.

The limitations of my work may include several aspects: (1) the possible alteration of regional water distribution by irrigation, reservoir regulation, water withdraw, ground water pumping, soil and water conservations have not been considered in the study of NC, due to a lack of historical records on these activities; (2) *ET* estimation of TEM does not consider the effects of CO_2 on stomatal conductance; (3) I have used climatological wind speed data in CRU TS3.1 due to unavailability of monthly time series, as well as a seasonal climatology for representation of snow dynamics due to lack of long-term (1948-2009) snow time series; (4) the uncertainty due to the scale mismatch between the coarser forcing data and finer *ET* processes has not been separately assessed; (5) the land cover has been assumed to remain unchanged during the entire study period for Chapter 3 and 4, despite the increasing frequency of forest fires and other land use practices in NE in recent years (McClelland et al. 2004); (6) the assumption of unlimited water in water bodies or no soil water stress in wetlands might be invalid throughout the whole study period; (7) the horizontal water flow between grid cells has not been considered in the model; (8) the effects of forest stand age on the rates of water and carbon fluxes have not been considered for NE where forest is the most important plant functional type; and (9) processes such as melting glaciers and permafrost thawing that regulate water dynamics in this region have not been taken into account in the model.

6.2 Future research directions

Following the dissertation work, there is large room that I could fill. I am going to proceed in several directions out of my research interests as well as the needs of the community.

Water and carbon (C) fluxes interact in the terrestrial ecosystems. There has been substantial progress in recent years in understanding global and regional C/water variations through satellite data, *in-situ* measurements, and model simulations. Nevertheless, most of model simulations ignore the effects of stand age on the interacted C/water fluxes for forest ecosystems, although the effects are apparent (Ewers et al. 2005, 2011; Pan et al. 2011). Moreover, the record of satellite products is limited, especially for C fluxes. These limitations affect the accuracy of model estimates of C/water fluxes and hinder their validation (Ewers et al. 2011; Deng et al. 2013). Fire disturbances also have important effects on C/water fluxes, including subsequent changes in forest stand age and other effects derived from the instantaneous fire emissions (Balshi et al. 2007; Pan et al. 2011). A follow-up research direction is to investigate the impacts of forest stand age and fire disturbances on water/C fluxes.

Previous studies show that elevation of CO_2 concentration has considerable effects on stomatal conductance (Field et al. 1995; De Boer et al. 2011; Lammertsma et al. 2011; Reid et al. 2003) and thus lead to changes in *ET* and stream flow (Gedney et al. 2006). These effects are still controversial in the community as different studies have various opinions. For example, De Boer et al. (2011) and Lammertsma et al. (2011) show that elevated CO_2 concentration leads to apparent decrease in stomatal conductance and reduction in transpiration. On the other hand, McNaughton et al. (1991) and Betts et al.

(1997) indicate that there is an offset of stomatal closure via atmospheric boundary layer feedback and changes in leaf area index. While recent years have seen investigation of the CO_2 effect via biogeochemical models, most current hydrological models have not considered this effect yet. It will be promising and interesting to examine those effects in hydrological model via an appropriate model representation of connection between water cycling and changes in CO_2 concentration. This could be a future direction for my research work.

In the context of global warming, there is a general tendency towards higher frequencies of extreme events such as droughts (IPCC 2013). As shown in Chapter 2, soil moisture and discharge decline have been exacerbated by intensification of agricultural activities. Meanwhile, the impacts of drought on regional carbon fluxes and yields of agriculture ecosystems have not been largely studied. Food sufficiency is currently and is projected to be in risk due to the negative effects of climate change on food productivity (Lobell et al. 2008, 2011; IPCC 2013). Then balance between food security and droughts deterioration is imperative in the future. Investigation on interactions between droughts and agriculture ecosystems would be out of personal interest as well as a support for sustainable agriculture and environment. Another relevant direction is to investigate drought-induced changes in carbon fluxes and their feedbacks to climate.

There is a growing consensus that water is becoming a crucial limiting resource for natural ecosystems as well as human life and economic development (Vörösmarty et al. 2010). With an increasing human population, the rapidly rising demand for water is causing this resource to become progressively scarce. Climatic change may exacerbate

this water limitation, as future warming is expected to raise the rates of *ET* leading to further drying of the land surface (Huntington, 2006; Douville et al. 2012). Then in the context of concurrent changes in climate, bioenergy production, socio-economy and land use, improvement in quantification of water demand in different sectors such as agricultural ecosystems, natural ecosystems, industrial and municipal use would be a necessary task for better water management. These research questions will be promisingly and efficiently addressed by using integrated model such as Global Change Assessment Model (GCAM, Edmonds et al. 1997). This research topic would be a future direction that I will be dedicating to.

REFERENCES

REFERENCES

Adam JC, Haddeland I, Su F, Lettenmaier DP (2007) Simulation of reservoir influences on annual and seasonal discharge changes for the Lena, Yenisei, and Ob'rivers. *Journal of Geophysical Research: Atmospheres*, (1984–2012) 112 D24.

Adam JC, Lettenmaier DP (2008) Application of new precipitation and reconstructed discharge products to discharge trend attribution in Northern Eurasia. *Journal of Climate*, 21(8): 1807-1828.

ADRC (Asian Disaster Reduction Center). (2003) Country report on natural disasters. ADRC, Kobe, Japan.

Alexeev VA, Birdsey RA (1998) Carbon storage in forests and peatlands of Russia. *General Technical Report* NE-244, U.S.D.A. Forest Service Northeastern Research Station, Radnor.

Allen RG, Pereira LS, Raes D, Smith M (1998) Crop evapotranspiration-Guidelines for computing crop water requirements. *FAO Irrigation and Drainage Paper*, 56 (Rome: FAO) pp 328.

Alley RB, Marotzke J, Nordhaus W, Overpeck J, Peteet D, Pielke R, Pierrehumbert R, Rhines P, Stocker T, Talley L (2003) Abrupt climate change. *Science*, 299:2005-2010.

An C, Feng Z, Barton L (2006) Dry or humid? Mid-Holocene humidity changes in arid and semi-arid China. *Quaternary Science Reviews*, 25:351-361.

An S, Xing J (1985) The modified palmer drought index and its application. *Meteorology*, 1985, 1(12): 17-19.

Anderson DB (1936) Relative humidity or vapor pressure deficit. *Ecology*, 17(2), 277-282.

Andrews DG (2010) An introduction to atmospheric physics. Cambridge University Press.

Anthoni PM, Law BE, Unsworth MH (1999) Carbon and water vapor exchange of an open-canopied ponderosa pine ecosystem. *Agricultural and Forest Meteorology*, 95 151-68.

Arctic Climate Impact Assessment (ACIA) (2005) Arctic Climate Impact Assessment. *ACIA Overview Report*, Cambridge University Press, New York, p 1042.

ASCE (American Society of Civil Engineers) (1996) Hydrology handbook. *ASCE Manuals and Reports on Engineering Practice No. 28. ASCE*, New York.

Aubinet M, Grelle A, Ibrom A, Rannik Ü, Moncrieff J, Foken T, Kowalski AS, Martin PH, Berbigier P,Bernhofer C (1999) Estimates of the annual net carbon and water exchange of forests: the EUROFLUX methodology. *Advances in Ecological Research*, 30, 113-175.

Balshi M, McGuire AD, Zhuang Q, Melillo J, Kicklighter DW, Kasischke E, Wirth C, Flannigan M, Harden J, Clein JS (2007) The role of historical fire disturbance in the carbon dynamics of the pan-boreal region: A process-based analysis. *Journal of Geophysical Research: Biogeosciences*, (2005–2012) 112.

Bates BC, Kundzewicz ZW, Wu S and Palutikof JP, Eds (2008) IPCC: Climate Change and Water. Technical Paper of the Intergovernmental Panel on Climate Change, IPCC Secretariat, Geneva.

Belward AS, Estes JE, and Kline KD (1999) The IGBP-DIS global 1-km land-cover data set DISCover: A project overview. *Photogrammetric Engineering and Remote Sensing*, 65:1013-1020.

Betts AK, Ball JH, Beljaars ACM, Miller MJ, Viterbo PA (1996) The land surface-atmosphere interaction: A review based on observational and global modeling perspectives. *Journal of Geophysical Research*, 101(D3), 7209.

Betts RA, Cox PM, Lee SE, Woodward FI (1997) Contrasting physiological and structural vegetation feedbacks in climate change simulations. *Nature*, 387:796-799.

Beyrich F, Mengelkamp HT (2006) Evaporation over a heterogeneous land surface: EVA_GRIPS and the LITFASS-2003 experiment—an overview. *Boundary Layer Meteorology*, 121:5-32.

Bohannon J (2008) The big thaw reaches Mongolia's pristine north. Science 319:567-568.

Bonan G (2008) Ecological Climatology. *Concepts and Applications*, Cambridge University Press, New York, pp. 690.

Budyko M (1974) Climate and Life. *International Geophysical Series*, Academic Press, New York.

Chen B, Ge Q, Fu D, Liu G, Yu G, Sun X, Wang S, Wang H (2009) Upscaling of gross ecosystem production to the landscape scale using multi-temporal Landsat images, eddy covariance measurements and a footprint model. *Biogeosciences Discuss*, 6, 11317-11345.

Chen C, Qian C, Deng A, Zhang W (2012) Progressive and active adaptations of cropping system to climate change in Northeast China. *European Journal of Agronomy*, 38:94-103.

Chen J, He D, Cui S (2003) The response of river water quality and quantity to the development of irrigated agriculture in the last 4 decades in the Yellow River Basin, China. *Water Resources Research*, 39.

Chen Z, Zhang X, Cui M, He X, Ding W, Peng J (2012) Tree-ring based precipitation reconstruction for the forest–steppe ecotone in northern Inner Mongolia, China and its linkages to the Pacific Ocean variability. *Global and Planetary Change*, 86, 45-56.

Cleugh HA, Leuning R, Mu Q, Running SW (2007) Regional evaporation estimates from flux tower and MODIS satellite data. *Remote Sensing of Environment*, 106(3), 285-304.

Coughlan JC, Running SW (1997) Regional ecosystem simulation: A general model for simulating snow accumulation and melt in mountainous terrain. *Landscape Ecology*, 12:119-136.

Daly E, Porporato A (2005) A review of soil moisture dynamics: from rainfall infiltration to ecosystem response. *Environmental Engineering Science*, 22:9-24.

De Boer HJ, Lammertsma EI, Wagner-Cremer F, Dilcher DL, Wassen MJ, Dekker SC (2011) Climate forcing due to optimization of maximal leaf conductance in subtropical vegetation under rising CO2. *Proceedings of the National Academy of Sciences*, 108:4041-4046.

Decker M, Brunke MA, MA, Wang Z, Sakaguchi K, Zeng X, Bosilovich MG (2011) Evaluation of the reanalysis products from GSFC, NCEP, and ECMWF using flux tower observations. *Journal of Climate*, 25, 1916-1944.

Dee DP, Uppala SM, Simmons AJ, et al (2011) The ERA-Interim reanalysis: Configuration and performance of the data assimilation system. *Quarterly Journal of the Royal Meteorological Society*, 137(656), 553-597.

Deng F, Chen J, Pan Y, Peters W, Birdsey R, McCullough K, Xiao J (2013) Forest stand age information improves an inverse North American carbon flux estimate. *Biogeosciences Discussions*, 10:4781-4817.

Dickinson RE, Shaikh M, Bryant R and Graumlich L (1998) Interactive canopies for a climate model. *Journal of Climate*, 11(11), 2823-2836.

Ding Y, Pan S (2007) Evolutionary characteristics of runoff into the sea of the Huanghe River and their causes in recent 50 years. *Quaternary Sciences*, 27 (5):709-717 (In Chinese).

Dolman AJ, De Jeu R (2010) Evaporation in focus. *Nature Geoscience*, 3(5): 296-296.

Dolman AJ, Gash JH, Roberts J and Shuttleworth WJ (1991) Stomatal and surface conductance of tropical rainforest. *Agricultural and Forest Meteorology*, 54(2), 303-318.

Dorigo WA, Chung D, Parinussa R, Liu Y, Wagner W, Fernández-Prieto D (2012) Evaluating global trends (1988–2010) in harmonized multi-satellite surface soil moisture. *Geophysical Research Letters*, 39.

Douville H (1998) Validation and sensitivity of the global hydrologic budget in stand-alone simulations with the ISBA land-surface scheme. *Climate Dynamics*, 14:151-172.

Douville H, Ribes A, Decharme B, Alkama R, Sheffield J (2012) Anthropogenic influence on multidecadal changes in reconstructed global evapotranspiration. *Nature Climate Change*, .

Dulamsuren C, Hauck M and Mühlenberg M (2009) Ground vegetation in the Mongolian taiga forest-steppe ecotone does not offer evidence for the human origin of grasslands. *Applied Vegetation Science*, 8(2), 149-154.

Dye DG, Tucker CJ (2003) Seasonality and trends of snow-cover, vegetation index, and temperature in northern Eurasia. *Geophysical Research Letters*, 30.

Edmonds J, Wise M, Pitcher H, Richels R, Wigley T, Maccracken C (1997) An integrated assessment of climate change and the accelerated introduction of advanced energy technologies-An application of MiniCAM 1 0. Mitigation and Adaptation Strategies for Global Change, 1:311-339.

Euskirchen ES, McGuire AD, Kicklighter DW, et al (2006) Importance of recent shifts in soil thermal dynamics on growing season length, productivity, and carbon sequestration in terrestrial high-latitude ecosystem. *Global Change Biology*, 12: 731-750.

Ewers B, Bond-Lamberty B, and Mackay DS (2011) Consequences of stand age and species' functional trait changes on ecosystem water use of forests. Size- and Age-Related Changes in Tree Structure and Function: Tree Physiology vol. 4, edited by FC Meinzer, B Lachenbruch and TE Dawson, pp. 481-505. Springer , New York.

Ewers B, Gower S, Bond-Lamberty B, Wang C (2005) Effects of stand age and tree species on canopy transpiration and average stomatal conductance of boreal forests. *Plant Cell and Environment*, 28:660-678.

Fang Q, Ma L, Green T, Yu Q, Wang T, Ahuja L (2010) Water resources and water use efficiency in the North China Plain: Current status and agronomic management options. *Agricultural Water Management*, 97:1102-1116.

Farr TG (2007) The shuttle radar topography mission. *Reviews of Geophysics and Space Physics*, 45 RG2004.

Feddes RA, Lenselink KJ (1994) Evapotranspiration. Drainage Principles and Applications, Water Resources Pubns, Wageningen, H.P. Ritzema (Ed.), The Netherlands, pp. 145.

Federov AN (1996) Effects of recent climate change on permafrost landscapes in central Sakha. *Polar Geography*, 20, 99-108.

Fekete BM, Vörösmarty CJ, Roads JO, Willmott CJ (2004) Uncertainties in precipitation and their impacts on runoff estimates. *Journal of Climate*, 17(2), 294-304.

Feng Z, Yang Y, Zhang Y, Zhang P, Li Y (2005) Grain-for-green policy and its impacts on grain supply in West China. Land Use Policy 22:301-312.

Ferguson CR, Sheffield J, Wood EF, and Gao H (2010) Quantifying uncertainty in a remote sensing-based estimate of evapotranspiration over continental USA. *International Journal of Remote Sensing*, 31:3821-3865.

Field C, Jackson R, Mooney H (1995) Stomatal responses to increased CO2: implications from the plant to the global scale. *Plant Cell and Environment*, 18:1214-1225.

Fisher JB, Tu KP, Baldocchi DD (2008) Global estimates of the land–atmosphere water flux based on monthly AVHRR and ISLSCP-II data, validated at 16 FLUXNET sites. *Remote Sensing of Environment*, 112(3), 901-919.

Frey KE, Smith LC (2003) Recent temperature and precipitation increase in West Sibria and their association with the Arctic Oscillation. *Polar Research*, 22(2):287-300.

Froehlich K (2000) Evaluating the water balance of inland seas using isotopic tracers: the Caspian Sea experience. *Hydrological Processes*, 14(8): 1371-1383.

Fu B, Wang J, Chen L, Qiu Y (2003) The effects of land use on soil moisture variation in the Danangou catchment of the Loess Plateau, China. *Catena*, 54:197-213.

Fu C, Yuan H (2001) An virtual numerical experiment to understand the impacts of recovering natural vegetation on the summer climate and environmental conditions in East Asia. *Chinese Science Bulletin*, 46:1199-1203.

Fu G, Chen S, Liu C, Shepard D (2004) Hydro-climatic trends of the Yellow River basin for the last 50 years. *Climatic Change*, 65:149-178.

Gaiser T, De Barros I, Lange F-M, Williams J (2004) Water use efficiency of a maize/cowpea intercrop on a highly acidic tropical soil as affected by liming and fertilizer application. *Plant and Soil*, 263:165-171.

Galloway J, Melillo J (1998) Asian change in the context of global climate change: Impact of natural and anthropogenic changes in Asia on global biogeochemical cycles. Cambridge University Press.

Gao C, Sun B, Zhang T-L (2006) Sustainable nutrient management in Chinese agriculture: challenges and perspective. *Pedosphere*, 16:253-263.

Gao F, Schaaf CB, Strahler AH, Roesch A, Lucht W, Dickinson R (2005) MODIS bidirectional reflectance distribution function and albedo Climate Modeling Grid products and the variability of albedo for major global vegetation types. *Journal of Geophysical Research*, 110(D01104), 2005.

Garnier E, Cordonnier P, Guillerm JL, Sonié L (1997) Specific leaf area and leaf nitrogen concentration in annual and perennial grass species growing in Mediterranean old-fields. *Oecologia*, 111(4), 490-498.

Gash JH and Shuttleworth WJ (2007) Vegetation controls on evaporation - Commentary. Benchmark papers in hydrology: Evaporation, IAHS Press, Wallingford, pp. 233-239.

Gedney N, Cox PM, Betts RA, Boucher O, Huntingford C, Stott PA (2006) Detection of a direct carbon dioxide effect in continental river runoff records. *Nature*, 439(7078), 835-838.

Gerten D, Schaphoff S, Haberlandt U, Lucht W, and Sitch S (2004) Terrestrial vegetation and water balance—hydrological evaluation of a dynamic global vegetation model. *Journal of Hydrology*, 286:249-270.

Glenn EP, Morino K, Didan K, Jordan F, Carroll CK, Nagler PL, Hultine K, Sheader L, Waugh J (2008) Scaling sap flux measurements of grazed and ungrazed shrub communities with fine and coarse-resolution remote sensing. *Ecohydrology*, 1(4): 316-29.

Gong D-Y, Shi P-J, Wang J-A (2004) Daily precipitation changes in the semi-arid region over northern China. *Journal of Arid Environments*, 59:771-784.

Groisman P, Gutman G, Reissell A (2010) Introduction: Climate and Land-Cover Changes in the Arctic. Eurasian Arctic Land Cover and Land Use in a Changing Climate, edited by G. Gutman and A. Reissell, Springer, pp 1-8.

Groisman PY, Clark EA, Kattsov VM, Lettenmaier DP et al (2009) The Northern Eurasia earth science partnership: an example of science applied to societal needs. *Bulletin of the American Meteorological Society*, 5: 671-688.

Groisman PY, Sun B, Vose RS, Lawrimore JH, Whitfield PH, Førland E, Hanssen-Bauer I, Serreze MC, Razuvaev VN, and Alekseev GV (2003) Contemporary climate changes in high latitudes of the Northern Hemisphere: daily time resolution. 14th Symp. on Global Change and Climate Variations, Long Beach, CA, American Meteorological Society, CD-ROM, 4.8.

Groisman, PY, Sherstyukov BG, Razuvaev VN, Knight RW, Enloe JG, Stroumentova NS, Whitfield PH, Forland E, Hannsen-Bauer I, Tuomenvirta H, Aleksandersson H, Mescherkaya AV and Karl TR (2007) Potential forest fire danger over Northern Eurasia: changes during the 20th century. *Global and Planetary Change*, 56, pp. 371–386.

Guo J, Liu X, Zhang Y, Shen J, Han W, Zhang W, Christie P, Goulding K, Vitousek P, Zhang F (2010) Significant acidification in major Chinese croplands. *Science*, 327:1008-1010.

Hamed KH, Rao AR (1998) A modified Mann–Kendall trend test for autocorrelated data. *Journal of Hydrology*, 204, 182-96.

Hamon WR (1963) Computation of direct runoff amounts from storm rainfall, International Association of Scientific Hydrology Publication, 63:52-62.

Harris I, Jones P, Osborn T, and Lister D (2013) Updated high-resolution grids of monthly climatic observations–the CRU TS3 10 Dataset. *International Journal of Climatology*, DOI: 10.1002/joc.3711.

He D, Liu Y, Pan Z, An P, Wang L, Dong Z, Zhang J, Pan X, Zhao P (2013) Climate change and its effect on reference crop evapotranspiration in central and western Inner Mongolia during 1961–2009. *Frontiers of Earth Science*, 7:417-428.

He, J, Kuhn N, Zhang X, Zhang X and Li H (2009) Effects of 10 years of conservation tillage on soil properties and productivity in the farming–pastoral ecotone of Inner Mongolia, China. *Soil Use and Management*, 25(2), 201-209.

Heim Jr RR (2002) A review of twentieth-century drought indices used in the United States. *Bulletin of the American Meteorological Society*, 83:1149-1165.

Heinsch FA, Zhao M, Running SW, Kimball JS, Nemani RR, Davis KJ, Bolstad PV, Cook BD, Desai AR, Ricciuto DM (2006) Evaluation of remote sensing based terrestrial productivity from MODIS using regional tower eddy flux network observations. *Geoscience and Remote Sensing*, IEEE Transactions on, 44(7), 1908-1925.

Held IM, Soden BJ (2000) Water vapor feedback and global warming. *Annual Review of Energy and The Environment*, 25:441-475.

Hollinger DY, Richardson AD (2005) Uncertainty in eddy covariance and its applicatino to physiological models. *Tree Physiology*, 25, 873-885.

Hu H, Huang G, Huang H (2013) Variation of runoff at Tieling station of Liaohe River basin and its influence factors. *Research of Soil and water conservation*, 20 (2), In Chinese.

Hu J, Su Y, Tan B, Huang D, Yang W, Schull M, Bull MA, Martonchik JV, Diner DJ, Knyazikhin Y, Myneni RB (2007) Analysis of the MISR LAI/FPAR product for spatial and temporal coverage, accuracy and consistency. *Remote Sensing of Environment*, 107(1-2), 334-347.

Huang M, Dang T, Gallichand J, Goulet M (2003) Effect of increased fertilizer applications to wheat crop on soil-water depletion in the Loess Plateau, China. *Agricultural Water Management*, 58:267-278.

Huang Y, Sass R, Sun W, Zhang W, Yu Y (2010) Reducing nitrogen fertilizer use to mitigate negative environmental impact in China. James A. Baker III institute for public policy. Houston, TX.

Huntington TG (2006) Evidence for intensification of the global water cycle: review and synthesis. *Journal of Hydrology*, 319(1):83-95.

Huxman TEet al (2005) Ecohydrological implications of woody plant encroachment. *Ecology*, 86(2), 308-319.

Idso SB, Jackson RD (1969) Thermal radiation from the atmosphere. *Journal of Geophysical Research*, 74: 5397−5402.

IPCC(Intergovernmental Panel on Climate Change) (2001) Climate change 2001: The Scientific Basis. *Contribution of Working Group I to the Third Assessment Report of the Intergovernmental Panel on Climate Change.* Cambridge University Press, New York.

IPCC(Intergovernmental Panel on Climate Change) (2007) Climate Change 2007: The Physical Science Basis. Cambridge University Press, Cambridge.

IPCC(Intergovernmental Panel on Climate Change) (2013) Climate Change 2007: The Physical Science Basis. Cambridge University Press, Cambridge.

Jacobsen A (1999) Estimation of the soil heat flux/net radiation ratio based on spectral vegetation indexes in high-latitude Arctic areas. *International Journal of Remote Sensing*, 20:445-461.

Jarvis PG (1976) The interpretation of the variations in leaf water potential and stomatal conductance found in canopies in the field. *Philosophical Transactions of the Royal Society of London. Series B, Biological Sciences*, 273(927), 593-610.

Jensen ME (2010) Estimating evaporation from water surfaces. CSU/ARS Evapotranspiration Workshop, pp. 1-27.

Jensen ME, Dotan A, Sanford R (2005) Penman-Monteith Estimates of Reservoir Evaporation, ASCE.

Jensen ME, Haise HR (1963) Estimating evapotranspiration from solar radiation. *Journal of the Irrigation and Drainage Division*, Proceedings of the American Society of Civil Engineers, 89, 15-41.

Jiang L, Islam S, Guo W, Singh Jutla A, Senarath SUS, Ramsay BH, Eltahir E (2009) A satellite-based daily actual evapotranspiration estimation algorithm over South Florida. *Global and Planetary Change*, 67(1-2), 62-77.

Jiang Y, Zhuang Q, Schaphoff S, Sitch S, Sokolov A, Kicklighter D, Melillo J (2012) Uncertainty analysis of vegetation distribution in the northern high latitudes during the 21st century with a dynamic vegetation model. *Ecology and Evolution*, 2(3), 593-614.

Jiménez Cet al (2011) Global intercomparison of 12 land surface heat flux estimates. *Journal of Geophysical Research: Atmospheres (1984–2012)*, 116(D2).

Jin Y, Schaaf CB, Gao F, Li X, Strahler AH, Zeng X, Dickinson RE (2002) How does snow impact the albedo of vegetated land surfaces as analyzed with MODIS data?. *Geophysical Research Letters*, 29(10).

Jin, Y, Schaaf CB, Woodcock CE, Gao F, Li X, Strahler AH, Lucht W, and Liang S (2003a) Consistency of MODIS surface bidirectional reflectance distribution function and albedo retrievals: 1 Algorithm performance. *Journal of Geophysical Research*, 108(D5).

Jin, Y, Schaaf CB, Woodcock CE, Gao F, Li X, Strahler AH, Lucht W, and Liang S (2003b) Consistency of MODIS surface bidirectional reflectance distribution function and albedo retrievals: 2 Validation. *Journal of Geophysical Research*, 108(D5).

John R et al (2013) Vegetation response to extreme climate events on the Mongolian Plateau from 2000-2010. *Environmental Research Letters*, 8:035033.

Jones PD, Lister DH, Osborn TJ, Harpham C, Salmon M, Morice CP (2012) Hemispheric and large-scale land-surface air temperature variations: An extensive revision and an update to 2010. *Journal of Geophysical Research.:Atmosphere*, (1984–2012) 117(D5).

Joshi C, Mohanty BP, Jacobs JM, Ines AV (2011) Spatiotemporal analyses of soil moisture from point to footprint scale in two different hydroclimatic regions. *Water Resources Research*, 47.

Ju X, Xing G, Chen X, Zhang S, Zhang L, Liu X, Cui Z, Yin B, Christie P, Zhu Z (2009) Reducing environmental risk by improving N management in intensive Chinese agricultural systems. Proceedings of the National Academy of Sciences, 106:3041-3046.

Jung Met al (2010) Recent decline in the global land evapotranspiration trend due to limited moisture supply. *Nature*, 467(7318), 951-954.

Kahrl F, Li Y, Roland-Holst D, Xu J, and Zilberman D (2010a) Toward sustainable use of nitrogen fertilizers in China. Giannini Foundation of Agricultural Economics, University of California, ARE Update 14(2):5-7.

Kahrl F, Li Y, Su Y, Tennigkeit T, Wilkes A, Xu J (2010b) Greenhouse gas emissions from nitrogen fertilizer use in China. *Environmental Science & Policy*, 13:688-694.

Katul GG, Oren R, Manzoni S, Higgins C, Parlange MB (2012) Evapotranspiration: a process driving mass transport and energy exchange in the soil-plant-atmosphere-climate system. *Reviews of Geophysics*, 50(RG3002).

Keeling CD, Whorf TP (2005) Atmospheric CO2 records from sites in the SIO air sampling network. *Trends: A Compendium of Data on Global Change (Oak Ridge. TN: Carbon Dioxide Information Analysis Center. Oak Ridge National Laboratory)*, 16-26.

Kistler R, Kalnay E, Collins W, Saha S, White G, Woollen J, Kalnay E, Chelliah M, Ebisuzaki W, Kanamitsu M, Kousky V, van den Dool H, Jenne R, Fiorino M (2001) The NCEP-NCAR 50-year reanalysis: Monthly means CD-ROM and documentation. *Bulletin of the American Meteorological Society*, 82:247-267.

Kumar S, Lawrence DM, Dirmeyer PA, Sheffield J (2014) Less reliable water availability in the 21st century climate projections. *Earth's Future*, 2:152-160.

Kurc AS, Small EE (2004) Dynamics of evapotranspiration in semiarid grassland and shrubland ecosystems during the summer monsoon season, central New Mexico. *Water Resources Research*, 40(9).

Kutner MH, Nachtsheim CJ, Neter J, Li W (2005) Chapter 22. Applied Linear Statistical Models, Fifth edition, McGraw-Hill Irwin, New York.

Lammertsma EI, de Boer HJ, Dekker SC, Dilcher DL, Lotter AF, Wagner-Cremer F (2011) Global CO2 rise leads to reduced maximum stomatal conductance in Florida vegetation. Proceedings of the National Academy of Sciences, 108:4035-4040.

Landsberg JJ, Gower ST (1996) Applications of physiological ecology to forest management. Academic Press.

Lehner B, Döll P (2004) Development and validation of a global database of lakes, reservoirs and wetlands. *Journal of Hydrology*, 296(1-4):1-22.

Li J, Lin B, Liang G and Shen G (2000) Prediction of chemical fertilizer consumption in China. Nutrient Cycling and Management in Agro-Ecosystem (in Chinese),edited by Zhou JM, Fan QZ, Xie JC and Hardter R, Hohai University Press, Nanjing. pp. 53-60.

Li M, Ma Z, Niu G-Y (2011) Modeling spatial and temporal variations in soil moisture in China. *Chinese Science Bulletin*, 56:1809-1820.

Li S, Asanuma J, Kotani A, Davaa G, Oyunbaatar D (2007) Evapotranspiration from a Mongolian steppe under grazing and its environmental constraints. *Journal of Hydrology*, 333(1), 133-143.

Li S, Eugster W, Asanuma J, Kotani A, Davaa G, Oyunbaatar D, Sugita M (2008) Response of gross ecosystem productivity, light use efficiency, and water use efficiency of Mongolian steppe to seasonal variations in soil moisture. *Journal of Geophysical Research*, 113(G1).

Li W, Zhao Z, Li X, Sun L (2003) The drought characteristics analysis in North China and its causes of formation. *Journal of Arid Meteorology*, 21(4):1–5 (in Chinese).

Liang X, Lettenmaier DP, Wood EF, and Burges SJ (1994) A simple hydrologically based model of land surface water and energy fluxes for general circulation models. *Journal of Geophysical Research.*, 99:14415-14428.

Lindroth A, Grelle A, Morén AS (1998) Long-term measurements of boreal forest carbon balance reveal large temperature sensitivity. *Global Change Biology*, 4:443-450.

Liu J, An S, Liao R, Ren S, Liang H (2009) Temporal variation and spatial distribution of the root system of corn in a soil profile. *Chinese Journal of Eco-Agriculture*, 17(3):517-521.

Liu J, Gao J, Lv S, Han Y, and Nie Y (2011) Shifting farming–pastoral ecotone in China under climate and land use changes. *Journal of Arid Environments*, 75(3), 298-308.

Liu R, Zhu Z, Fang W, Deng T, Zhao G (2008) Distribution pattern of winter wheat root system. *Chinese Journal of Ecology*, 37(11): 2024-2027.

Liu S, Mao D, and Lu L (2006) Measurement and estimation of the aerodynamic resistance. *Hydrology and Earth System Sciences Discussions*, 3(3), 681-705.

Liu Y, Zhuang Q, Chen M, Tchebakova N, Pan Z, et al (2013) Response of evapotranspiration and water availability to changing climate and land cover on the Mongolian Plateau during the 21st century. *Global Planet Change*, 108: 85-99.

Liu Y, Zhuang Q, Miralles D, Pan Z, Tchebakova N, et al (2014) Responses of evapotranspiration and water availability to the changing climate in Northern Eurasia. *Climatic Change*, DOI 10.1007/s10584-014-1234-9.

Liu Y, Zhuang Q, Pan Z, Miralles D, Tchebakova N, et al (2014) Impact of forcing data uncertainty on the estimation of evapotranspiration in Northern Eurasia. *Journal of Geophysical Research: Atmospheres*, in review (available upon request).

Livneh B, Lettenmaier DP (2012) Multi-criteria parameter estimation for the unified land model. *Hydrology and Earth System Sciences*, 16:3029-3048.

Lobell DB, Burke MB, Tebaldi C, Mastrandrea MD, Falcon WP, Naylor RL (2008) Prioritizing climate change adaptation needs for food security in 2030. *Science*, 319:607-610.

Lobell DB, Schlenker W, Costa-Roberts J (2011) Climate trends and global crop production since 1980. *Science*, 333:616-620.

Loveland TR, Reed BC, Brown JF, Ohlen DO, Zhu Z, Yang L, and Merchant JW (2000) Development of a global land cover characteristics database and IGBP DISCover from 1 km AVHRR data. *Journal. International Journal of Remote Sensing*, 21: 1303-1330.

Lu N, Chen S, Wilske B, Sun G, and Chen J (2011) Evapotranspiration and soil water relationships in a range of disturbed and undisturbed ecosystems in the semi-arid Inner Mongolia, China. *Journal of Plant Ecology*, 4: 49-60.

Lu Y, Zhuang Q, Zhou G, Sirin A, Melillo J, Kicklighter D (2009) Possible decline of the carbon sink in the Mongolian Plateau during the 21st century. *Environmental Research Letters*, 4(4), 045023.

Ma Z, Fu C (2006) Some evidence of drying trend over northern China from 1951 to 2004. *Chinese Science Bulletin*, 51:2913-2925.

Mallick K, Jarvis AJ, Boegh E, Fisher J, et al (2014) A surface temperature initiated closure (STIC) for surface energy balance fluxes. *Remote Sensing of Environment*, 141, 243-261.

Massmana WJ, Lee X (2002) Eddy covariance flux corrections and uncertainties in long-term studies of carbon and energy exchanges. *Agricultural and Forest Meteorology*, 113, 121-144.

McClelland JW, Holmes RM, Peterson BJ, and Stieglitz M (2004) Increasing river discharge in the Eurasian Arctic: Consideration of dams, permafrost thaw, and fires as potential agents of change. *Journal of Geophysical Research: Atmospheres*, (1984–2012) 109 D18.

McGuire AD, Melillo JM, Joyce LA, Kicklighter DW, Grace AL, Moore IIIB, Vorosmarty CJ (1992) Interactions between carbon and nitrogen dynamics in estimating net primary productivity for potential vegetation in North America. *Global Biogeochemical Cycles*, 6, 101-124.

McGuire AD, Melillo JM, Kicklighter DW, Pan Y, Xiao X, Helfrich J, Moore B, Vorosmarty CJ, Schloss AL (1997) Equilibrium responses of global net primary production and carbon storage to doubled atmospheric carbon dioxide: Sensitivity to changes in vegetation nitrogen concentration. *Global Biogeochemical Cycles*, 11(2), 173-189.

McNaughton KG, Jarvis PG (1991) Effects of spatial scale on stomatal control of transpiration. *Agricultural and Forest Meteorologyis*, 54, 279–302.

Melillo JM, McGuire AD,Kicklighter D, Moore B,Vorosmarty CJ, Schloss AL (1993) Global climate change and terrestrial net primary production. *Nature*, 363(6426): 234-240.

Mengelkamp HT, Beyrich F, Heinemann G, Ament F, JBange, Berger F, Bösenberg J, Foken T,Hennemuth B, and Heret C (2006) Evaporation over a heterogeneous land surface: the EVA-GRIPS project. *Bulletin of the American Meteorological Society*, 87:775-786.

Miglietta F, Peressotti A, Viola R, Körner C, Amthor JS (2011) Stomatal numbers, leaf and canopy conductance, and the control of transpiration. Proceedings of the National Academy of Sciences, 108(28), E275-E275.

Milner KS, Coble DW, McMahan AJ, Smith EL (2003) FVSBGC: a hybrid of the physiological model STAND-BGC and the forest vegetation simulator. *Canadian Journal of Forest Research*, 33(3), 466-479.

Minayeva T, Gunin P, Sirin A, Dugardzhav C, Bazha S (2004) Peatlands in Mongolia: The typical and disappearing landscape. *Peatlands International*, 2004. N 2. P. 44–47.

Minayeva T, Sirin A, Dorofeyuk N, et al (2005) Mongolian Mires: from taiga to desert. Stapfia 85. zugleich Kataloge der OÖ. Landesmuseen Neue Serie 35, 335–352.

Miralles DG, De Jeu RAM, Gash JH, Holmes TRH, Dolman AJ (2011a) Magnitude and variability of land evaporation and its components at the global scale. *Hydrology and Earth System Sciences*, 15(3): 967-981.

Miralles DG, Gash JH, Holmes TR, de Jeu RA, Dolman AJ (2010) Global canopy interception from satellite observations. *Journal of Geophysical Research: Atmospheres (1984–2012)*, 115(D16).

Miralles DG, Holmes TRH, De Jeu R, Gash JH, Meesters AGCA, Dolman AJ (2011b) Global land-surface evaporation estimated from satellite-based observations. *Hydrology and Earth System Sciences*, 15(2): 453-469.

Mitchell TD, Jones PD (2005) An improved method of constructing a database of monthly climate observations and associated high-resolution grids. *International Journal of Climatology*, 25(6), 693-712.

Mo X, Liu S, Lin Z, Guo R (2009) Regional crop yield, water consumption and water use efficiency and their responses to climate change in the North China Plain. *Agriculture Ecosystems & Environment*, 134:67-78.

Mohamed YA, Bastiaanssen WGM, Savenije HHG, van den Hurk BJJM, Finlayson CM (2012) Wetland versus open water evaporation: An analysis and literature review. *Physics and Chemistry of the Earth*, 47-48: 114-121.

Monteith JL (1965) Evaporation and environment. *Symposium of the Society of Experimental Biology*, 19: 205-224.

Moore CJ (1986) Frequency response corrections for eddy correlation systems. *Boundary Layer Meteorology*, 37, 17-35.

Mu Q, Heinsch FA, Zhao M, Running SW (2007) Development of a global evapotranspiration algorithm based on MODIS and global meteorology data. *Remote Sensing of Environment*, 111(4): 519-537.

Mu Q, Zhao M, Running SW (2011) Improvements to a MODIS global terrestrial evapotranspiration algorithm. *Remote Sensing of Environment*, 115(8): 1781-1800.

Mueller B, et al (2011) Evaluation of global observations-based evapotranspiration datasets and IPCC AR4 simulations. *Geophysical Research Letters*, 38(6), L06402.

Mueller B, Hirschi M, Jimenez C, Ciais P, Dirmeyer PA, Dolman AJ, Fisher JB, Jung M, Ludwig F, and Maignan F (2013) Benchmark products for land evapotranspiration: LandFlux-EVAL multi-data set synthesis. *Hydrology and Earth System Sciences*, 17: 3707-3720.

Muramatsu N (2003) County-level income inequality and depression among older Americans. *Health Services Research*, 38:1863-1884.

NEESPI (2004) The Northern Eurasia Earth Science Partnership Initiative (NEESPI). Executive Overview, Version 2.1.

New M, Hulme M, Jones P (1999) Representing twentieth-century space-time climate variability, Part I: Development of a 1961-90 mean monthly terrestrial climatology. *Journal of Climate*, 12(3), 829-856.

New M, Hulme M, Jones P (2000) Representing twentieth-century space-time climate variability, Part II: Development of 1901-96 monthly grids of terrestrial surface climate. *Journal of Climate*, 13(13), 2217-2238.

Niu G, Yang Z, Mitchell KE, Chen F, et al (2011) The Community Noah Land Surface Model with Multi-Parameterization Options (Noah-MP): 1 Model Description and Evaluation with Local-scale Measurements. *Journal of Geophysical Research*, 116, D12, D12109.

Niyogi D, Alapaty K, Raman S, and Chen F (2009) Development and Evaluation of a Coupled Photosynthesis-Based Gas Exchange Evapotranspiration Model (GEM) for Mesoscale Weather Forecasting Applications. *Journal of Applied Meteorology and Climatology*, 48, 349-368.

Noy-Meir I (1973) Desert ecosystems: environment and producers. *Annual review of ecology and systematics*, 4, 25-51.

Oki T, Hanasaki N, Ikoma E, Yasukawa M, Kitsuregawa M, and Dirmeyer PA (2006) GSWP-2 intercomparison and data distribution center. *GEWEX news*, 16(3): 11–12.

Oki T, Kanae S (2006) Global hydrological cycles and world water resources. *Science*, 313(5790), 1068-72.

Pan Y, Chen JM, Birdsey R, McCullough K, He L, Deng F (2011) Age structure and disturbance legacy of North American forests. *Biogeosciences*, 8:715-732.

Pan Y, Mcguire AD, Kicklighter DW, Melillo JM (1996) The importance of climate and soils for estimates of net primary production: a sensitivity analysis with the terrestrial ecosystem model. *Global Change Biology*, Biol. 2(1): 5-24.

Papale D, Valentini R (2003) A new assessment of European forests carbon exchanges by eddy fluxes and artificial neural network spatialization. *Global Change Biology*, 9(4): 525-536.

Parmentier F, MVan Der Molen, JVan Huissteden, Karsanaev S, Kononov A, Suzdalov D, Maximov T, and Dolman A (2011) Longer growing seasons do not increase net carbon uptake in the northeastern Siberian tundra. *Journal of Geophysical Research: Biogeosciences*, (2005–2012) 116.

Penman HL (1948) Natural evaporation from open water, bare soil and grass. Proceedings of the Royal Society of London, Series A Mathematical and Physical Sciences, 193(1032): 120-145.

Penman HL (1956) Evaporation: An introductory survey. *Netherlands Journal of Agricultural Science*, 4(1): 9-29.

Penman HL (1963) *Vegetation and Hydrology*, Commonwealth Bureau of Soils, Technical Communications 53, England, Harpenden.

Peterson BJ, et al (2006) Trajectory shifts in the Arctic and subarctic freshwater cycle. *Science*, 313(5790), 1061-6.

Peterson BJ, Holmes RM, McClelland JW, Vorosmarty CJ, Lammers RB, Shiklomanov AI, Shiklomanov IA, and Rahmstorf S (2002) Increasing river discharge to the Arctic Ocean. *Science*, 298(5601): 2171-2173.

Piao S, Ciais P, Huang Y, Shen Z, Peng S, Li J, Zhou L, Liu H, Ma Y, Ding Y (2010) The impacts of climate change on water resources and agriculture in China. *Nature*, 467:43-51.

Pierce LL, Running SW, Walker J (1994) Regional-scale relationships of leaf area index to specific leaf area and leaf nitrogen content. *Ecological Applications*, 4(2), 313-321.

Poorter H, Evans JR (1998) Photosynthetic nitrogen-use efficiency of species that differ inherently in specific leaf area. *Oecologia*, 116(1), 26-37.

Population census Office of China (2011) Main statistics on sixth national population census in China. China Statistics Press, Beijing.

Priestley C, Taylor R (1972) On the assessment of surface heat flux and evaporation using large-scale parameters. *Monthly Weather Review*, 100:81-92.

Rahmstorf S, and Ganopolski A (1999) Long-term global warming scenarios computed with an efficient coupled climate model. *Climatic Change*, 43:353-367.

Raich JW, Rastetter EB, Melillo JM, Kicklighter DW, Steudler PA, Peterson BJ, Grace AL, Moore III B, Vorosmarty CJ (1991) Potential net primary productivity in South America: application of a global model. *Ecological Applications*, 1(4), 399-429.

Raun WR, Johnson GV (1999) Improving nitrogen use efficiency for cereal production. Agronomy journal 91:357-363.

Rawlins M, Frolking S, Lammers R, and Vörösmarty CJ (2006) Effects of uncertainty in climate inputs on simulated evapotranspiration and runoff in the Western Arctic. *Earth interactions*, 10:1-18.

Reference Book on Climate of the USSR, Leningrad: Gidrometeoizdat.

Reid CD, Maherali H, Johnson HB, Smith SD, Wullschleger SD, Jackson RB (2003) On the relationship between stomatal characters and atmospheric CO2. *Geophysical Research Letters*, 30.

Ren H, Luo Y (2004) The Exper imen ta l Research on the Water-consumpion of Winter Wheat and Summer Maize in the Northwest Plain of Shandong Province. *Journal of Irrigation and Drainage*, 23 (4):37-39, (in Chinese).

Rienecker MM, Suarez MJ, Gelaro R, Todling R, Bacmeister J, Liu E, Bosilovich MG, Schubert SD, Takacs L, and Kim G-K (2011) MERRA: NASA's modern-era retrospective analysis for research and applications. *Journal of Climate*, 24:3624-3648.

Rodríguez-Iturbe I, Porporato A (2004) Ecohydrology of water-controlled ecosystems. *Soil Moisture and Plant Dynamics*, .

Romanou A, Tselioudis G, Zerefos CS, Clayson CA, Curry JA, Andersson A (2010) Evaporation-precipitation variability over the Mediterranean and the Black Seas from satellite and reanalysis estimates. *Journal of Climate*, 23(19): 5268-5287.

Romanovsky VE (2002) Book Review: A guide to frozen ground in transition, by Neil Davis. *Journal of Glaciology*, Vol. 48, No. 162, 478.

Rosenzweig C, Karoly D, Vicarelli M, Neofotis P, Wu Q, Casassa G, Menzel A, Root TL, Estrella N, Seguin B (2008) Attributing physical and biological impacts to anthropogenic climate change. *Nature*, 453:353-357.

Running SW, Coughlan JC (1988) A general model of forest ecosystem processes for regional applications I. *Hydrologic balance*, canopy gas exchange and primary production processes. Ecological Modelling, 42(2), 125-154.

Salomon J, Schaaf CB, Strahler AH, Gao F,and Jin Y (2006) Validation of the MODIS Bidirectional Reflectance Distribution Function and Albedo Retrievals Using Combined Observations From the Aqua and Terra Platforms. *IEEE Transactions on Geoscience and Remote Sensing*, 44(6), 1555-1565.

Sankey TT, Montagne C, Graumlich L, Lawrence R, and Nielsen J (2006) Lower forest–grassland ecotones and 20th Century livestock herbivory effects in northern Mongolia. *Forest Ecology and Management*, 233(1), 36-44.

Saurer M, Siegwolf RT, Schweingruber FH (2004) Carbon isotope discrimination indicates improving water-use efficiency of trees in northern Eurasia over the last 100 years. *Global Change Biology*, 10:2109-2120.

Schaaf CB, Gao F, Strahler AH, Lucht W, Li X, Tsang T, Strugnell NC, Zhang X, Jin Y, Muller JP (2002) First operational BRDF, albedo nadir reflectance products from MODIS. *Remote Sensing of Environment*, 83(1-2), 135-148.

Seneviratne SI, Corti T, Davin EL, Hirschi M, Jaeger EB, Lehner I, Orlowsky B, Teuling AJ (2010) Investigating soil moisture–climate interactions in a changing climate: A review. *Earth-Science Reviews*, 99:125-161.

Serreze MC, Barry RG (2005) The Arctic Climate System, Cambridge University Press.

Serreze MC, Walsh JE, Chapin III FS, Osterkamp T, Dyurgerov M, Romanovsky V, Oechel WC, Morison J, Zhang T, and Barry RG (2000) Observational evidence of recent change in the northern high-latitude environment. *Climatic Change*, 46:159–207.

Sheffield J, Goteti G, and Wood EF (2006) Development of a 50-year high-resolution global dataset of meteorological forcings for land surface modeling. *Journal of Climate*, 19:3088-3111.

Shepard DA (1968) A two-dimensional interpolation function for irregularly-spaced data. Proceedings of the 1968 23rd ACM national conference, ACM, pp. 517-524.

Shuttleworth WJ (1992) Evaporation. Handbook of hydrology, Maidment DR (Eds.) McGraw Hill, New York.

Shvidenko A, Schepaschenko D, Nilsson S, McCallum I (2008) Boreal forests in high latitudes of the NEESPI domain. Proceedings of the Northern Eurasian Earth Science Partnership Initiative (NEESPI) Regional Science Team Meeting devoted to the High Latitudes, 2-6 June, Helsinki, Finland. iLEAPS Report Series No 1.

Simmons A, et al (2004) Comparison of trends and low-frequency variability in CRU, ERA-40, and NCEP/NCAR analyses of surface air temperature. *Journal of Geophysical Research: Atmospheres*, (1984–2012) 109.

Simpson EH (1951) The interpretation of interaction in contingency tables. *Journal of the Royal Statistical Society*, Series B (Methodological):238-241.

Soja AJ, Cofer III WR, Shugart HH, Sukhinin AI, Stackhouse Jr PW, McRae DJ and Conard SG (2004a) Estimating fire emissions and disparities in boreal Siberia (1998 through 2002). *Journal of Geophysical Research*, 109 (D14S06).

Soja AJ, Sukhinin AI, Cahoon Jr DR, Shugart HH and Stackhouse Jr PW (2004b) AVHRR-derived fire frequency, distribution and area burned in Siberia. *International Journal of Remote Sensing*, 25 (10):1939–1960.

Sokolov AP, Schlosser CA, Dutkiewicz S, Paltsev S, Kicklighter DW, Jacoby HD, Prinn RG, Forest CE, Reilly JM, Wang C (2005) MIT integrated global system model(IGSM) version 2: model description and baseline evaluation. MIT Joint Program on the Science and Policy of Global Change Report, Report 124, Cambridge, Massachusetts.

Sprintsin M, Karnieli A, Berliner P, Rotenberg E, Yakir D, Cohen S (2009) Evaluating the performance of the MODIS Leaf Area Index (LAI) product over a Mediterranean dryland planted forest. *International Journal of Remote Sensing*, 30(19), 5061-5069.

Stephens GL, et al (2012) An update on Earth's energy balance in light of the latest global observations. *Nature Geoscience*, 5:691-696.

Sukhinin AI, French NHF, Kasischke ES, Hewson JH, Soja AJ, Csiszar IA, Hyer EJ, Loboda T, Conard SG, Romasko VI, Pavlichenko EA, Miskiv SI, and Slinkina OA (2004) AVHRR-based mapping of fires in Russia: new products for fire management and carbon cycle studies. *Remote Sensing of Environment*, 93: 546–564.

Sun G, Alstad K, Chen J, Chen S, Ford CR, Lin G, Liu C, Lu N, McNulty SG, Miao H (2011a) A general predictive model for estimating monthly ecosystem evapotranspiration. *Ecohydrology*, 4(2), 245-255.

Sun G, Caldwell P, Noormets A, McNulty SG, Cohen E, Moore Myers J, Domec JC, Treasure E, Mu Q, Xiao J (2011b) Upscaling key ecosystem functions across the conterminous United States by a water-centric ecosystem model. *Journal of Geophysical Research: Biogeosciences (2005–2012)*, 116(G3).

Sun W, Wu W, Zhang B (2002) An approach to the fluctuation mechanism of ecotone. *Journal of Environmental Sciences*, 14(1), 127-131.

Tao F, Yokozawa M, Hayashi Y, Lin E (2003) Changes in agricultural water demands and soil moisture in China over the last half-century and their effects on agricultural production. *Agricultural and Forest Meteorology*, 118:251-261.

Tchebakova NM, Kolle O, et al (2002) Inter-annual and seasonal variations of energy and water vapour fluxes above a Pinus sylvestris forest in the Siberian middle taiga. *Tellus B*, 54(5) 537-551.

Tchebakova NM, Parfenova E, Soja AJ (2009) The effects of climate, permafrost and fire on vegetation change in Siberia in a changing climate. *Environmental Research Letters*, 4(4), 045013.

Tchebakova NM, Parfenova EI, Soja AJ (2011) Climate change and climate-induced hot spots in forest shifts in central Siberia from observed data. *Regional Environmental Change*, 11(4), 817-827.

Thornthwaite CW (1948) An approach toward a rational classification of climate. *Geographical Review*, 38:55-94.

Tong C, Hall CA, Wang H (2003) Land use change in rice, wheat and maize production in China (1961–1998). *Agriculture Ecosystems & Environment*, 95:523-536.

Trenberth KE, Dai A, van der Schrier G, Jones PD, Barichivich J, Briffa KR, Sheffield J (2014) Global warming and changes in drought. *Nature Climate Change*, 4:17-22.

Turc L (1961) Evaluation des besoins en eau d'irrigation, évapotranspiration potentielle. *Annales Agronomiques*, 12:13-49.

Turner DP, Ritts, Cohen WD, Gower WB, et al. 2003. Scaling Gross Primary Production (GPP) over boreal and deciduous forest landscapes in support of MODIS GPP product validation. Remote Sensing of Environment, 88(3), 256-270.

Valiantzas JD (2006) Simplified versions for the Penman evaporation equation using routine weather data. *Journal of Hydrology*, 331(3-4), 690-702.

Vinukollu RK, Wood EF, Ferguson CR, and Fisher JB (2011) Global estimates of evapotranspiration for climate studies using multi-sensor remote sensing data: Evaluation of three process-based approaches. *Remote Sensing of Environment*, 115(3), 801-823.

Vörösmarty CJ, et al (2010) Global threats to human water security and river biodiversity. *Nature*, 467(7315): 555-561.

Vörösmarty CJ, Federer CA, Schloss AL (1998) Potential evaporation functions compared on US watersheds: possible implications for global-scale water balance and terrestrial ecosystem modeling. *Journal of Hydrology*, 207(3-4): 147-169.

Vorosmarty CJ, Green P, Salisbury J, Lammers RB (2000) Global Water Resources: Vulnerability from Climate Change and Population Growth. *Science*, 289(5477), 284-288.

Wang A, Lettenmaier DP, Sheffield J (2011) Soil moisture drought in China, 1950-2006. *Journal of Climate*, 24:3257-3271.

Wang E, Harman WL, Williams JR, Xu C (2002) Simulated effects of crop rotations and residue management on wind erosion in Wuchuan, west-central Inner Mongolia, China. *Journal of Environmental Quality*, 31:1240-1247.

Wang J, Liu W, Dang T (2011) Responses of soil water balance and precipitation storage efficiency to increased fertilizer application in winter wheat. *Plant and Soil*, 347:41-51.

Wang K, Dickinson RE (2012) A review of global terrestrial evapotranspiration: Observation, modeling, climatology, and climatic variability. *Reviews of Geophysics*, 50(2).

Wang Q, Tenhunen J, Dinh NQ, Reichstein M, Otieno D, Granier A, Pilegarrd K (2005) Evaluation of seasonal variation of MODIS derived leaf area index at two European deciduous broadleaf forest sites. *Remote Sensing of Environment*, 96(3), 475-484.

Wang X, Pan Y, Zhang Y, Dou D, Hu R, Zhang H (2013) Temporal stability analysis of surface and subsurface soil moisture for a transect in artificial revegetation desert area, China. *Journal of Hydrology*, 507:100-109.

Wang Y, Woodcock CE, Buermann W, Stenberg P, Voipio P, Smolander H, Häme T, Tian Y, Hu J, Knyazikhin Y, Myneni RB (2004) Evaluation of the MODIS LAI algorithm at a coniferous forest site in Finland. *Remote Sensing of Environment*, 91(1), 114-127.

Wang Y, Yu P, Feger KH, Wei X, Sun G, Bonell M, Xiong W, Zhang S, Xu L (2011) Annual runoff and evapotranspiration of forestlands and non-forestlands in selected basins of the Loess Plateau of China. *Ecohydrology*, 4(2), 277-287.

Wang, K., Dickinson, R.E., Wild, M., Liang, S., 2010. Evidence for decadal variation in global terrestrial evapotranspiration between 1982 and 2002: 1. Model development. Journal of Geophysical Research, 115(D20), D20112.

Webster MD, et al (2002) Uncertainty in emissions projections for climate models. *Atmospheric Environment*, 36(22), 3659-3670.

Weiß M, Menzel L (2008) A global comparison of four potential evapotranspiration equations and their relevance to stream flow modelling in semi-arid environments. *Advances in Geosciences*, 18, 15-23.

Wetherald RT, Manabe S (2002) Simulation of hydrologic changes associated with global warming. *Journal of Geophysical Research: Atmospheres*, (1984–2012) 107:ACL 7-1-ACL 7-15.

White MA, Thornton PE, Running SW, Nemani RR (2000) Parameterization and sensitivity analysis of the BIOME-BGC terrestrial ecosystem model: net primary production controls. *Earth Interactions*, 4(3), 1-85.

Wilson K, Goldstein A, Falge E, Aubinet M, Baldocchi D, Berbigier P, Bernhofer C, Ceulemans R, Dolman H, Field C (2002) Energy balance closure at FLUXNET sites. *Agricultural and Forest Meteorology*, 113 223-243.

Wright IR, Manzi AO, Da Rocha HR (1995) Surface conductance of Amazonian pasture: model application and calibration for canopy climate. *Agricultural and Forest Meteorology*, 75(1), 51-70.

Wu C, Ren G, Li J (2009) Experimental study on water requirements and irrigation schedule of Potato. *Journal of Irrigation and Drainage*, 28(3): 93-95, (in Chinese).

Wu K, Chen J, Xie X (1997) On the water consumption characteristics of winter wheat and water-saving in agriculture. *Acta Geographica Sinica*, 52(5): 455-460, (in Chinese).

Xiao J, Chen J, Davis KJ, Reichstein M (2012) Advances in upscaling of eddy covariance measurements of carbon and water fluxes. *Journal of Geophysical Research*, 117, G00J01.

Xie A, Liu H (2004) Drying of soil in the central Inner Mongolia region in the recent 50-year. *Journal of Nanjing Institute of Meteorology*, 4(27), 480-486 (in Chinese).

Xin L, Li X, Tan M (2012) Temporal and regional variations of China's fertilizer consumption by crops during 1998–2008. *Journal of Geographical Sciences*, 22:643-652.

Xu L, Dennis PL, Wood EF, Burges SJ (1994) A simple hydrologically based model of land surface water and energy fluxes for general circu-lation models. *Journal of Geophysical Research*, 99, 14415-14428.

Yang W, Tan B, Huang D, et al. (2006) MODIS leaf area index products: From validation to algorithm improvement. *Geoscience and Remote Sensing*, IEEE Transactions on, 44(7), 1885-1898.

Zhang P (1993) Model Selection Via Multifold Cross Validation. *Annals of Statistics*, 21(1) 299-313.

Zhang Y, Kadota T, Ohata T, Oyunbaatar D (2007) Environmental controls on evapotranspiration from sparse grassland in Mongolia. *Hydrological Processes*, 21(15), 2016-2027.

Zhao M, Running SW, Nemani RR (2006) Sensitivity of moderate resolution imaging spectroradiometer (MODIS) terrestrial primary production to the accuracy of meteorological reanalyses. *Journal of Geophysical Research*, 111(G1), G01002.

Zhu X, Li Y, Li M, Pan Y, Shi P (2013) Agricultural irrigation in China. *Journal of Soil and Water Conservation*, 68:147A-154A.

Zhu X, Zhuang Q, Chen M, Sirin A, Melillo J, Kicklighter D, Sokolov A, and Song L (2011) Rising methane emissions in response to climate change in Northern Eurasia during the 21st century. *Environmental Research Letters*, 6(4), 045211.

Zhuang Q, He J, Lu Y, Ji L, Xiao J, and Luo T (2010) Carbon dynamics of terrestrial ecosystems on the Tibetan Plateau during the 20th century: an analysis with a process-based biogeochemical model. *Global Ecology and Biogeography*, 19(5), 649-662.

Zhuang Q, et al. (2003) Carbon cycling in extratropical terrestrial ecosystems of the Northern Hemisphere during the 20th Century: A modeling analysis of the influences of soil thermal dynamics. *Tellus*, 55B, 751-776.

Zhuang Q, McGuire AD, O'Neill KP, Harden JW, Romanovsky VE, Yarie J (2002) Modeling soil thermal and carbon dynamics of a fire chronosequence in interior Alaska. *Journal of Geophysical Research*, 108(D1).

Zhuang Q, Melillo JM, Kicklighter DW, Prinn RG, McGuire DA, Steudler PA, Felzer BS, and Hu S (2004) Methane fluxes between terrestrial ecosystems and the atmosphere at northern high latitudes during the past century: A retrospective analysis with a process-based biogeochemistry model. *Global Biogeochemical Cycles*, 18, GB3010.

Zhuang Q, Melillo JM, Sarofim MC, et al (2006) CO2 and CH4 exchanges between land ecosystems and the atmosphere in northern high latitudes over the 21st century. *Geophysical Research Letters*, 33, L17403.

Zhuang Q, Romanovsky VE, and McGuire AD (2001) Incorporation of a permafrost model into a large-scale ecosystem model: Evaluation of temporal and spatial scaling issues in simulating soil thermal dynamics. *Journal of Geophysical Research*, 106(D24), 33,649-33,670.

Zobler L (1986) A world soil file for global climate modeling. *NASA Technical Memorandum 87802*, National Aeronautics and Space Administration, New York.

Zou X, Zhai P, Zhang Q (2005) Variations in droughts over China: 1951–2003. *Geophysical Research Letters*, 32.

VITA

VITA

YALING LIU
liu516@purdue.edu
+1 (765) 775-6055
http://web.ics.purdue.edu/~liu516/

Education

- Ph.D., **Atmospheric Sciences**, Purdue University, 01/2011- 12/2014
  Dissertation: The Impact of Climate Change and Agricultural Activities on Water Cycling of Northern Eurasia
- M.S., **Meteorology**, China Agricultural University, 09/2002 – 07/2005
  Thesis: Dynamics of Vegetation Cover and its Driving Forces in the North Piedmont of Yinshan Mountain
- B.S., **Geography**, Hubei University, 09/1998 – 07/2002

Research Interests

- Hydrological impacts
- Water and Carbon Cycling
- Land-atmosphere interactions
- Land Surface Modeling

Publications

- **Liu, Y.**, Zhuang, Q., Pan, Z., Miralles, D., Tchebakova, N., Kicklighter, D., Chen., J., Sirin, A., He, Y., Zhou, G., Melillo, J. (2014) Responses of evapotranspiration and water availability to the changing climate in evapotranspiration and water availability to the changing climate in Northern Eurasia, *Climatic Change*, 126, 413-427
- **Liu, Y.**, Zhuang, Q., Miralles, D., Pan, Z., Tchebakova, N., Kicklighter, D., Zhu, Q., He, Y., Chen, J., Tchebakova, N., Sirin, A., Niyogi, D., Melillo, J. Impact of forcing data uncertainty on the estimation of evapotranspiration in Northern Eurasia, in review at *JGR:Atmosphere*
- **Liu, Y.**, Pan, Z., Zhuang, Q., Miralles, D., Teuling, A.J., Zhang, T., An, P., Dong, Z., Zhang, J., He, D., Wang, L., Pan, X., Niyogi, D. Agricultural activities aggravate drought in the Northern China, under revision, in review at *Scientific Reports*
- He, Y., Zhuang, Q., Harden, J.W., McGuire, A.D., Fan, Z., **Liu, Y.**, Wickland, K.P. (2014), The implications of microbial and substrate limitation for the fates of carbon in different organic soil horizon types: a mechanistically based model analysis, *Biogeosciences*, 11(16) , 4477-4491
- He, Y., Yang, J., Zhuang, Q., McGuire, A.D., Zhu, Q., **Liu, Y.**, Teskey, R., (2014), Uncertainty in the fate of soil organic carbon: A comparison of three conceptually different decomposition models at a larch plantation, *JGR: Biogeosciences*, 1-14, doi/10.1002/2014JG002701
- Zhu, Q., Zhuang, Q., Henze, D., Bowman, K., **Liu Y.** He, J., Matsueda, H., Machida, T., Sawa, Y., Oechel, W. (2014), Constraining terrestrial ecosystem CO2 fluxes by integrating models of biogeochemistry and atmospheric transport and data of surface carbon fluxes and atmospheric CO2 concentrations, Atmospheric Chemistry and Physics Discussion, 14, 22587-22638

- **Liu, Y.**, Zhuang, Q., Chen, M., Tchebakova, N., Pan, Z., Sokolov, A., Kicklighter, D., Melillo, J., Zhou, G., He., Y., Chen, J., Bowling, L., Miralles, D., Parfenov, E. (2013) Response of evapotranspiration and water availability to changing climate and land cover on the Mongolian Plateau during the 21st century, *Global and Planetary Change*, 108(0), 85-99.
- He, D., **Liu, Y.**, Pan, Z., An, P., Wang, L., Dong, Z., Zhang, J., Pan, X., Zhao, P. (2013). Climate change and its effect on reference crop evapotranspiration in central and western Inner Mongolia during 1961–2009. *Frontiers of Earth Science*, 7(4):417-428
- Zhao, L., **Liu, Y.**, Pan, Z., An, P., Pan, X., Zhao., P., (2013), Impacts of Climate Change on the Dry-land Crop Water Consumption in Recent Decades in the North Agro-pastoral Transitional Zone of China, *Acta Meteorological Sinica,*27(4), 585-590
- He, Y., Q. Zhuang, A. D. McGuire, **Liu, Y.**, and M. Chen (2013), Alternative ways of using field-based estimates to calibrate ecosystem models and their implications for carbon cycle studies, *JGR: Biogeosciences* 118, 1-11
- **Liu, Y.**, Pan, Z., Fan, J., and Zheng, D., (2005), Spatial and Temporal Analysis on Vegetation Cover Dynamics in North Piedmont of Yinshan Mountain, *Resource Science*, 27(4), 168-174
- **Liu, Y.**, (2005), Dynamics of Vegetation Cover and its Driving Forces in the North Piedmont of Yinshan Mountain, *China Excellent Doctoral Dissertations and Master's Theses Full-Text Databases*
- **Liu, Y.**, Pan, Z., Fan, J., (2004), Time-series Analysis of Vegetation Cover in North Piedmont of Yinshan Mountain, *IEEE International Geoscience and Remote Sensing Symposium,* 6,3618-3621

- **Liu, Y.**, Pan, Z., (2004), Research on Vegetation Cover Degeneration and Restoration in North Ecotone, *Ecology Economics*, 9:51-53
- Pan, Z., An, P., **Liu, Y.**, (2004), Research on Environment Change of Ecology System in North Ecotone—for the example of Wuchuan County, *Chinese Agriculture and District*, Vol.24.No.5:37-41
- Pan, Z., An, P., **Liu, Y.,** Zheng, D., Tuo, D. (2004). "Change of eco-systematical function in northern ecotone: A case study in Wuchuan." *Journal of China Agricultural University*, 9(1): 37-40.

Awards

- American Geophysical Union (AGU) student Travel grant, 2013
- Travel grant for Women in Science of Purdue University, 2013& 2014

Public Services

- Reviewer for *Water Resources Research*, *Hydrology and Earth System Sciences* and *PLOS ONE*

Professional Experience

- **Research Assistant**, Department of Earth, Atmospheric, and Planetary Sciences, Purdue University, 01/2011 – 12/2014
- **Research Assistant**, Beijing Oriental Wisdom Tech Dev. Co., Ltd, Beijing, China, 05/2006 – 03/2010
- **Geography Teacher**, Beijing Experimental Foreign Language School, Beijing, China, 07/2005 – 05/2006